
Journal of
Mechanics of
Materials and Structures
Volume 10, No. 4
July 2015
msp

JOURNAL OF MECHANICS OF MATERIALS AND STRUCTURES

msp.org/jomms

Founded by Charles R. Steele and Marie-Louise Steele

Cover photo: Mando Gomez, www.mandolux.com

See msp.org/jomms for submission guidelines.

JoMMS (ISSN 1559-3959) at Mathematical Sciences Publishers, 798 Evans Hall #6840, c/o University of California, Berkeley, CA 94720-3840, is published in 10 issues a year. The subscription price for 2015 is US $565/year for the electronic version, and $725/year (+$60, if shipping outside the US) for print and electronic. Subscriptions, requests for back issues, and changes of address should be sent to MSP.

JoMMS peer-review and production is managed by EditFLOW® from Mathematical Sciences Publishers.

PUBLISHED BY

mathematical sciences publishers

nonprofit scientific publishing

http://msp.org/

JOURNAL OF MECHANICS OF MATERIALS AND STRUCTURES
Vol. 10, No. 4, 2015
dx.doi.org/10.2140/jomms.2015.10.447

RELATION BETWEEN THE MAXWELL EQUATIONS AND BOUNDARY CONDITIONS IN PIEZOELECTRIC AND PIEZOMAGNETIC FRACTURE MECHANICS AND ITS APPLICATION

HAO TIAN-HU

This paper presents the relation between the Maxwell equations and the boundary conditions in piezoelectric and piezomagnetic fracture mechanics. In addition, considering that the case after deformation (current configuration in nonlinear elasticity) is very important for these conditions, the significance of them has been studied for this case. The application of them has also been researched. Moreover, the stress field of the solid material caused by the electric field has been discussed. In the conclusion, it is briefly discussed how to determine the crack open or not, which is of vital importance for semipermeable and impermeable boundary conditions.

1. Introduction

In mechanics, along with rapid development of the computing technology, the methods of solution have been various. Accordingly, the equations of constitutive and the boundary conditions should be paid more attention. Consequently, in the research on the solid fracture mechanics of piezoelectric and piezomagnetic materials, the exploration of the relation between the Maxwell equations and the electromagnetic boundary conditions is necessary. Although many authors have researched on these boundary conditions such as Kumar and Singh [1997], yet the study of this relation is not enough. In this paper, firstly, the relation between the permeable electromagnetic boundary conditions and Maxwell equations has been studied. Then, the permeable, the semipermeable and the impermeable electromagnetic boundary conditions have been discussed [Zhang et al. 2002]. In particular, for the semipermeable electromagnetic boundary condition, the body after deformation must be dealt with. Therefore, we must cope with the nonlinear elasticity. We know that this theory is very complicated. In order to avoid this difficulty, we consider using the approximated direct method instead of the iteration method. Consequently, we don't need to carry out this repeat calculation.

Lastly, the problem of the stress field of the solid material caused by the electric field had been discussed. It is briefly discussed how to determine the crack open or not.

2. Maxwell equations and permeable conditions

It is known that the Maxwell equations can be written in two forms. They are differential form and integral form. The Maxwell equations in these forms are

$$\int_S \boldsymbol{D}\cdot d\boldsymbol{S} = q_0 \quad \text{or} \quad \mathrm{Div}\,\boldsymbol{D} = q_1, \quad (\partial D_1/\partial x_1 + \partial D_2/\partial x_2 + \partial D_3/\partial x_3 = q_1), \tag{1}$$

Keywords: Maxwell equations, electric-magnetic boundary condition.

where $\boldsymbol{D}$ is the electric displacement vector, S is the whole surface of a body, q_0 is the total charge in the body, q_1 is the charge density and $d\boldsymbol{S}$ is a vector as in the course of vector analysis.

$$\begin{gathered}\int_k \boldsymbol{E}\cdot d\boldsymbol{k} = -\int_{S_k} (\partial \boldsymbol{B}/\partial t)\cdot d\boldsymbol{S} \quad \text{or} \quad \text{Curl}\boldsymbol{E} = -\partial \boldsymbol{B}/\partial t,\\ \partial E_2/\partial x_1 - \partial E_1/\partial x_2 = -\partial B_3/\partial t,\\ \partial E_1/\partial x_3 - \partial E_3/\partial x_1 = -\partial B_2/\partial t,\\ \partial E_3/\partial x_2 - \partial E_2/\partial x_3 = -\partial B_1/\partial t.\end{gathered} \tag{2}$$

where $\boldsymbol{E}$ is electric field vector, $\boldsymbol{B}$ is magnetic induction vector, k is a closed curve, $d\boldsymbol{k}$ is the tangential vector of k and S_k is a surface whose boundary curve is k.

$$\int_S \boldsymbol{B}\cdot d\boldsymbol{S} = 0 \quad \text{or} \quad \text{div}\boldsymbol{B} = 0, \quad (\partial B_1/\partial x_1 + \partial B_2/\partial x_2 + \partial B_3/\partial x_3 = 0), \tag{3}$$

$$\begin{gathered}\int_k \boldsymbol{H}\cdot d\boldsymbol{k} = \boldsymbol{J}_0 + \int_{S_k} (\partial \boldsymbol{D}/\partial t)\cdot d\boldsymbol{S} \quad \text{or} \quad \text{Curl}\boldsymbol{H} = \boldsymbol{J}_0 + \partial \boldsymbol{D}/\partial t,\\ \partial H_2/\partial x_1 - \partial H_1/\partial x_2 = J_{03} + \partial D_3/\partial t,\\ \partial H_1/\partial x_3 - \partial H_3/\partial x_1 = J_{02} + \partial D_2/\partial t,\\ \partial H_3/\partial x_2 - \partial H_2/\partial x_3 = J_{01} + \partial D_1/\partial t,\end{gathered} \tag{4}$$

where $\boldsymbol{H}$ is magnetic field intensity vector and J_{01}, J_{02}, J_{03}, are the components of the current intensity vector $\boldsymbol{J}_0$.

Only the static condition and the cases $q_0 = 0$, $q_1 = 0$, $\boldsymbol{J}_0 = 0$ are dealt with.

The equations (1) and (3) become

$$\begin{gathered}\int_S \boldsymbol{D}\cdot d\boldsymbol{S} = 0 \quad \text{or} \quad \text{Div}\boldsymbol{D} = 0 \quad (\partial D_1/\partial x_1 + \partial D_2/\partial x_2 + \partial D_3/\partial x_3 = 0), \quad \text{and}\\ \int_S \boldsymbol{B}\cdot d\boldsymbol{S} = 0 \quad \text{or} \quad \text{Div}\boldsymbol{B} = 0 \quad (\partial B_1/\partial x_1 + \partial B_2/\partial x_2 + \partial B_3/\partial x_3 = 0).\end{gathered} \tag{5}$$

Considering $\partial \boldsymbol{D}/\partial t = 0$ and $\partial \boldsymbol{B}/\partial t = 0$ (static condition) and $\boldsymbol{J}_0 = 0$, the equations (2) and (4) become

$$\begin{gathered}\int_k \boldsymbol{E}\cdot d\boldsymbol{k} = 0 \quad \text{or} \quad \text{Curl}\boldsymbol{E} = 0\\ (\partial E_2/\partial x_1 - \partial E_1/\partial x_2 = 0, \quad \partial E_1/\partial x_3 - \partial E_3/\partial x_1 = 0, \quad \partial E_3/\partial x_2 - \partial E_2/\partial x_3 = 0), \quad \text{and}\\ \int_k \boldsymbol{H}\cdot d\boldsymbol{k} = \boldsymbol{0} \quad \text{or} \quad \text{Curl}\boldsymbol{H} = 0\\ (\partial H_2/\partial x_1 - \partial H_1/\partial x_2 = 0, \quad \partial H_1/\partial x_3 - \partial H_3/\partial x_1 = 0, \quad \partial H_3/\partial x_2 - \partial H_2/\partial x_3 = 0).\end{gathered} \tag{6}$$

On the basis of Equation (6), we have

$$E_i = \partial\phi/\partial x_i \text{ and } H_i = \partial\phi_1/\partial x_i \tag{6a}$$

where ϕ is the electric potential and ϕ_1 is the magnetic potential.

For plane case, on the Ox_1x_2 plane, two integrals in (5) are all computed along the surface curve p of the area and become

$$\begin{gathered}\int_p D_n\,dp = 0 \quad \text{and} \quad \int_p B_n\,dp = 0, \quad \text{or} \\ \partial D_1/\partial x_1 + \partial D_2/\partial x_2 = 0 \quad \text{and} \quad \partial B_1/\partial x_1 + \partial B_2/\partial x_2 = 0,\end{gathered} \tag{7}$$

where p is the surface curve in the plane, D_n is the normal component of vector D and B_n is the normal component of vector B.

The two integrals in (6) become

$$\begin{gathered}\int_p E_t\,dp = 0 \quad \text{or} \quad \partial E_2/\partial x_1 - \partial E_1/\partial x_2 = 0, \quad \text{and} \\ \int_p H_t\,dp = 0 \quad \text{or} \quad \partial H_2/\partial x_1 - \partial H_1/\partial x_2 = 0,\end{gathered} \tag{8}$$

where E_t is the tangential component of vector E and H_t is the tangential component of vector H.

Now, based on Maxwell equations, the permeable boundary conditions for the static electric and magnetic case are studied. One considers a surface, which can be the interface of two materials. A short segment of this surface is studied (we shall discuss it in detail in Appendix). For convenience, the segment in the studied plane is a part of Ox_1 axis. In order to study the conditions on the segment, a rectangle is taken, as shown in the figure:

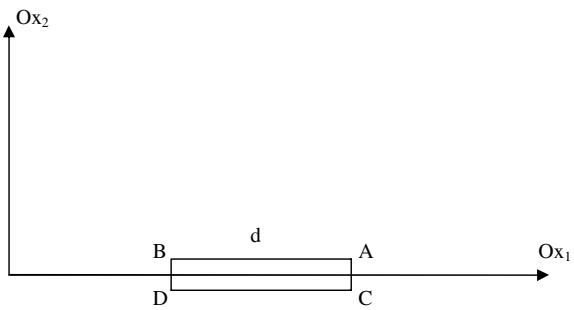

The longer side is parallel to the segment, i.e., Ox_1 axis with width d. The shorter is perpendicular to the segment, i.e., Ox_2 axis and its length trends to zero. For the rectangle, the two integrals in (5) and (7) can be computed.

Considering the area is very small, one can be sure that the value of D, $E(\phi)$, B and $H(\phi_1)$ are constants on one side but can be different on other side. Therefore, the contribution on the shorter side tends to zero. For the longer side, they are parallel to Ox_1. The tangent component of vector $\boldsymbol{E}$ is E_1. Similarly, the normal component of vector $\boldsymbol{D}$ is D_2. The equation $\int_p D_n\,dp = 0$ and $\int_p E_t\,dp = 0$ becomes

$$(D_2^+ - D_2^-)d = 0, \quad \text{i.e.,} \quad D_2^+ = D_2^-, \quad \text{and} \quad (E_1^+ - E_1^-)d = 0, \quad \text{i.e.,} \quad E_1^+ = E_1^-(\phi^+ = \phi^-), \tag{9}$$

where D_2^+ is the D_2 on the upper surface of the interface and D_2^- is that on the lower surface. Similarly, E_1^+ and E_1^- can be understand as D_2^+ and D_2^-.

For the magnetic field, one has

$$B_2^+ = B_2^{--} \quad \text{and} \quad H_1^+ = H_1^-(\phi_1^+ = \phi_1^-). \tag{10}$$

It is the permeable boundary conditions for a surface in static electric and magnetic field. For the static electric field, in the piezoelectric fracture mechanics, it is the well known boundary condition of [Parton 1976; Mikhailov and Parton 1990].

As a matter of fact, that is an old boundary condition. In any textbook of the theory of electromagnetism, for the interface between two materials, one can find this boundary condition.

3. Semipermeable conditions and impermeable condition

Although the permeable boundary conditions are deduced from Maxwell equations, yet they have not considered the existence of crack and only for a surface or an interface in the materials. When one directly uses them for the piezoelectric and piezomagnetic fracture mechanics, they may result in larger deviations sometime. However, the importance of these conditions is that they can be the basis of the further discussion on the boundary conditions for the piezoelectric and piezomagnetic fracture mechanics.

Now, the semipermeable boundary conditions and the impermeable boundary conditions are considered. Firstly, the cracks can be divided into two kinds. The first is for the cracks with the opening voids full of fluid (air) after deformation. We always dealt with this kind. The second has not the opening voids such as the antiplane case (as $u_1 = u_2 = 0$, the crack can not be opening), the crack subjected to compression stress, etc. For the second, as the void does not exist after deformation, the permeable equations $D_2^+ = D_2^-$ and $E_1^+ = E_1^-(\phi^+ = \phi^-)$, $B_2^+ = B_2^{--}$ and $H_1^+ = H_1^-(\phi_1^+ = \phi_1^-)$ can be accepted.

Then, for the first, when studying the crack full of air, it is improper to write the boundary condition before deformation as the classical theory; otherwise the crack is only a slit without void and no air can be exist in it. Therefore, we must consider the boundary condition after deformation (the current configuration in nonlinear elasticity). In the meantime, the opening crack becomes a void. At the surface of the void, on the interface between the fluid (in void) and the solid (outside void), we have the interface boundary conditions

$$D_2^+ = D_2^- \quad \text{and} \quad E_1^+ = E_1^-(\phi^+ = \phi^-), \quad B_2^+ = B_2^{--} \quad \text{and} \quad H_1^+ = H_1^-(\phi_1^+ = \phi_1^-), \tag{11}$$

where D_2^+, D_2^-, E_1^+, $E_1^-(\phi^+, \phi^-)$, B_2^+, B_2^-, H_1^+, $H_1^-(\phi_1^+, \phi_1^-)$ belong to the fluid (in void) and the solid (outside void).

In the fluid (in void), there are the various basic equations of the fluid (air), such as

$$\partial^2\phi_i/\partial x_1^2 + \partial^2\phi_i/\partial x_2^2 + \partial^2\phi_i/\partial x_3^2 = 0 \quad \text{and} \quad \partial^2\phi_{1i}/\partial x_1^2 + \partial^2\phi_{1i}/\partial x_2^2 + \partial^2\phi_{1i}/\partial x_3^2 = 0, \tag{12}$$

where ϕ_i and ϕ_{1i} are the electric and magnetic potentials of the fluid components in the void. For the solid (outside void), the basic equations are well known and we shall not discuss them here. It is the all conditions satisfied by the body with void including air. To solve it is a complicated problem. Generally, it is better to use the nonlinear elasticity to solve this problem but the nonlinear elasticity is too tough to study. Now, a simpler method is accepted in study. This method is as follows. For convenience, when studying the crack void full of air, the boundary after deformation can be accepted as the boundary before deformation (a closed slit) adding the evaluated boundary displacement. Naturally, we know that this

displacement is also found by classical theory. In this theory, the displacement field is calculated from the boundary before deformation, i.e., on the nondeformation body. This result is not precise but results in the little deviation. Nevertheless, to the case of crack void full of air, the deviation is not negligible.

As mentioned above, the approximate boundary after deformation is determined. Now we consider the solid (outside void) and the fluid (in void). As mentioned above, the constitutive equation of the solid is well known and that of the fluid are various and complicated. In order to avoid that of fluid, considering the void is very small after deformation, Hao [1993] and Hao and Shen [1994] have used the linear change of ϕ and ϕ_1 along the surface normal to replace the rigorous solution of the complicated equation (that is one of the basic assumption of this boundary condition). In the void, E_2 and H_2 (for small deformation case, E_n and H_n are replaced by E_2 and H_2) become $-(\phi^+ - \phi^-)/(u_2^+ - u_2^-)$ and $-(\phi_1^+ - \phi_1^-)/(u_2^+ - u_2^-)$, and u_2 is the evaluated boundary displacement component as above mentioned.

Considering $D_2 = \epsilon_a E_2$ and $B_2 = \epsilon_{a1} H_2$ in air, one obtains

$$(u_2^+ - u_2^-)D_2 = -\epsilon_a(\phi^+ - \phi^-), \quad (u_2^+ - u_2^-)B_2 = -\epsilon_{a1}(\phi_1^+ - \phi_1^-) \tag{13}$$

where ϵ_a and ϵ_{a1} are the electric and magnetic permitivities of air.

Since in the void, E_2 and H_2 become the constants along the normal, D_2 and B_2 are also the constants along the normal. Then, we obtain

$$D_2^+ = D_2^- = -\epsilon_a \frac{\phi^+ - \phi^-}{u_2^+ - u_2^-}, \quad B_2^+ = B_2^- = -\epsilon_{a1} \frac{\phi_1^+ - \phi_1^-}{u_2^+ - u_2^-}. \tag{14}$$

In fact, this boundary condition is obtained from the conception of current configuration in finite deformation theory and the linear change of potential as [Hao 2004]. In short, the conception of current configuration is that we must deal with the crack boundary after deformation when studying a crack.

The equation (14) is the semipermeable boundary condition. For the piezoelectric case, it is suggested by [Hao 1993; Hao and Shen 1994].

It is approximate to use an average rate of change of potential ϕ to take the place of the actual rate. However, as it is only an approximate boundary condition rather than an exact result, I can be sure that for disagreeing it we must be based on some contrary examples, not one exact example.

It is apparent that Equation (13) will be reduced to $\phi^+ = \phi^-$ or $\phi_1^+ = \phi_1^-$ (one of the permeable boundary conditions) when $u_2^+ - u_2^- = 0$ (closed), and to the following equation under the condition $\epsilon_a = 0$ and $\epsilon_{a1} = 0$:

$$D_2^+ = D_2^- = 0, \ B_2^+ = B_2^- = 0. \tag{15}$$

The Equation (15) is the impermeable boundary conditions.

4. Some problems about the application of these boundary conditions

In order to avoid the irrationality in the result, we must decide to suitably use these boundary conditions. The permeable boundary condition is obtained from the Maxwell equations exactly. Therefore, we must determine in what situation this boundary may be accepted. If we can be sure that the crack is closed, the permeable boundary condition should be accepted. However, it is not easy to determine the crack

being closed. In order to do it, from [Hao 2001], we know

$$u_2^+ - u_2^- = 2\mathrm{Re}\sum_{j=1}^{4}(\beta_{2r}k_{rj} + \eta_{2\alpha}d_{\alpha j})[f_j'(x_1)^+ - f_j'(x_1)^-]/\mu, \tag{16a}$$

where the constants can be found in [Hao 2001].

It is an exact formula to decide whether the crack is closed or not but it is too complicated to be used. We shall discuss it in detail later.

When we know that the crack is closed, the permeable boundary condition can be accepted.

From the Equation (16), we can also decide that the crack is open. At this time, the semipermeable or the impermeable boundary condition can be considered.

About the semipermeable boundary condition, although it has considered the electric field in the air, yet it seems to be too complicated to deal with. However, many results can be accepted by us to study this problem without difficulty. These results tell us that D_2^+ can be determined directly without complicated computing. For an example, to the common multiple collinear cracks (naturally, single crack) under the simple remote load case, we have following result.

In general case, there are four functions of complex variables $f_j''(z_j)$ and the displacements and potential can be

$$\begin{aligned}\phi^+ - \phi^- &= 2\mathrm{Re}\sum_{j=1}^{4}(h_{1r}k_{rj} - \xi_{1\alpha}d_{\alpha j})[f_j'(x_1)^+ - f_j'(x_1)^-],\\ u_2^+ - u_2^- &= 2\mathrm{Re}\sum_{j=1}^{4}(\beta_{2r}k_{rj} + \eta_{2\alpha}d_{\alpha j})[f_j'(x_1)^+ - f_j'(x_1)^-]/\mu_j\end{aligned} \tag{16b}$$

where the constants can be found in [Hao 2001].

The functions $f_j''(z_j)$ can be obtained from

$$\begin{gathered}\sum_{j=1}^{4} l_{ij}f_j''(z) = e_i + if_i + e_i[Q(z) - 1], \quad i = 1, \ldots, 4,\\ Q(z) = \frac{z^n + c_1z^{n-1} + \cdots + c_{n-1}z + c_n}{\prod_{k=1}^{n}[(z - a_k)(z - b_k)]^{1/2}},\end{gathered} \tag{17}$$

where $c_1, c_2, \ldots, c_{n-1}, c_n$ are defined by single value requirements of displacements and potential and a_k and b_k are the two tips of the k-th crack but no relation with material constants.

Then, using linear algebra method, one can find functions $f_j''(z_j)$ as [Hao 2001]

$$f_i''(z_i) = \sum_{j=1}^{4} x_{ij}\{D_j + e_jQ(z_i)\}, \quad D_j = e_j + if_j - e_j, \tag{18}$$

where x_{ij} is determined by linear algebra method as [Hao 2001].

We introduce

$$P'(x_1) = -Q(x_1). \tag{19}$$

Then, there is

$$\begin{aligned} f_i''(x_1)^+ - f_i''(x_1)^- &= -\left[\sum_{j=1}^{4} x_{ij} e_j Q(x_1)\right]^- + \left[\sum_{j=1}^{4} x_{ij} e_j Q(x_1)\right]^+ \\ &= \left[\sum_{j=1}^{4} x_{ij} e_j P'(x_1)\right]^- - \left[\sum_{j=1}^{4} x_{ij} e_j P'(x_1)\right]^+ \\ &= \sum_{j=1}^{4} x_{ij} e_j [P'(x_1)^- - P'(x_1)^+]. \end{aligned} \tag{20}$$

From Equation (20), we obtain

$$\begin{aligned} f_i'(x_1)^+ - f_i'(x_1)^- &= \sum_{j=1}^{4} x_{ij} e_j [P(x_1)^- - P(x_1)^+] \\ &= [P(x_1)^- - P(x_1)^+] \sum_{j=1}^{4} x_{ij} e_j \\ &= A_i [P(x_1)^- - P(x_1)^+], \end{aligned} \tag{21}$$

$$A_i = \sum_{j=1}^{4} x_{ij} e_j. \tag{22}$$

Then, we have

$$\begin{aligned} \phi^+ - \phi^- &= 2\mathrm{Re} \sum_{j=1}^{4} (h_{1r} k_{rj} - \xi_{1\alpha} d_{\alpha j}) A_j [P(x_1)^- - P(x_1)^+] \\ &= 2\mathrm{Re}[P(x_1)^- - P(x_1)^+] \sum_{j=1}^{4} (h_{1r} k_{rj} - \xi_{1\alpha} d_{\alpha j}) A_j, \\ u_2^+ - u_2^- &= 2\mathrm{Re} \sum_{j=1}^{4} (\beta_{2r} k_{rj} + \eta_{2\alpha} d_{\alpha j}) A_j [P(x_1)^- - P(x_1)^+]/\mu_j \\ &= 2\mathrm{Re}[P(x_1)^- - P(x_1)^+] \sum_{j=1}^{4} (\beta_{2r} k_{rj} + \eta_{2\alpha} d_{\alpha j}) A_j/\mu_j. \end{aligned} \tag{23}$$

One can find that the function $[P(x_1)^+ - P(x_1)^-]$ is imaginary. Therefore, we have

$$\begin{aligned} \phi^+ - \phi^- &= 2\mathrm{i}[P(x_1)^- - P(x_1)^+]\mathrm{Im} \sum_{j=1}^{4} (h_{1r} k_{rj} - \xi_{1\alpha} d_{\alpha j}) A_j, \\ u_2^+ - u_2^- &= 2\mathrm{i}[P(x_1)^- - P(x_1)^+]\mathrm{Im} \sum_{j=1}^{4} (\beta_{2r} k_{rj} + \eta_{2\alpha} d_{\alpha j}) A_j/\mu_j. \end{aligned} \tag{24}$$

Therefore, D_2^+ can be approximately expressed as

$$D_2^+ = -\epsilon_a \frac{[P(x_1)^- - P(x_1)^+]\,\mathrm{Im}\sum_{j=1}^4 (h_{1r}k_{rj} - \xi_{1\alpha}d_{\alpha j})A_j}{[P(x_1)^- - P(x_1)^+]\,\mathrm{Im}\sum_{j=1}^4 (\beta_{2r}k_{rj} + \eta_{2\alpha}d_{\alpha j})A_j/\mu_j}$$
$$= -\epsilon_a \frac{\mathrm{Im}\sum_{j=1}^4 (h_{1r}k_{rj} - \xi_{1\alpha}d_{\alpha j})A_j}{\mathrm{Im}\sum_{j=1}^4 (\beta_{2r}k_{rj} + \eta_{2\alpha}d_{\alpha j})A_j/\mu_j}, \tag{25}$$

D_2^+ is no relation with these coordinates x_i and can be determined directly without the iteration method.

We must pay attention to that although the expressions of $\phi^+ - \phi^-$ and $u_2^+ - u_2^-$ are exact, yet for D_2^+ it is approximate. For an example, we consider a crack. In general case, its $\phi^+ - \phi^-$ and $u_2^+ - u_2^-$ may be proportional to $(a^2 - z^2)^{1/2}$. When the load leads $u_2^+ - u_2^-$ tending to zero, the crack should be closed. Therefore, we must accept the permeable condition. As $\phi^+ - \phi^-$ can also tend to zero, the value $(\phi^+ - \phi^-)/(u_2^+ - u_2^-)$ may tend to a constant. However, because the crack is closed, there is no air in the crack void and $(\phi^+ - \phi^-)/(u_2^+ - u_2^-)$ is a constant without significance.

5. Stress field caused by the electric field

Now, we study the stress field caused by the electric field. Essentially it is the acting force of electric field on the solid element. The acting force caused by the electric field is a body force. It is known that the stress field caused by the electric field is a square but that by the piezoelectric field is linear [Fang and Yin 1989, 4.7.1, p. 209]. Therefore, the stress field caused by the electric field is always smaller than that by the piezoelectric field [ibid., 4.7.2, p. 210] and always can be neglected.

Due to the complexity of this problem, the stress distribution caused by the electric field will be discussed in detail in another paper.

6. Conclusions

For the electric-magnetic fracture mechanics, the relation between the Maxwell equations and the permeable, semipermeable and impermeable electromagnetic boundary conditions has been studied. Then, the application of these boundary conditions has been discussed. Lastly, the stress field caused by the electric field also has been discussed. It is known that permeable electromagnetic boundary conditions are exact for the closed crack. When we can be sure that the crack is not closed, the semipermeable or the impermeable electromagnetic boundary condition is accepted. Naturally, it has some trouble to use formula (16a) to decide whether the crack is open or not. However, for the cracks on a straight line (for example, the cracks on Ox_1) and $D_2^\infty = 0$, it is easy to deal with. From the equation (24), we know

$$u_2^+ - u_2^- = 2\mathrm{i}[P(x_1)^- - P(x_1)^+]\,\mathrm{Im}\sum_{j=1}^4 (\beta_{2r}k_{rj} + \eta_{2\alpha}d_{\alpha j})A_j/\mu_j \tag{26}$$

where $A_j = m_j\sigma_2^\infty$ and m_j is a constant and no use for our discussion.

Substituting them into (26), we have

$$u_2^+ - u_2^- = 2\mathrm{i}[P(x_1)^- - P(x_1)^+]\sigma_2^\infty\,\mathrm{Im}\sum_{j=1}^4 (\beta_{2r}k_{rj} + \eta_{2\alpha}d_{\alpha j})m_j/\mu_j. \tag{27}$$

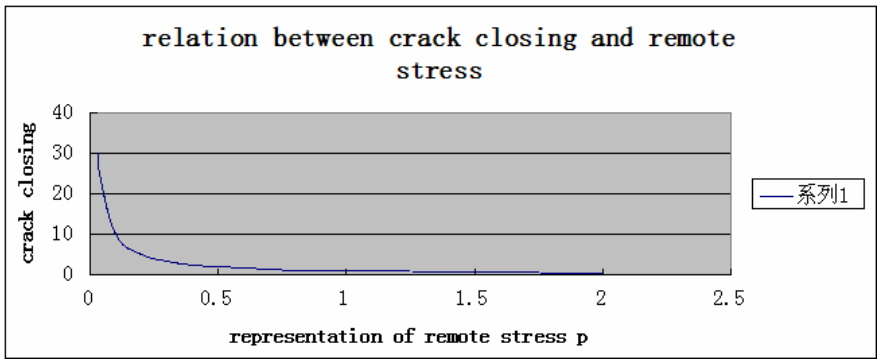

Figure 1. The relation between the crack closing and the representation of remote stress p.

It is clear that the value $u_2^+ - u_2^-$ is proportional to the value σ_2^∞ which is the same with the theory of elasticity.

For one crack case, we know

$$u_2^+ - u_2^- = -2\mathrm{i}[P(x_1)^+ - P(x_1)^-](k_2/\pi^{1/2}a^{1/2})\,\mathrm{Im}\sum_{j=1}^{4}(\beta_{2r}k_{rj} + \eta_{2\alpha}d_{\alpha j})m_j/\mu_j, \tag{28}$$

where k_2 is the stress intensity factor and a is the half length of the crack.

In order to clarify the crack closing, it is explained in Figure 1.

For convenience, the term $4a\sigma_2^\infty\,\mathrm{Im}\sum_{j=1}^{4}(\beta_{2r}k_{rj} + \eta_{2\alpha}d_{\alpha j})m_j/\mu_j$ is replaced by $10^{11}p$, where $2a$ is the crack length.

From Figure 1 we know that when the representation of remote stress p tends to 0, the crack closing to infinite.

Previously, we only consider the crack being traction free at its surface. When there is homogeneous load σ_0 on crack surface and $\sigma_2^\infty = 0$, we resolve it into two cases. The one is homogeneous stress σ_0 on the whole solid and the another is $\sigma_2^\infty = -\sigma_0$. On the basis of the sum of the two cases, all boundary conditions are satisfied. The case of homogeneous stress σ_0 on the whole solid is a homogeneous field. It is easy to deal with. The case of $-\sigma_0$ at infinite is that of $\sigma_2^\infty = -\sigma_0$. It has been discussed in the equation (27).

Appendix: About the boundary condition

In order to discuss the boundary condition easily, we consider the plane potential fluid mechanics. Firstly, we introduce the conception of source, sink and vortex point. Naturally, they are the plane potential fluid field which has two components parallel to Ox_1 and Ox_2. The velocity fields of source and sink are radius. At every point, the velocity is parallel to the radius. The vortex point is tangential velocity field. At every point, the velocity is perpendicular to the radius. Therefore, the vortex point velocity field is a circular ring field. In fluid mechanics, we call this field in rotational field. We know that the conception of source seems to be the water spring. The conception of sink is contrary to that of source. For the vortex point, we always seem to observe it at the water surface. Sometimes, the sources (naturally, sinks

and vortex points) can be considered a line source. That seems to be observed at the water surface. For convenience, we deal with the plane problem on the plane with axis Ox_1 and Ox_2. Now, we consider a slit on the interface of two materials. The slit is on the axis Ox_1. We must be sure that because there are two materials, the velocity must be different in the two materials. Letting the velocities be V_1 and V_2 in the two materials. When there is no source and sink in the slit, letting the values V_{12} and V_{22} are components of V_1 and V_2 paralleling to Ox_2. $V_{12} = V_{22}$. When there is no vortex point in the slit, letting the values V_{11} and V_{21} are components of V_1 and V_2 paralleling to Ox_1. $V_{11} = V_{21}$. When there are some sources or sinks in the slit, $V_{12} \neq V_{22}$ across the slit. When there are some vortex points in the slit, $V_{11} \neq V_{21}$ across the slit.

On the basis of above discussed, the static electric field is easy to deal with. The positive and negative charge is corresponding to the source and sink. Naturally, it seems to be difficult to find anything corresponding to the vortex point. However, when we study the magnetic field around the wire, we seem to meet the point corresponding to it. Therefore, for the slit of the interface of two materials on Ox_1 in the electric field, we can be sure that $D_{12} = D_{22}$ (corresponding to $V_{12} = V_{22}$ in fluid). Now, we must pay attention to the condition $V_{11} = V_{21}$ in fluid. We know that in fluid mechanics, we prove the condition $V_{11} = V_{21}$ based on the condition no vortex point in the slit. In fluid mechanics, as above mentioned, the condition no vortex point is corresponding to that of nonrotation. In Maxwell equations, as above mentioned, the condition nonrotation is discussed in equations (2) and (6). Here, the physical quantity E pays a leading role. Therefore, the condition $V_{11} = V_{21}$ in fluid mechanics, is corresponding to the condition $E_{11} = E_{21}$ in Maxwell equations.

Therefore, we obtain the boundary condition on the interface

$$D_{12} = D_{22}, \quad E_{11} = E_{21}, \tag{29}$$

where D_{1j} is the j-th of D_1, D_{2j} is the j-th of D_2, E_{1j} is the j-th of E_1 and E_{2j} is the j-th of E_2.

Naturally, these boundary conditions above mentioned, are obtained based on the analogy method. Now, we shall prove it by integral form of Maxwell equations exactly.

Letting BA and CD being the two longer sides of the rectangle (their length equals d) and AC, BD being the two shorter sides (their length tends to 0) and the segment of Ox_1 in the rectangle being the interface, we have $\int_p D_n\, dp = 0$ and $\int_p E_t\, dp = 0$. We consider the right spiral rule. The direction of four tops of the rectangle is $BACDB$. As BA and CD are parallel to Ox_1, their normal is parallel to Ox_2. The vector D_n becomes D_2. As their tangent is parallel to Ox_1, the vector E_t becomes E_1. The equation $\int_p D_n\, dp = 0$ becomes

$$-D_{12BA}AB + D_{22CD}CD + \text{ small contribution of the sides } AC \text{ and } DB = 0, \tag{30}$$

where D_{12} is the second component of the electric displacement D_1 in upper half plane $x_2 > 0$, D_{22} is the second component of the electric displacement D_2 in lower half plane $x_2 < 0$, D_{12BA} is D_{12} on BA and D_{22CD} is D_{22} on CD.

Considering the contribution of the shorter sides AC and DB tending to zero, we neglect it and consider the two sides AC and DB being the upper and lower surfaces of the interface. Therefore,

$$-D_{2BA}AB + D_{2CD}CD = -D_2^+AB + D_2^-CD = 0, \tag{31}$$

where $D_2^+ = D_{2BA}$ is the D_2 on the upper surface of the interface and $D_2^- = D_{2CD}$ is the D_2 on the lower surface of the interface.

Substituting $BA = CD = d$, we obtain

$$d(-D_2^+ + D_2^-) = 0. \tag{32}$$

Therefore, we have

$$D_2^+ = D_2^-. \tag{33}$$

Considering the E_t becomes E_1, the equation $\int_p E_t\, dp = 0$ becomes

$$-E_{11BA}BA + E_{21CD}CD + \text{ small contribution of the sides } AC \text{ and } DB = 0,$$

where E_{11} is the first component of the electric field E_1 in upper half plane $x_2 > 0$, E_{21} is the first component of the electric field E_1 in lower half plane $x_2 < 0$, E_{11BA} is E_1 on BA and E_{21CD} is E_1 on CD.

Considering the contribution of the shorter sides AC and DB being very little, we neglect it and consider the two sides AC and DB being the upper and lower surfaces of the interface. Therefore,

$$-E_{11BA}AB + E_{21CD}CD = -E_1^+ AB + E_2^- CD = 0, \tag{34}$$

where $E_1^+ = E_{11BA}$ is the E_1 on the upper surface of the interface and $E_2^- = E_{21CD}$ is the E_2 on the lower surface of the interface.

Substituting $BA = CD = d$, we obtain

$$d(-E_1^+ + E_1^-) = 0. \tag{35}$$

And so we have

$$E_1^+ = E_1^-. \tag{36}$$

Therefore, on the upper and lower surface of the interface, the components of vectors E_1 and D_2 on both surfaces are equal. When on the upper and lower surface of the interface, the components of vector E_1 on both surfaces are equal, on the upper and lower surface, the function ϕ ($\phi = \partial E_1/\partial x_1$) on both surfaces is equal (when the interface is $-\infty$–$+\infty$, on the upper and lower surface, the difference between the two functions ϕ^+ and ϕ^- may be a constant).

This result is the famous permeable condition in piezoelectric fracture mechanics [Parton 1976; Parton and Kudryavtsev 1988; Mikhailov and Parton 1990].

In fact, this is an old result in electrodynamics: $\int_q D_n\, dq = 0$. We can find it in any textbook such as [Coelho 1979].

Acknowledgment

Thanks for Professor Huang K. C. thanks to whom I have overcome many difficulties. Thanks for Professor Shen Z. Y. for his valuable help on English.

References

[Coelho 1979] R. Coelho, *Physics of dielectrics for the engineer*, Fundamental studies in engineering **1**, Elsevier, Amsterdam, 1979.

[Fang and Yin 1989] J. X. Fang and Z. W. Yin, 电介质物理学 , Science Press, Beijing, 1989.

[Hao 1993] T. H. Hao, "A boundary condition in electromagnetic fracture mechanics", *J. China Text. Univ.* **19**:1 (1993), 53. In Chinese.

[Hao 2001] T. H. Hao, "Multiple collinear cracks in a piezoelectric material", *Int. J. Solids Struct.* **38**:50–51 (2001), 9201–9208.

[Hao 2004] T. H. Hao, "Perturbation method of the piezoelectric fracture mechanics considering the permittivity of the medium in the crack gap", *Int. J. Fract.* **126**:1 (2004), 57–69.

[Hao and Shen 1994] T.-H. Hao and Z.-Y. Shen, "A new electric boundary condition of electric fracture mechanics and its applications", *Eng. Fract. Mech.* **47**:6 (1994), 793–802.

[Kumar and Singh 1997] S. Kumar and R. N. Singh, "Influence of applied electric field and mechanical boundary condition on the stress distribution at the crack tip in piezoelectric materials", *Mater. Sci. Eng. A* **231**:1–2 (1997), 1–9.

[Mikhailov and Parton 1990] G. K. Mikhailov and V. Z. Parton, *Electromagnetoelasticity*, Hemisphere, New York, 1990.

[Parton 1976] V. Z. Parton, "Fracture mechanics of piezoelectric materials", *Acta Astronaut.* **3**:9–10 (1976), 671–683.

[Parton and Kudryavtsev 1988] V. Z. Parton and B. A. Kudryavtsev, *Electromagnetoelasticity: piezoelectrics and electrically conductive solids*, Gordon and Breach, New York, 1988.

[Zhang et al. 2002] T.-Y. Zhang, M. Zhao, and P. Tong, "Fracture of piezoelectric ceramics", *Adv. Appl. Mech.* **38** (2002), 147–289.

Received 8 Mar 2014. Revised 4 Oct 2014. Accepted 27 Apr 2015.

HAO TIAN-HU: haoth0000@aliyun.com
State Key Lab for Modification of Polymer Materials and Chemical Fibers, Donghua University, P.O. Box 220, Shanghai, 200051, China

JOURNAL OF MECHANICS OF MATERIALS AND STRUCTURES
Vol. 10, No. 4, 2015
dx.doi.org/10.2140/jomms.2015.10.459

AXISYMMETRIC LOADING OF AN ELASTIC-PLASTIC PLATE ON A GENERAL TWO-PARAMETER FOUNDATION

LUCA LANZONI, ANDREA NOBILI, ENRICO RADI AND ANDREA SORZIA

The load carrying capacity and collapse scenarios for an infinite elastic-plastic plate resting on a two-parameter elastic foundation uniformly loaded on a small circular footprint are investigated in a general framework of stiffness and yield parameters. The present work extends the study already presented for a specific value of the Pasternak modulus and it allows the investigation of the influence of the stiffness property of the underlying soil and the amplitude of the loaded region on the load carrying capacity of the plate and the corresponding collapse mechanism. Moreover, the present analysis allows for the evaluation of the transverse deflection, slope, radial and circumferential bending moments, shearing force within the plate and the reactive pressure of the elastic subgrade at the onset of the plastic collapse together with their dependence on the foundation moduli. The effect of the ratio between negative and positive yield moments is also investigated. The amplitude and assembly of plastic regions at the onset of the plastic collapse are discussed in some detail.

1. Introduction

The problem of a plate resting on an elastic subgrade has been extensively investigated in the literature because of its relevance in many structural and geotechnical applications. Indeed, plate and slab-like elements supported by an elastic foundation are commonly encountered in many engineering systems, with particular reference to design spread building foundations (particularly, shallow mat-like foundations), e.g., [Gazetas and Tassios 1978; Gazetas 1981a], industrial and airport pavements [Caliendo and Parisi 2010], and rigid or flexible roadways [Helwany et al. 1998].

According to its relative slenderness, a shallow building foundation can be modeled as a thin Kirchhoff plate or as a thick Reissner–Mindlin plate, whereas the supporting medium can be simulated in different ways. As is well known, the perhaps most popular foundation model was proposed by Winkler in 1867, and it has enjoyed wide popularity ever since on account of its greater simplicity with respect to other soil descriptions at a reasonable cost in terms of result reliance in the supported structure. Nonetheless, owing to its local nature, the Winkler model cannot produce accurate results for the displacement field of the soil-foundation system. Accordingly, a variety of nonlocal subgrade models (e.g., Pasternak, Reissner, Filonenko-Borodich, Hetényi, Kerr and Vlazov models, among others) has been proposed over the years to improve upon the Winkler-type soil model [Selvadurai 1979].

Several analytical and numerical studies have been performed to evaluate the mechanical interaction between a raft slab foundation and the supporting medium. The analytical solution of a thin Kirchhoff plate resting on a Winkler-type subgrade under various load conditions is reported in detail in the classical

Keywords: two-parameter subgrade, Kirchhoff plate, Johansen's yield criterion, axisymmetric loading conditions, contour integral, elastic-plastic collapse.

book of Timoshenko and Woinowsky-Krieger [1959]. The axisymmetric flexure of an infinite elastic plate resting on an incompressible elastic half-space is considered by Selvadurai [1977] by making use of the potential functions and Hankel transforms. The problem of an elastic plate supported by an elastic two-parameter subgrade is studied in [Wen-da and Shu 1987] in order to model the circular foundation of a cooling hyperbolic tower. Results are compared with a numerical solution obtained through a FE package. The mechanical interaction between an infinite cracked Kirchhoff plate resting on a two-parameter elastic subgrade can be found in [Nobili et al. 2014, 2015]. A full-field solution is obtained therein by means of the Wiener–Hopf method and the influence of the subgrade parameters on the stress intensity factors at the crack tip are evaluated in detail.

Recently, Shukla et al. [2011] have obtained the solution of a circular plate supported by a tensionless Pasternak-type subgrade by using the strain energy approach and assuming a power series expansion for the transverse deflection of the plate. Variational boundary conditions for a beam resting on a two-parameter tensionless elastic foundation have been developed in [Nobili 2012]. Shell- and plate-like elements in contact with elastic media have been adopted as a reliable model to study micro- or nano-structures in the framework of modern microelectronics based on the use of special composite materials. As an example, Ru [2001] studied the critical loading for a double-walled carbon nanotube embedded in an elastic matrix. There, the nanotube is modeled as a thin elastic cylindrical shell supported by a Winkler subgrade, which accounts for the van der Waals forces. Likewise, in order to investigate the vibrations of carbon nanotubes, Liew et al. [2006] consider a plate embedded into a Pasternak elastic medium and solve the problem by means of Fourier analysis. It is found that the resonant frequencies of the system can be significantly affected by van der Waals interaction. Later, Pradhan and Kumar [2010] extended the vibration analysis to orthotropic single layered graphene sheets, taking into account scale effects by adopting Eringen nonlocal constitutive relations for the plate. These authors extend a previous work by Duan and Wang [2007] concerning the axisymmetric bending of circular plates under static loading and find that scale effects can produce a decrease of stiffness and, in turn, larger deflection of the plate.

Numerical simulations have been extensively adopted to study plate and slabs supported by or embedded in an elastic medium. As an example, Çelik and Saygun [1999] develop an iterative FE numerical method to simulate a plate on a two-parameter foundation. In that study, the soil surrounding the plate has been modeled by a finite region having amplitude comparable with the thickness of the compressible soil layer underneath the plate. Caliendo and Parisi [2010] studied the stress field in jointed concrete airport pavements under aircraft loads and thermal gradients. Through a commercial FE package, the authors carried out 3D numerical simulations wherein the pavement is modeled as a square-shaped plate bonded to an isotropic elastic half-space, thus incorporating the effect of the subgrade Young modulus on the maximum tensile stress at the interior as well as at the edge of the plate. A recent application of a FE-boundary integral equation coupling method is adopted in [Tullini et al. 2012] to investigate the interaction problem between a bar and an elastic half-plane. In this work, the Green function of the half-plane is implemented in the variational formulation.

Analytical and numerical models based on plates supported by an elastic subgrade can be readily used to simulate insulated building foundation. In fact, in order to adequately insulate the base of a building with the aim to reduce heat loss and, in turn, cut down on energy cost, an insulating layer (typically, high-compressive-strength polystyrene sheets and foams) can be placed right under the foundation concrete slab. Through this layer, moisture absorption, humidity infiltration and frost penetration phenomena are

hampered, the latter being a relevant issue in frost-susceptible soils [Bowles 1997]. The contribution of the insulating layer to the pressure distribution under the foundation is usually neglected, but it can be properly considered by adopting a two-parameter soil model.

Despite its potential and simplicity, linear elastic analysis cannot be used to predict the mechanical behavior of systems under the collapse load, when nonlinearity plays an essential role. In particular, models based on plasticity theory have been widely used to assess the load carrying capacity of mat building foundations. One of the first studies concerning the load-carrying capacity of rigid-plastic plates supported by a Winkler subgrade under a uniform static loading distribution was performed by Meyerhof [1960; 1962]. He assumed a fan-like collapse mechanism for the plate and thus he found an upper-bound for the collapse load, since the corresponding radial bending moment overcomes the yield moment of the plate. After those studies, a lot of works about this topic have appeared in the literature. By using potential functions to represent stress and displacements fields of the foundation, Gazetas [1981b] studied a transversely isotropic elastic half-space indented by a rigid-plastic plate under a uniform load distribution. He considered a conical shape of the plate after yielding, which can lift off the foundation. Sokól-Supel [1985; 1988] studied elastic-plastic Kirchhoff plates resting on an elastic subgrade. Solutions of elastic-plastic plates under different loading conditions and variously clamped at the ends may be found in the book by Save et al. [1997]. Lewandowski and Świtka [1991] solved the problem of a plate in tensionless contact with an underlying elastic-plastic Winkler subgrade obeying a bilinear constitutive law via a variational formulation. The authors solved the problem by using a FE method implemented through an iterative procedure. Kocatürk [1997] considered an elastic perfectly plastic plate in tensionless contact with an elastic-plastic Winkler foundation.

Recently, the problem of an infinite elastic-plastic plate resting on an elastic Winkler-type subgrade and uniformly loaded on a circular area has been solved by Radi and Di Maida [2014] by assuming the Johansen yield criterion for the plate [Johansen 1962] and associative flow rule. In that work, the exact ultimate bearing capacity of the system has been assessed varying the radius of the loaded region. It is also shown that the behavior of the plate is governed by a single parameter, namely the amplitude of the loaded region over the characteristic length of the plate-foundation system, and an approximate formula for the collapse load is also proposed.

Then, the study has been extended by Lanzoni et al. [2014] by considering a nonlocal behavior of the soil. In that study, a two-parameter foundation with a specific value of the Pasternak modulus has been assumed, resulting in closed-form solutions of the governing equations for the elastic-plastic regions that may occur within the plate. The analysis shows that the collapse mechanism of the plate differs from that found by Radi and Di Maida [2014], due to the nonlocal response of the Pasternak foundation.

The present work is the natural extension of the work by Lanzoni et al. [2014]. Here a general value of the Pasternak modulus is taken into account and the effects of the subgrade on the load-bearing capacity of the plate are investigated. A method based on a contour integral is adopted to solve in closed form the fourth-order linear ODE with nonconstant coefficients governing the mechanical behavior within the elastic-plastic region of the plate.

It is remarked that the plate is perfectly bonded to the elastic subgrade, thus the reactive soil pressure can be compressive as well as tensile. The study concerns the mechanical behavior of the system at the onset of plastic collapse. Nonetheless, it is worth noting that the system can sustain further increases in the external load after the plastic mechanism is achieved, owing to the presence of the elastic subgrade.

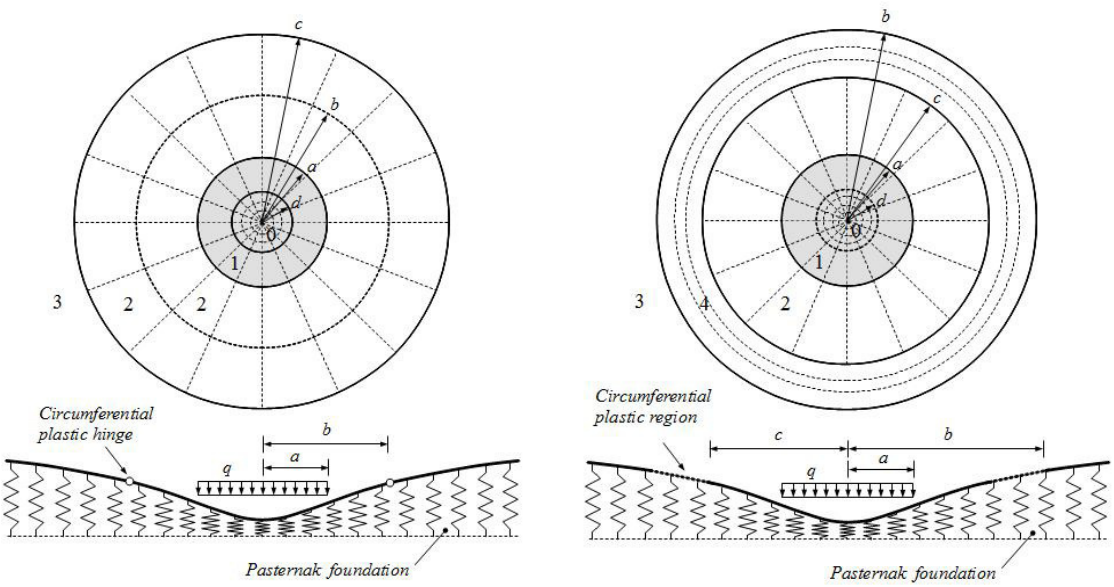

Figure 1. Sketch of the plastic mechanism for $b < c$ (left) and for $c < b$ (right). The loaded region $0 \le r \le a$ has been highlighted. (0) plastic corner region $r \le d$; (1) elastic-plastic region under load $d \le r \le a$; (2) unloaded elastic-plastic region; (3) elastic outer region; (4) annular elastic-plastic region.

The paper is organized as follows. Section 2 deals with the governing ODEs for the elastic-plastic regions that may arise within the plate. Solutions of these ODEs are found for a general value of the Pasternak subgrade modulus. The boundary conditions for each considered collapse mechanism are set in Section 3. The main results are reported in Section 4 in terms of ultimate load-bearing capacity, bending moments, shear forces, reactive soil pressure together with the size of each subregion. An experimental setup is briefly presented in Section 5. Finally, conclusions are drawn in Section 6.

2. Governing equations

In this section, the governing equations adopted in [Lanzoni et al. 2014] are briefly reviewed. The plate is subject to an external uniform pressure distribution q acting on its upper surface within a circular area of radius a and positive in the downward direction (see Figure 1). Elastic-perfectly plastic and isotropic behavior is adopted for the plate, which is assumed to obey Johansen's yield condition with associative flow rule. Due to the axisymmetrical conditions affecting the system, all variables depend on the radial coordinate r only.

The plate rests on an elastic two-parameter Pasternak foundation. Therefore, the reactive soil pressure p (positive if upwards) reads

$$p = k_1 w - k_2 \Delta w, \tag{1}$$

where k_1 and k_2 are the (positive) subgrade moduli, w represents the transversal deflection (positive if downward), and Δ is the Laplacian operator in two dimensions.

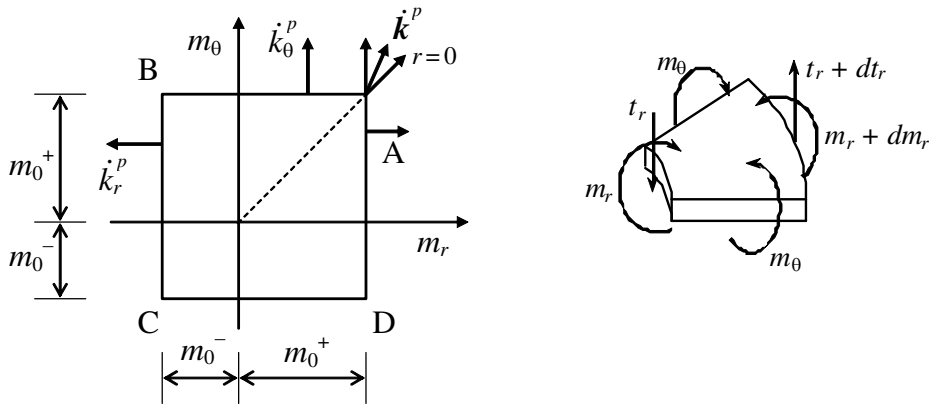

Figure 2. Left: Johansen's yield locus for elastic-plastic plates and corresponding flow rule. Right: positive bending moments and shear force per unit length.

Both in the elastic and in the elastic-plastic regions of the plate, the equilibrium conditions under axisymmetric loading conditions require

$$(rm_r)' - m_\theta + rt_r = 0, \tag{2}$$

$$(rt_r)' + r[k_1 w - k_2(w'' + w'/r) - q] = 0, \tag{3}$$

where m_r and m_θ are the bending moments per unit length, t_r is the transverse shear force per unit length, whose positive directions are shown in Figure 2, right, and prime denotes differentiation with respect to the radial coordinate r.

Johansen's square yield condition is assumed to hold for the plate (Figure 2, left), namely

$$-m_0^- \le m_r \le m_0^+, \quad -m_0^- \le m_\theta \le m_0^+, \tag{4}$$

where m_0^+ and m_0^- are the positive and negative yield moments per unit length.

Under proportional loadings, the elastic-plastic constitutive equations can be assumed in the integrated form

$$m_r = D(k_r^e + \nu k_\theta^e), \quad m_\theta = D(k_\theta^e + \nu k_r^e), \tag{5}$$

where k_r and k_θ are the components of the curvature tensor, $D = Eh^3/12(1-\nu^2)$ is the flexural rigidity of the plate, h is the plate thickness, E is the Young's modulus and ν is the Poisson's coefficient of the material. The curvature tensor can be separated into elastic and plastic contributions according to

$$k_r = k_r^e + k_r^p = -w''(r), \quad k_\theta = k_\theta^e + k_\theta^p = -w'(r)/r, \tag{6}$$

where the elastic components of the curvature tensor follow from (5) as

$$k_r^e = \frac{m_r - \nu m_\theta}{D(1-\nu^2)}, \quad k_\theta^e = \frac{m_\theta - \nu m_r}{D(1-\nu^2)}. \tag{7}$$

Following the classical Kirchhoff theory for thin plates, the rotation of the cross-sections of the plate orthogonal to the radial direction can be evaluated through the derivative of the displacement with respect

to the radial coordinate, i.e.,

$$\phi_\theta = -w'. \tag{8}$$

In the following, a dimensionless parameter ξ is introduced to make clear the role of the Pasternak stiffness parameter k_2, leading to a useful normalization of the ODEs governing the problem:

$$k_2 = \xi k_1 L^2, \tag{9}$$

where

$$L = \sqrt[4]{D(1-\nu^2)/k_1} \tag{10}$$

is a characteristic length of the plate/subgrade system. It follows that, for $\xi \to 0$, the Winkler foundation is retrieved.

As found in [Lanzoni et al. 2014], the plate at the onset of collapse may exhibits two different plastic mechanisms, characterized by different elastic-plastic regions. For the sake of clarity, the governing equation for the transversal deflection of the plate and the corresponding solutions for each plastic region are presented in the following, the numbering of the letters being presented in Figure 1.

2.1. ***Elastic-plastic region 0 lying at the corner A of the yield surface*** **($0 \le r \le d$).** Due to the axisymmetry of the problem, the conditions

$$m_r(0) = m_\theta(0), \quad k_r^p(0) = k_\theta^p(0) \tag{11}$$

are met for $r = 0$. Moreover, the condition

$$m_r(r) = m_\theta(r) = m_0^+ \quad \text{for } 0 \le r \le d \tag{12}$$

must hold within the central region of the plate lying on the corner A of the yield surface. It is worth noting that the yield locus is not smooth and the plastic flow can assume different directions at the corner of the yield surfaces. However, the condition $m_r(0) = m_\theta(0)$ holds at the center of the plate due to axisymmetry and, thus, also the plastic contributions of the curvature tensor are expected to be equal, i.e., $k_r^p(0) = k_\theta^p(0)$, according to (11). On the other hand, the condition $m_\theta(r) = m_0^+$ holds within the elastic plastic regions 1 and 2, namely for $d < r < b$, together with the normality law for the plastic flow $k_\theta^p(r) > 0$ and $k_r^p(r) = 0$, so that the flow of the plastic curvature is aligned with the outward normal to the boundary AB of the yield domain, according to the Johansen associative yield criterion, as shown in Figure 2, left. Thus, within the fully plasticized region (region 0), the plastic flow must lie arbitrarily in the cone delimited by the bisector (OA direction) and the outward normal to the boundary AB of the strength domain.

This assumption leads to the fulfillment of the maximum dissipation postulate also at the corner A of the yield domain [Salençon 2013, Chapter 11.3.2]. In particular, the plastic curvature $k_\theta^p(r)$ is assumed to vary continuously with r from the center of the plate ($r = 0$) where $k_\theta^p(0) = k_r^p(0)$ to the outer border of the region 0 ($r = d^-$) where $k_\theta^p(d^-) = k_\theta^p(d^+)$, so that the circumferential component of the plastic curvature tensor is continuous between the regions 0 and 1. As discussed in [Lanzoni et al. 2014], continuity of this component also implies continuity of the rotation ϕ_θ between the regions 0 and 1 at $r = d$, according to relation $(6)_2$, since the elastic component of the curvature is continuous due to the continuity of the bending moments.

The yield condition (12) and the balance equation (2) imply the vanishing of the transverse shear force within the inner elastic-plastic region 0, i.e.,

$$t_r(r) = 0 \quad \text{for } 0 \le r \le d, \tag{13}$$

and, thus, the load is entirely supported by the subgrade therein.

By using relations (9) and (13), the general expression for the transversal deflection of the plate within the elastic-plastic region 0 can be found from the balance condition (3) in the form

$$w_0(r) = (m_0^+ L^2/D)\big[\chi + a_0 I_0\big(r/\sqrt{\xi}L\big)\big], \tag{14}$$

where I_0 is the modified Bessel function of first kind of order zero, a_0 is an arbitrary constant and

$$\chi = qD/(k_1 m_0^+ L^2) \tag{15}$$

is a dimensionless parameter proportional to the intensity q of the external load distribution.

2.2. ***Elastic-plastic regions 1 and 2 lying on the side AB of the yield surface*** **($d \le r \le c$).** On the side AB of the yield locus (Figure 2, left) the bending moment m_θ attains its positive limit value m_0^+, namely

$$m_\theta(r) = m_0^+ \quad \text{for } d \le r \le c, \tag{16}$$

and thus positive radial yield lines occur within the corresponding elastic-plastic region of the plate, which can be split into the inner loaded region 1 and the outer unloaded region 2, as sketched in Figure 1. According to the associative flow rule, the plastic curvature components for the side AB of the yield locus are given by

$$k_r^p = 0, \quad k_\theta^p \ge 0. \tag{17}$$

Therefore, by using (16) and $(17)_1$, equations $(6)_1$, $(7)_1$ and (2) yield the following expressions for the bending moment m_r and the transverse shear force t_r per unit length in the elastic-plastic regions 1 and 2:

$$m_r = \nu m_0^+ - D(1-\nu^2)w'', \tag{18}$$

$$t_r = \frac{1-\nu}{r}[m_0^+ + D(1+\nu)(w'' + rw''')]. \tag{19}$$

Introduction of (19) in the balance equation (3) then provides the governing ODE for these regions:

$$rw'''' + 2w''' - \frac{\xi}{L^2}w''r - \frac{\xi}{L^2}w' + \frac{1}{L^4}wr - \frac{q}{k_1 L^4}r = 0. \tag{20}$$

The general solution of the fourth-order linear ODE (19) has been found in closed form by Lanzoni et al. [2014] only for the special case $\xi = 2$.

Different methods can be used to solve the ODE (20). For example, the solution can be obtained numerically, or by using the method of Frobenius, i.e., by seeking the unknown function w as a power series of r and solving the corresponding indicial equation. Here, we use a contour integration instead (see for example [Ince 1944]). Assume that $w(r)$ has the form

$$w(r) = \int_C S(p)e^{pr/L}\,dp, \tag{21}$$

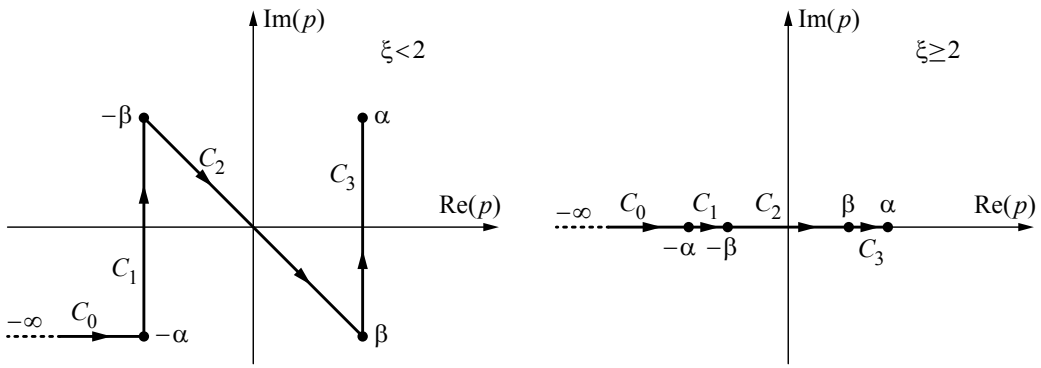

Figure 3. Path of integration in the complex domain for complex conjugate roots (left) and real roots (right).

where $S(p)$ is an unknown function of the complex variable p and C a contour to be defined later. Therefore, introduction of the representation (21) in (20) and taking $q = 0$ gives

$$\frac{r}{L}\int_C (p^4 - \xi p^2 + 1)S(p)e^{pr/L}\,dp + \int_C (2p^3 - \xi p)S(p)e^{pr/L}\,dp = 0. \tag{22}$$

Integration by parts of the first integral in (22) then yields

$$\int_C (2p^3 - \xi p)S(p)e^{pr/L}\,dp + \int_C (p^4 - \xi p^2 + 1)S'(p)e^{pr/L}\,dp - (p^4 - \xi p^2 + 1)S(p)e^{pr/L}\Big|_{p_i}^{p_f} = 0, \tag{23}$$

where prime denotes differentiation with respect to the function argument p. If the contour C is chosen in such a way that the last term vanishes, then the function $S(p)$ must satisfy the ODE

$$(2p^3 - \xi p)S(p) + (p^4 - \xi p^2 + 1)S'(p) = 0, \tag{24}$$

namely,

$$\frac{S'(p)}{S(p)} = -\frac{(2p^3 - \xi p)}{(p^4 - \xi p^2 + 1)}. \tag{25}$$

Integration of (25) gives the general expression of the function $S(p)$ as

$$S(p) = A(p^4 - \xi p^2 + 1)^{-1/2}, \tag{26}$$

where A is an arbitrary constant.

The contour C must be chosen in order to satisfy the condition

$$(p^4 - \xi p^2 + 1)e^{pr/L}\Big|_{p_i}^{p_f} = 0. \tag{27}$$

The latter condition is satisfied for $p = \pm\alpha, \pm\beta$, and for $p \to -\infty$, where

$$\alpha = \sqrt{\xi/2 + \sqrt{\xi^2/4 - 1}}, \quad \beta = \sqrt{\xi/2 - \sqrt{\xi^2/4 - 1}}, \tag{28}$$

and the contour C can be defined as sketched in Figure 3 for complex and real values of the variable p, respectively, in order to obtain four independent solutions of (20) in the form given by (21). Namely, the contours C_k $(k = 1, 2, 3)$ are chosen to coincide with the three straight paths joining the points

$-\alpha, -\beta, \beta, \alpha$ of the complex plane, respectively, and the fourth path is defined by $C_0 = \{x - i\,\mathrm{Im}(\alpha) \mid -\infty \le x \le -\mathrm{Re}(\alpha)\}$. Note that the roots (28) are real for $\xi \ge 2$, whereas they become complex conjugates for $\xi \le 2$ (see Figure 3). Therefore, the function $w(r)$ can be assumed in the form

$$w_1(r) = \frac{m_0^+ L^3}{D}\left[\frac{\chi}{L} + \sum_{k=0}^{3} b_k \int_{C_k} \frac{e^{pr/L}}{\sqrt{p+\alpha}\sqrt{p+\beta}\sqrt{p-\alpha}\sqrt{p-\beta}}\,dp\right] \quad \text{for } d \le r \le a. \tag{29}$$

Equation (29) defines the displacement field within the annular loaded region, whereas the displacement field within the elastic-plastic annular region not directly loaded (namely for $q = 0$) is given by

$$w_2(r) = \frac{m_0^+ L^3}{D} \sum_{k=0}^{3} c_k \int_{C_k} \frac{e^{pr/L}}{\sqrt{p+\alpha}\sqrt{p+\beta}\sqrt{p-\alpha}\sqrt{p-\beta}}\,dp \quad \text{for } a \le r \le c. \tag{30}$$

2.3. ***Elastic-plastic region 4 lying on the side BC of the yield surface*** **($c \le r \le b$).** On the side BC of the yield locus (Figure 2, left) the bending moment m_r attains its negative limit value, namely

$$m_r(r) = -m_0^- \quad \text{for } c \le r \le b, \tag{31}$$

according to the associative flow rule, and thus negative circumferential yield lines occur within the corresponding elastic-plastic region 4 in Figure 1, right, where $c \le r \le b$. The plastic curvature components are given by the associative flow rule for the side BC of the yield locus, namely,

$$k_r^p \le 0, \quad k_\theta^p = 0. \tag{32}$$

Therefore, from $(6)_2$, $(7)_2$ and $(32)_2$ the bending moment per unit length m_θ in the present elastic-plastic region reads

$$m_\theta = -\nu m_0^- - D(1-\nu^2)w'/r. \tag{33}$$

Then, from (2) and (33) the transverse shear force per unit length follows as

$$t_r = \frac{1-\nu}{r}[m_0^- - D(1+\nu)w'/r]. \tag{34}$$

Substitution of (34) in the balance equation (3), also using (9), then yields the governing equation in terms of displacement for the elastic-plastic region 4 as

$$\left(1+\xi\frac{r^2}{L^2}\right)w'' - \left(1-\xi\frac{r^2}{L^2}\right)\frac{w'}{r} - \frac{r^2}{L^4}w = 0. \tag{35}$$

The general solution of the fourth-order linear ODE (35) in closed form is

$$w_4(r) = \frac{m_0^+ L^2}{D}\sqrt{2/\xi}\left[a_1 I_0\left((1/\xi)\sqrt{1+\xi r^2/L^2}\right) + a_2 K_0\left((1/\xi)\sqrt{1+\xi r^2/L^2}\right)\right], \tag{36}$$

where K_0 is the modified Bessel function of the second kind of order zero [Abramowitz and Stegun 1972], and a_1 and a_2 are arbitrary constants.

2.4. ***Elastic region 3.*** The governing differential equation in terms of the transversal displacement $w(r)$ for the elastic region 3 of the plate under symmetrical bending reads

$$w'''' + \frac{2}{r}w''' - \frac{1}{r^2}w'' + \frac{1}{r^3}w' - a\left(w'' + \frac{1}{r}w'\right) + \frac{1-\nu^2}{L^4}w = 0, \tag{37}$$

where $a = k_2/D = \xi(1-\nu^2)/L^2$. It can be shown that, if $\eta = aL^2/(2\sqrt{1-\nu^2}) \le 1$, the general solution of the ODE (37) as r becomes very large reads [Selvadurai 1979]

$$w_3(r) = \frac{m_0^+ L^2}{D}\left\{d_1 \mathrm{Re}[H_0^{(1)}(\beta r/L)] + d_2 \mathrm{Im}[H_0^{(1)}(\beta r/L)]\right\} \quad \text{for } r \ge c, \tag{38}$$

where $H_0^{(1)}$ is the Hankel function of the first kind [Abramowitz and Stegun 1972], d_1 and d_2 are dimensionless real constants and

$$\beta = \mathrm{i}\sqrt[4]{1-\nu^2}\left(\sqrt{\eta + \sqrt{\eta^2 - 1}}\right). \tag{39}$$

The general solution of the ODE (37) for $\eta > 1$ reads

$$w_3(r) = \frac{m_0^+ L^2}{D}\left\{d_1 \mathrm{Re}[Y_0(\mathrm{i}\beta_1 r/L)] + d_2 \mathrm{Re}[Y_0(\mathrm{i}\beta_2 r/L)]\right\} \quad \text{for } r \ge c, \tag{40}$$

where

$$\beta_1 = \sqrt[4]{1-\nu^2}\left(\sqrt{\eta + \sqrt{\eta^2 - 1}}\right), \quad \beta_2 = \sqrt[4]{1-\nu^2}\left(\sqrt{\eta - \sqrt{\eta^2 - 1}}\right). \tag{41}$$

It is worth noting that, for $\xi = 2/\sqrt{1-\nu^2}$, the solution of the elastic region reported in [Lanzoni et al. 2014] is retrieved from (38).

The relationship between the curvature components and the bending moments per unit length is given by [Timoshenko and Woinowsky-Krieger 1959]

$$m_r = -D(w_3'' + (\nu/r)w_3'), \quad m_\theta = -D(w_3'/r + \nu w_3''), \tag{42}$$

whereas the expression of the shear force t_r per unit length reads

$$t_r = D(w_3''' + w_3''/r - w_3'/r^2). \tag{43}$$

3. Boundary conditions

The dimensionless constants a_0, d_1, d_2, b_0, b_1, b_2, b_3, c_0, c_1, c_2, c_3, a_1 and a_2 appearing in the expressions for the displacement in the different regions considered in Section 2 can be evaluated by imposing proper continuity conditions for the displacement w, rotation ϕ_θ, bending moment m_r and shear force t_r per unit length across the boundaries between the regions at $r = a$, c and d, together with the fulfillment of the yield condition at the inner boundary of the elastic region and the conditions about the occurrence of a plastic mechanism in the plate at the onset of collapse.

As discussed in [Lanzoni et al. 2014], two different plastic mechanisms may occur in the plate at the onset of collapse, depending on the amplitude a/L of the loaded region. Continuity of displacement w, rotation ϕ_θ, bending moment m_r and shear force t_r across the boundary at $r = d$ and $r = a$ must be

imposed for both plastic mechanisms as

$$w_0(d) = w_1(d), \quad w_0'(d) = w_1'(d), \quad D(1+\nu)w_1''(d) = -m_0^+, \quad w_1'''(d) = 0, \tag{44}$$

$$w_1(a) = w_2(a), \quad w_1'(a) = w_2'(a), \quad w_1''(a) = w_2''(a), \quad w_1'''(a) = w_2'''(a), \tag{45}$$

where expressions (8), (18) and (19) have been used. One kind of plastic mechanism takes place with $b < c$ (see Figure 1, left). In this case, continuity across the boundaries at $r = c$ requires the further four conditions

$$\begin{gathered} w_2(c) = w_3(c), \quad w_2'(c) = w_3'(c), \\ \frac{\nu m_0^+}{D} - (1-\nu^2)w_2''(c) = -w_3''(c) - \frac{\nu}{c}w_3'(c), \\ (1-\nu)\frac{m_0^+}{D} + (1-\nu^2)[w_2''(c) + cw_2'''(c)] = cw_3'''(c) + w_3''(c) - \frac{1}{c}w_3'(c), \end{gathered} \tag{46}$$

where (8), (18), (19), $(42)_1$ and (43) have been used. Making use of $(42)_2$, accomplishment of the yield condition as r approaches c from the outer elastic region requires

$$\nu w_3''(c) + \frac{1}{c}w_3'(c) = -\frac{m_0^+}{D}. \tag{47}$$

Moreover, the negative circumferential yield line must take place within the elastic-plastic region, i.e., at $r = b$, where $d \le b \le c$. In this case, the onset of collapse occurs when the bending moment m_r within the elastic-plastic region attains a minimum value equal to the ultimate negative bending moment right at $r = b$, i.e.,

$$D(1-\nu^2)w_2''(b) = (\nu+\mu)m_0^+, \quad w_2'''(b) = 0, \tag{48}$$

for $b \le c$, where

$$\mu = m_0^-/m_0^+ \tag{49}$$

is the ratio between negative and positive yield moments.

Conditions (44)–(48) yield a system of 15 equations, which are linear in the 12 constants a_0, b_0, b_1, b_2, b_3, c_0, c_1, c_2, c_3, d_1, d_2 and χ. Once 12 such quantities are found in terms of the radii b, c and d, the last three equations can be solved numerically in order to obtain the remaining unknowns b, c and d. Finally, the collapse load P of the plate follows from (15) as

$$P = \pi a^2 \chi k_1 m_0^+ L^2/D. \tag{50}$$

The other possible scenario of plastic collapse occurs for $b > c$, namely when the negative circumferential yield line first appears within the elastic region (see Figure 1, right). In this case, the collapse load can be found by imposing the continuity conditions between the inner elastic-plastic region 2 and the annular elastic-plastic region 4 at $r = c$, where

$$\begin{gathered} w_2(c) = w_4(c), \quad w_2'(c) = w_4'(c), \\ D(1-\nu^2)w_2''(c) = m_0^- + \nu m_0^+, \\ D(1-\nu^2)\left[cw_2'''(c) + \frac{1}{c}w_4'(c)\right] + (m_0^+ + \nu m_0^-) = 0, \end{gathered} \tag{51}$$

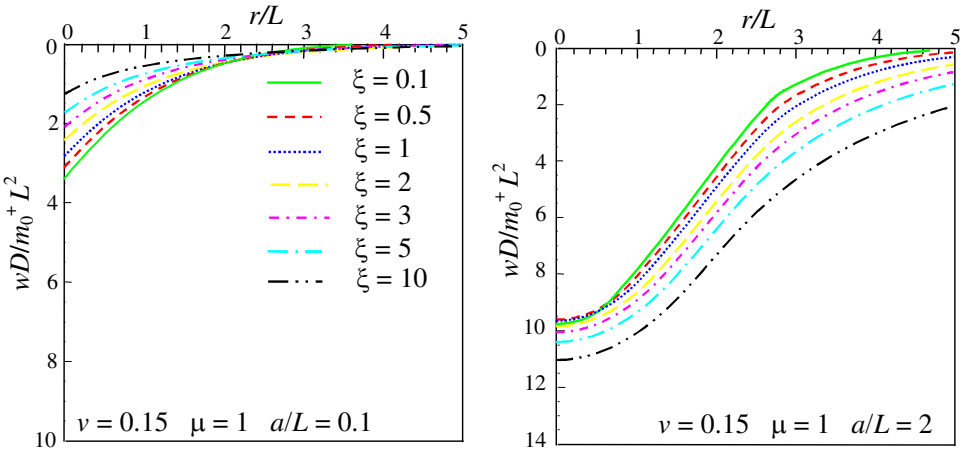

Figure 4. Radial variation of the dimensionless plate deflection for $\mu = 1$, varying the parameter ξ of the soil, for $a/L = 0.1$ (left) and $a/L = 2$ (right).

as well as between the annular elastic-plastic region 4 and the outer elastic region 3 at $r = b$, where

$$\begin{gathered} w_3(b) = w_4(b), \quad w_3'(b) = w_4'(b), \\ D\Big[w_3''(b) + \frac{\nu}{b} w_3'(b)\Big] = m_0^-, \\ D\Big[w_3'''(b) + \frac{1}{b} w_3''(b) - \frac{1}{b^2} w_3'(b)\Big] = \frac{1-\nu}{b}\Big[m_0^- - \frac{1}{b} D(1+\nu) w_4'(b)\Big]. \end{gathered} \tag{52}$$

By using $(52)_2$, $(42)_2$ and (33), Equation $(52)_3$ implies continuity of the bending moment m_θ (and vice versa) across the boundary at $r = b$. Condition $(52)_4$ also implies the stationarity of the bending moment m_r within the elastic region at $r = b$.

Continuity of the bending moment m_θ across the boundary at $r = c$ must be imposed by using (33), thus giving

$$m_0^+ + \nu m_0^- + D(1-\nu^2)\frac{w_4'(c)}{c} = 0. \tag{53}$$

The substitution of the functions $w_k(r)$ $(k = 0, 1, 2, 3, 4)$ introduced in Section 2 and their derivatives in conditions (44), (45), (51), (52) and (53) yield a system of 17 equations, which are linear in the 14 constants a_0, a_1, a_2, b_0, b_1, b_2, b_3, c_0, c_1, c_2, c_3, d_1, d_2 and χ. Once such constants are found in terms of the radii b, c and d, the numerical solution of the last three equations provides the values of b, c and d. Finally, the collapse load P of the plate can be calculated by using (50).

4. Results

In the following, the radial variation of transverse displacement, slope, bending moments, shear force and reactive soil pressure at the onset of plastic collapse are reported and discussed. For the sake of definiteness, we assumed $\nu = 0.15$. The radial variation of the transverse deflection of the plate $wD/m_0^+L^2$ for different values of the subgrade parameter ξ has been reported in Figure 4 for $a/L = 0.1$ and 2. Note that, if the Winkler modulus k_1 and the flexural rigidity of the plate D are kept constant, the variation of

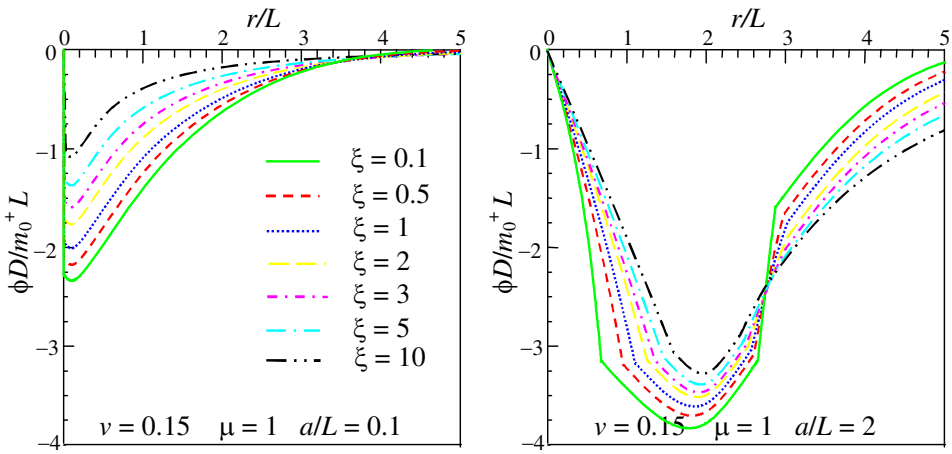

Figure 5. Radial variation of the dimensionless rotation of the plate cross-section for $\mu = 1$, varying the parameter ξ of the soil, for $a/L = 0.1$ (left) and $a/L = 2$ (right).

the parameter coincides with the variation of the Pasternak modulus k_2, where $\xi = k_2/(k_1 L^2)$, according to (9) and (10). As shown in Figure 4, left, for small sizes of the loaded region, the plate deflection under the loaded region monotonically decreases as ξ increases, whereas an opposite trend is observed for large sizes of the loaded region, as depicted in Figure 4, right. This effect is due to the fact that the reaction of the Pasternak foundation also depends on the first and second derivatives of the transverse deflection. In particular, the variation of the slope and, in turn, the second derivative of the displacement, assumes negative values in the inner region of the plate, and decreases going outward from the loaded region, as shown in Figure 5. Thus, in the inner region of the plate, the reactive soil pressure is compressive and very high for small sizes of the loaded region (see also Figure 9). Moreover, for large sizes of the loaded region, the slope displays a rapid variation out of the loaded area (from Figure 5, right, plotted for $a/L = 2$, it occurs approximately for $r/L = 3$). It follows that, in the neighborhood of this region, the second derivative becomes positive and, thus, the soil reaction tends to become tensile due to the second term in (1). Consequently, as the parameters k_2 and ξ increase while keeping constant the Winkler modulus k_1, the soil reaction becomes tensile out of the loaded region for large values of a/L, thus producing an increase in the transverse deflection of the plate, as shown in Figure 4, right. This effect does not occur for small values of a/L. In this case, an increase in the parameter ξ corresponds to a decrease of the displacement of the system, as revealed by Figure 4, left.

The radial variation of the slope ϕ_θ is shown in Figure 5 for $a/L = 0.1, 2$. The magnitude of the slope decreases under the loaded region as the Pasternak modulus k_2 and the parameter ξ become larger, whereas an opposite trend is observed out of the loaded region for large sizes of the loaded region (Figure 5, right). Note also that the function $\phi_\theta(r)$ is continuous, as required by the boundary conditions, but not monotonic, since its magnitude exhibits a maximum near the border of the loaded region.

The radial variations of bending moments $m_r(r)$ and $m_\theta(r)$ along the radial direction are plotted in dimensionless form in Figures 6 and 7 for different values of the parameter ξ. As shown in Figure 7, the circumferential bending moment $m_\theta(r)$ attains the positive yield limit m_0^+ within a circular region whose radius c increases with the size a of the loaded region and decreases as the parameter ξ becomes larger. Radial yield lines occur within this region.

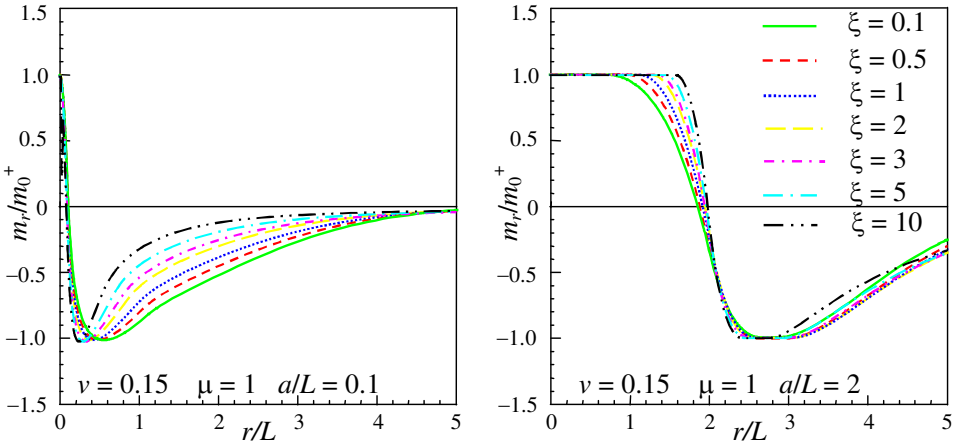

Figure 6. Radial variation of the dimensionless radial bending moment for $\mu = 1$, varying the parameter ξ of the soil, for $a/L = 0.1$ (left) and $a/L = 2$ (right).

For small sizes of the loaded area, the radial bending moment $m_r(r)$ displays a positive peak just at the center of the loaded area where the positive yield moment m_0^+ is attained (Figure 6, left) and then decreases outwards till the negative yield moment m_0^- is reached at $r = b$, where a negative circumferential yield line develops within region 2 and triggers the collapse mechanism within the plate. It is worth noting that the radius b of the negative circumferential yield line becomes smaller as the parameter ξ increases (Figure 6, left). For large sizes of the loaded area a, a circular region where both radial and circumferential bending moments attain the positive yield limit appears and extends outwards (Figure 6, right) as the size of the loaded region is increased. Both radial and circumferential yield lines take place within this region 0 of radius d. The amplitude of this fully yielded region at the onset of collapse increases with ξ, as shown in Figure 6, right. Out of this region, the radial bending moment $m_r(r)$ decreases and becomes negative. The negative yield moment m_0^- is then reached within an annular

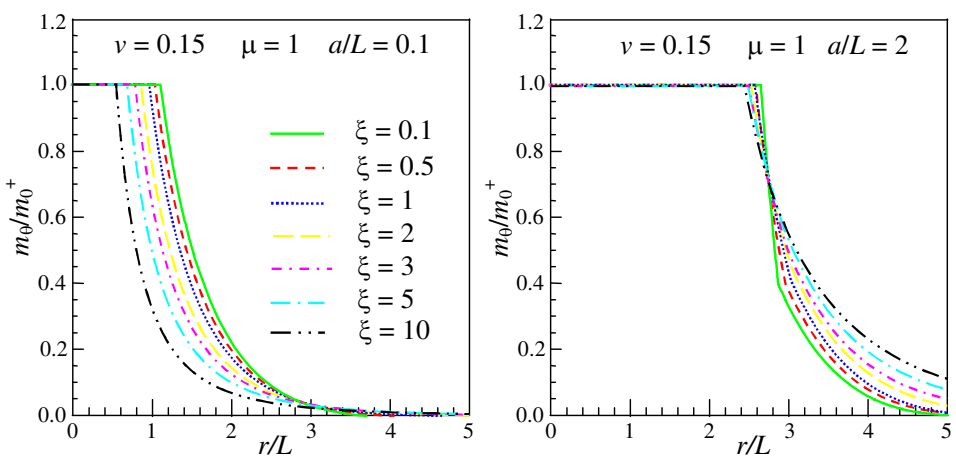

Figure 7. Radial variation of the dimensionless circumferential bending moment for $\mu = 1$, varying the parameter ξ of the soil, for $a/L = 0.1$ (left) and $a/L = 2$ (right).

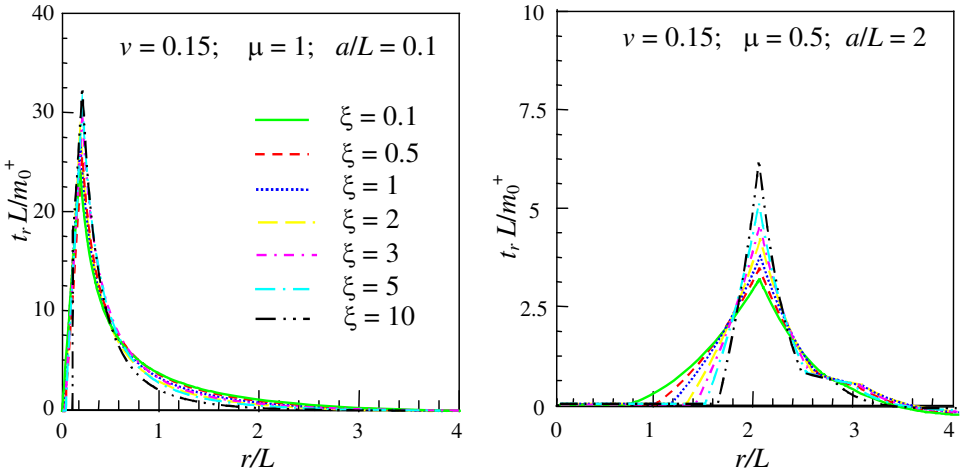

Figure 8. Radial variation of the dimensionless shear force for $\mu = 1$, varying the parameter ξ of the soil, for $a/L = 0.1$ (left) and $a/L = 2$ (right).

region, whose width increases with the load until it joins together with the inner radially yielded region, thus creating a plastic mechanism within the plate.

The bending moments within the outer elastic region decrease until they vanish at a large distance from the loaded area. For small sizes of the loaded area, the rate of decrease is faster for large values of the Pasternak modulus, i.e., of the parameter ξ, whereas for large sizes of the loaded area an opposite trend is observed.

The radial variations of shear force are plotted in Figure 8 in dimensionless form. These variations show a peak near the border of the loaded area, whose magnitude increases with the Pasternak modulus k_2. This behavior is expected since a stiffer foundation requires a larger applied load in order to achieve a plastic mechanism, thus producing an increase in the maximum shear force.

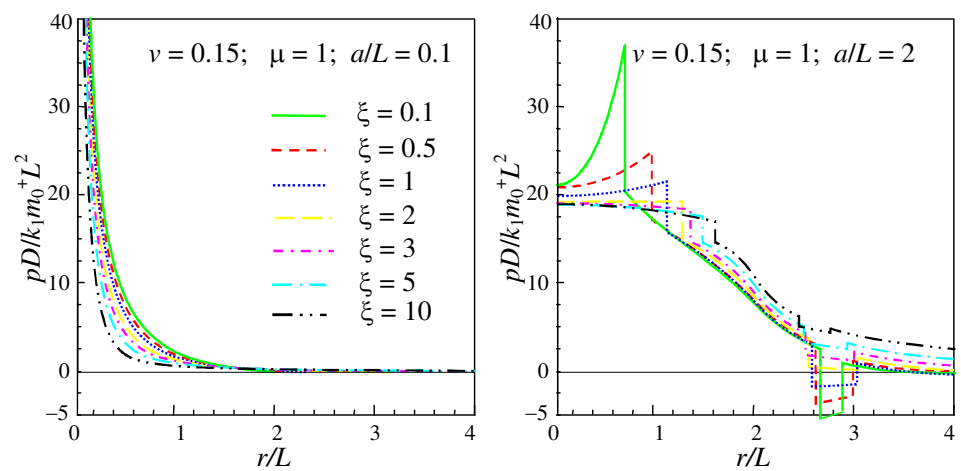

Figure 9. Radial variation of the dimensionless reacting soil pressure for $\mu = 1$, varying the parameter ξ of the soil, for $a/L = 0.1$ (left) and $a/L = 2$ (right).

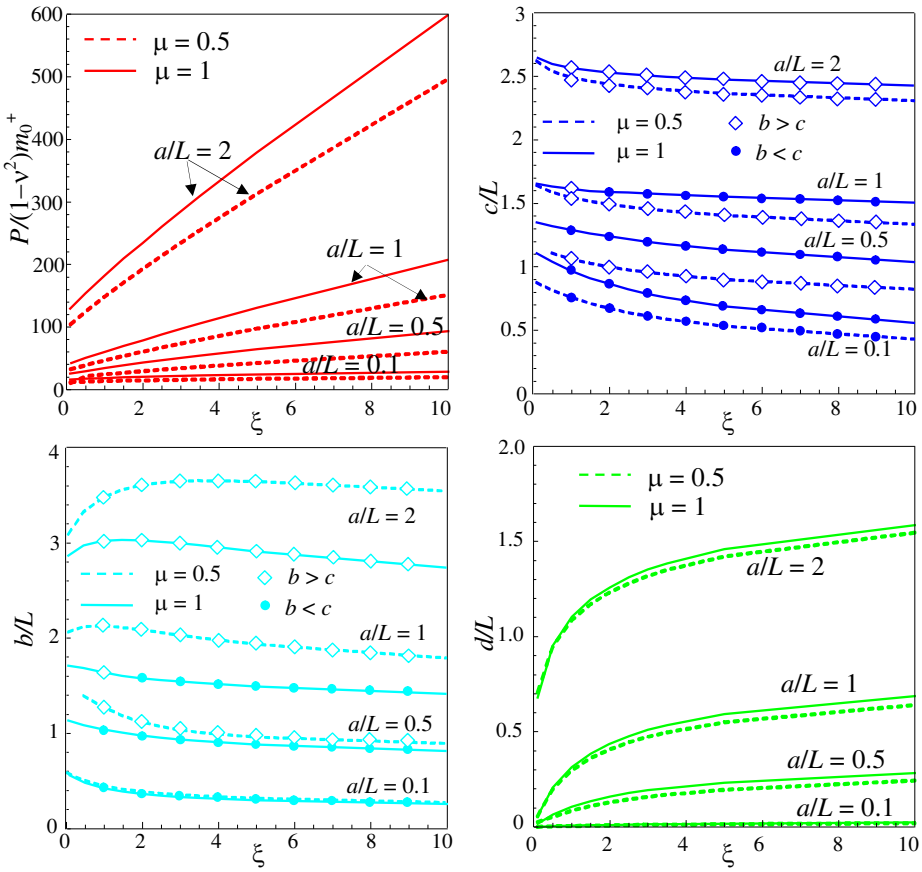

Figure 10. Top left: dimensionless ultimate load and dimensionless loci. Top right: x/L. Bottom left: y/L. Bottom right: d/L versus the parameter ξ of the soil for different values of the amplitude a of the loaded region, for $\mu = 0.5, 1$.

An interesting trend is observed for the curves of the reacting pressure, depicted in Figure 9. As the Pasternak modulus increases, the reactive soil pressure increases under the loaded region and decreases outside that region. In particular, Figure 9, right, highlights an increase of the peak of the soil pressure near the edge of region 0 for low values of the parameter ξ. This is due to the fact that the reacting pressure of the Pasternak soil depends on the Laplacian of the transverse deflection, namely on the slope and curvature. The latter exhibits a rapid variation at the border of region 0, as proved by the corner in the curves of Figure 5, right, and by the drop of the bending moment m_r from m_0^+ to m_0^- shown in Figure 6, right.

Figure 10, top left, displays the dimensionless ultimate load versus ξ for some values of the amplitude a/L of the loaded region, both for $\mu = 1$ and 0.5. As expected, the ultimate carrying capacity of the system increases with the soil stiffness for every value of the ratio a/L, as confirmed by the monotonic trend of the curves plotted in Figure 10, top left. If the parameters m_0^+, a/L and ξ are kept constant, the collapse load obviously decreases as μ decreases and thus m_0^- is reduced. Indeed, a decrease in μ implies a reduction of the negative yield moment m_0^-, thus allowing the activation of the collapse

mechanism at a lower level of the external load. The variations of the ratios c/L, b/L and d/L versus ξ are plotted in Figure 10 (top right, bottom left, bottom right, respectively). In particular, the dimensionless radius c/L monotonically decreases as the stiffness parameter ξ increases, whereas the variation of the radius $b/L$with ξ is not monotonic, as shown in Figure 10, top right and bottom left. These figures show also that the border of the elastic-plastic region (i.e., the radius c or b of the plastic mechanism for $b < c$ or $c < b$, respectively) displays a nonmonotonic trend for large values of a/L, whereas for moderate values of a/L the amplitude of the elastic-plastic zone monotonically decreases as the parameter ξ increases. Note that, for $a/L = 1$, the collapse mechanism for $b > c$ takes place for small values of the parameter ξ (approximately, until $\xi \leq 1.5$). Increasing ξ, the collapse mechanism occurs for $c > b$. The parameter μ significantly affects the size of the elastic-plastic region, mainly for large sizes of the loaded region, as shown by Figure 10, bottom left. Moreover, if the parameter ξ is kept constant, an increase in the parameter μ produces a decrease (increase) of the size of the elastic-plastic region for large (small) values of the amplitude of the loaded region a/L. From Figure 10, bottom right, it can be recognized that the radius d increases monotonically with ξ. Note that the influence of the parameter μ on c and d is lower than that found for radius b.

Finally, the variation of the ultimate load and ratios c/L, b/L, d/L versus μ are plotted in Figure 11 for $a/L = 0.5$ and for some values of the parameter μ. Figure 11, top left, shows that the ultimate load increases monotonically both with ξ and μ, as expected from an increase in the soil stiffness and negative yield moment. Figure 10, top right, shows that the radius c of the circumferential yield line becomes smaller as μ becomes vanishing small, and its variation with the parameter μ is monotonic. Conversely, the radius b of the circumferential yield line monotonically decreases as μ increases (Figure 11, bottom left). Moreover, the analysis shows that there exists a specific value of μ that minimizes the amplitude of the elastic-plastic region of the plate depending on the value of ξ. For $a/L = 0.5$, this occurs for values of $\mu \leq 1$ regardless of the value of the soil stiffness ξ. However, the influence of the parameter ξ on the radii c and b is limited. As expected, the amplitude d of the fully yielded region 0 increases both with μ and ξ, as confirmed by Figure 11, bottom right.

5. Experiments and possible applications

The model proposed here can be reliably used to predict the mechanical behavior of ductile elements (e.g., FRC slabs, metallic sheets, etc.) bonded to an elastic support under axisymmetric load distributions. For an example, it may be used to assess the failure mechanism of plastic or rubbery sheets covered by metallic thin films. This kind of composites finds important applications for many industrial purposes. For instance, plastic sheets coated by an aluminium film are widely used in the pharmaceutical, food and cosmetic industries to achieve hygienic packaging.

For example, Figure 12 shows a ductile polycarbonate sheet supported by a 6 mm thick sheet of rubber and coated by an Al thin film. The polycarbonate sheet is 5 mm thick, whereas the Al film thickness equals 50 μm. A load distribution has been imparted to the sample by means of a hydraulic cylinder mounted into a suitable metallic frame. The Al film allows the identification of the occurrence of the yield lines. Indeed, in the neighboring of the negative circumferential yield line, a detachment of the Al film occurs, thus producing small wrinkles, as shown in Figure 12, top right. In the proximity of positive radial yield lines, radial cracks within the Al film can also be detected (see Figure 13). These findings thus confirm the plastic mechanisms investigated in the present work.

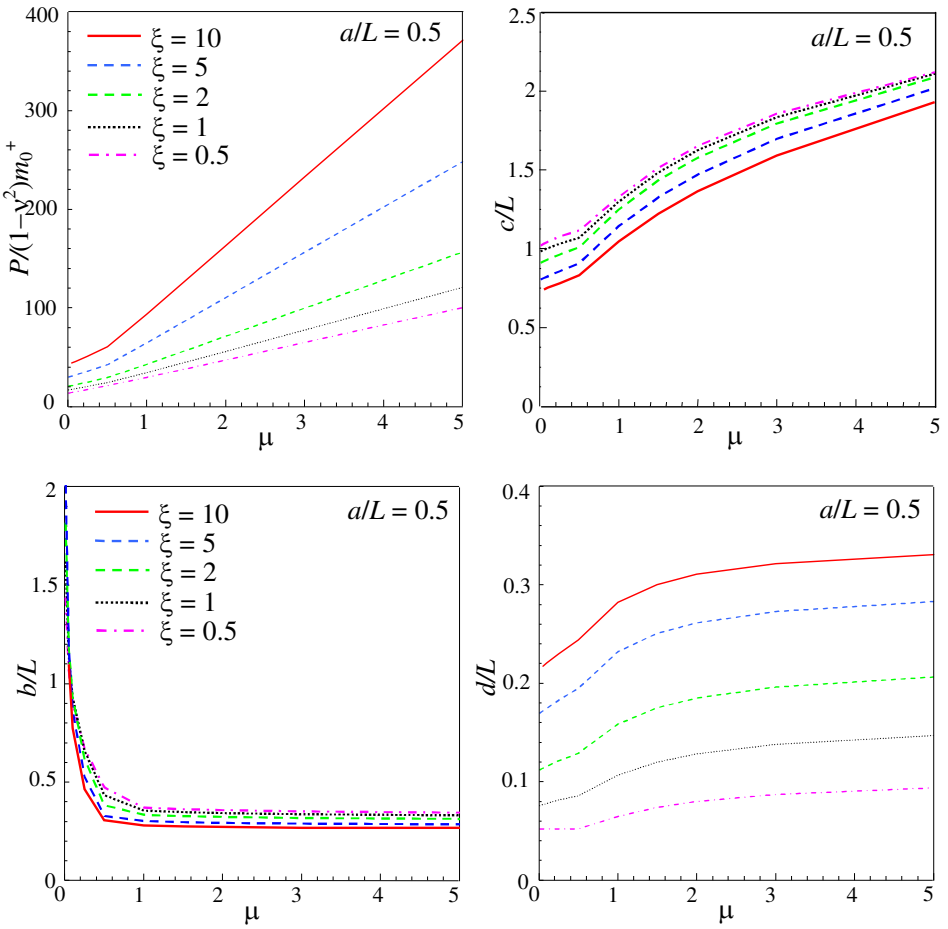

Figure 11. Top left: dimensionless ultimate load and dimensionless loci. Top right: x/L. Bottom left: y/L. Bottom right: d/L versus the parameter μ for different values of the amplitude a of the loaded region, for $\alpha = 0.5$.

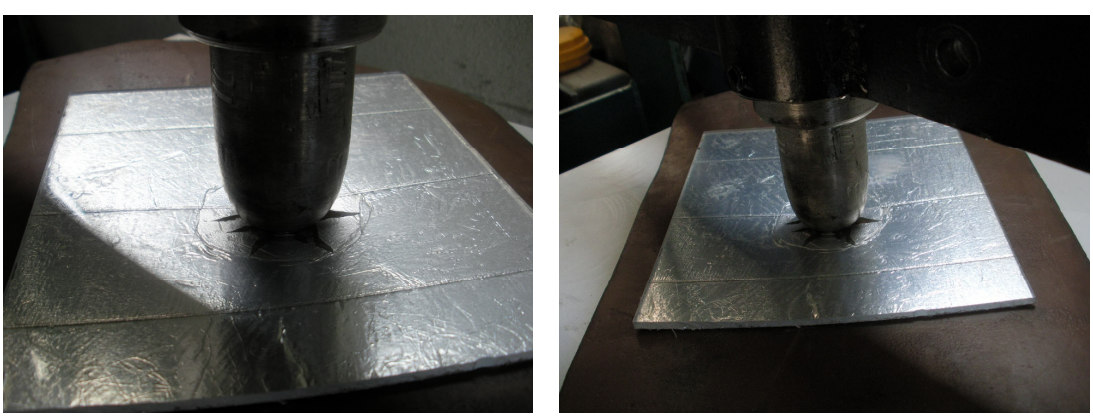

Figure 12. Load test on a polycarbonate sheet supported by an elastic support.

Figure 13. Circumferential and radial yield lines in the polycarbonate sheet.

6. Conclusions

In this paper, the analysis of an infinite elastic-plastic Kirchhoff plate supported by an elastic two-parameter subgrade has been performed for an arbitrary value of the Pasternak modulus. The elastic-plastic behavior of the plate is assumed to follow Johansen's yield criterion with associative flow rule. A bilateral contact between the paper and the underlying subgrade is assumed, leading to reactive soil pressure which can be compressive as well as tensile.

The analysis shows that the Pasternak modulus k_2 significantly affects through ξ both the load-carrying capacity of the plate and the size of the elastic-plastic regions at the onset of collapse. However, the effects induced by a variation in the Pasternak modulus are different for small or large amplitudes of the loaded region. For instance, the load-carrying capacity significantly increases as the Pasternak modulus k_2 increases for large sizes a/L of the loaded region, whereas the increase in the load-carrying capacity is rather moderate for small values of a/L. Furthermore, an increase in the stiffness of the subgrade in terms of the Pasternak modulus produces a monotonic decrease of the elastic-plastic region of the plate if the loaded region is small, whereas this trend is not monotonic for large amplitudes of the loaded region.

The size of the loaded region a/L affects the mechanical response of the system also. For large values of the parameter a/L, an increase in the stiffness parameter ξ produces indeed an increase of the transverse deflection of the plate; conversely, for moderate values of the parameter a/L, an increase of the parameter ξ generates a decrease of the transverse plate deflection. Furthermore, keeping the stiffness of the foundation (i.e., both moduli k_1 and k_2) constant, as the size of the load region a/L increases, the load-carrying capacity of the system increases, as does the amplitude of the elastic-plastic region of the plate.

The effects produced by the ratio μ between negative and positive yield moments have been investigated also. It is found that, as μ increases, the load-carrying capacity and the radius d of the fully yielded region 0 monotonically increase. It is worth noting that the parameter μ has a pronounced influence on the load-carrying capacity and amplitude of the annular elastic-plastic regions, but it has almost no effect on the amplitude of the fully plastic inner region 0 of the plate.

As suggested in Section 5, the model can be applied to assess the mechanical behavior of a plate-like element supported by an elastic medium, providing a prediction of both the load-carrying capacity and plastic mechanism taking place in the elastic-plastic plate.

With the aim of investigating the dynamic behavior of elastic-plastic plates supported by a nonlocal ground, the proposed model can be extended by taking into account also the inertial terms in the equilibrium equations, as in the recent study concerning the dynamical behavior of beams on elastic foundations performed by Piccolroaz and Movchan [2014].

Acknowledgements

Financial support from "Fondazione Cassa di Risparmio di Modena" within the project "Bando di Ricerca Applicata 2013/2014 — fibra di carbonio e resina IPN" (convention C15414 protocol no. 182.14.8C) is gratefully acknowledged. Lanzoni also gratefully acknowledges support from "Progetto Giovani 2015" by the National Group of Mathematical Physics (GNFM-INdAM).

References

[Abramowitz and Stegun 1972] M. Abramowitz and I. A. Stegun (editors), *Handbook of mathematical functions: With formulas, graphs, and mathematical tables*, 10th ed., Wiley, New York, 1972. Reprinted Dover, New York, 1992.

[Bowles 1997] J. E. Bowles, *Foundation analysis and design*, 5th ed., McGraw-Hill, New York, 1997.

[Caliendo and Parisi 2010] C. Caliendo and A. Parisi, "Stress-prediction model for airport pavements with jointed concrete slabs", *J. Transp. Eng.* (*ASCE*) **136**:7 (2010), 664–677.

[Çelik and Saygun 1999] M. Çelik and A. Saygun, "A method for the analysis of plates on a two-parameter foundation", *Int. J. Solids Struct.* **36**:19 (1999), 2891–2915.

[Duan and Wang 2007] W. H. Duan and C. M. Wang, "Exact solutions for axisymmetric bending of micro/nanoscale circular plates based on nonlocal plate theory", *Nanotechnology* **18** (2007), 385704.

[Gazetas 1981a] G. Gazetas, "Ultimate behavior of continuous footings in tensionless contact with a three-parameter soil", *J. Struct. Mech.* **9**:3 (1981), 339–362.

[Gazetas 1981b] G. C. Gazetas, "Indentation of anisotropic halfspace by yielding circular foundation", *J. Eng. Mech. Div.* (*ASCE*) **107**:4 (1981), 695–704.

[Gazetas and Tassios 1978] G. C. Gazetas and T. P. Tassios, "Elastic-plastic slabs on elastic foundation", *J. Struct. Div.* (*ASCE*) **104**:4 (1978), 621–636.

[Helwany et al. 1998] S. Helwany, J. Dyer, and J. Leidy, "Finite-element analyses of flexible pavements", *J. Transp. Eng.* (*ASCE*) **124**:5 (1998), 491–499.

[Ince 1944] E. L. Ince, *Ordinary differential equations*, Dover Publications, New York, 1944.

[Johansen 1962] K. W. Johansen, *Yield-line theory*, Cement and Concrete Association, London, 1962.

[Kocatürk 1997] T. Kocatürk, "Elastoplastic analysis of circular plates on elastoplastic foundation", *J. Struct. Eng.* (*ASCE*) **123**:6 (1997), 808–815.

[Lanzoni et al. 2014] L. Lanzoni, E. Radi, and A. Nobili, "Ultimate carrying capacity of elastic-plastic plates on a Pasternak foundation", *J. Appl. Mech.* (*ASME*) **81**:5 (2014), Article ID 051013.

[Lewandowski and Świtka 1991] R. Lewandowski and R. Świtka, "Unilateral plate contact with the elastic-plastic Winkler-type foundation", *Comput. Struct.* **39**:6 (1991), 641–651.

[Liew et al. 2006] K. M. Liew, X. Q. He, and S. Kitipornchai, "Predicting nanovibration of multi-layered graphene sheets embedded in an elastic matrix", *Acta Mater.* **54**:16 (2006), 4229–4236.

[Meyerhof 1960] G. G. Meyerhof, "Bearing capacity of floating ice sheets", *J. Eng. Mech. Div.* (*ASCE*) **86**:5 (1960), 113–146.

[Meyerhof 1962] G. G. Meyerhof, "Load-carrying capacity of concrete pavements", *J. Soil Mech. Found. Div.* **88**:3 (1962), 89–116.

[Nobili 2012] A. Nobili, "Variational approach to beams resting on two-parameter tensionless elastic foundations", *J. Appl. Mech.* (*ASME*) **79**:2 (2012), 021010.

[Nobili et al. 2014] A. Nobili, E. Radi, and L. Lanzoni, "A cracked infinite Kirchhoff plate supported by a two-parameter elastic foundation", *J. Eur. Ceram. Soc.* **34**:11 (2014), 2737–2744.

[Nobili et al. 2015] A. Nobili, E. Radi, and L. Lanzoni, "On the effect of the backup plate stiffness on the brittle failure of a ceramic armor", *Acta Mechanica* (online publication August 2015). DOI 10.1007/s00707-015-1412-5.

[Piccolroaz and Movchan 2014] A. Piccolroaz and A. B. Movchan, "Dispersion and localisation in structured Rayleigh beams", *Int. J. Solids Struct.* **51**:25–26 (2014), 4452–4461.

[Pradhan and Kumar 2010] S. C. Pradhan and A. Kumar, "Vibration analysis of orthotropic graphene sheets embedded in Pasternak elastic medium using nonlocal elasticity theory and differential quadrature method", *Comput. Mater. Sci.* **50**:1 (2010), 239–245.

[Radi and Di Maida 2014] E. Radi and P. Di Maida, "Analytical solution for ductile and FRC plates on elastic ground loaded on a small circular area", *J. Mech. Mater. Struct.* **9**:3 (2014), 313–331.

[Ru 2001] C. Q. Ru, "Axially compressed buckling of a doublewalled carbon nanotube embedded in an elastic medium", *J. Mech. Phys. Solids* **49**:6 (2001), 1265–1279.

[Salençon 2013] J. Salençon, *Yield design*, Wiley, Hoboken, NJ, 2013.

[Save et al. 1997] M. A. Save, C. E. Massonnet, and G. de Saxcé (editors), *Plastic limit analysis of plates, shells and disks*, 2nd ed., North-Holland Series in Applied Mathematics and Mechanics **43**, Elsevier, New York, 1997.

[Selvadurai 1977] A. P. S. Selvadurai, "Axisymmetric flexure of an infinite plate resting on a finitely deformed incompressible elastic halfspace", *Int. J. Solids Struct.* **13**:4 (1977), 357–365.

[Selvadurai 1979] A. P. S. Selvadurai, *Elastic analysis of soil-foundation interaction*, Developments in Geotechnical Engineering **17**, Elsevier, New York, 1979.

[Shukla et al. 2011] S. K. Shukla, A. Gupta, and N. Sivakugan, "Analysis of circular elastic plate resting on Pasternak foundation by strain energy approach", *Geotech. Geol. Eng.* **29**:4 (2011), 613–618.

[Sokól-Supel 1985] J. Sokól-Supel, "Elastoplastic bending of plates resting on elastic subgrade under rotational symmetry conditions", *J. Struct. Mech.* **13**:3–4 (1985), 323–341.

[Sokół-Supel 1988] J. Sokół-Supel, "Biegung metallischer Kreisplatten mit elastischer Unterlage", *Ing. Arch.* **58**:3 (1988), 185–192.

[Timoshenko and Woinowsky-Krieger 1959] S. Timoshenko and S. Woinowsky-Krieger, *Theory of plates and shells*, 2nd ed., McGraw-Hill, New York, 1959.

[Tullini et al. 2012] N. Tullini, A. Tralli, and L. Lanzoni, "Intefacial shear stress analysis of bar and thin film bonded to 2D elastic substrate using a coupled FE–BIE method", *Finite Elem. Anal. Des.* **55** (2012), 42–51.

[Wen-da and Shu 1987] L. Wen-da and W. Shu, "On the circular footing plates on two-parameters foundation under arbitrary loads", *Appl. Math. Mech.* **8**:9 (1987), 815–823.

Received 13 Jan 2015. Revised 17 Mar 2015. Accepted 22 Mar 2015.

LUCA LANZONI: luca.lanzoni@unimo.it
DET — Dipartimento di Economia e Tecnologia, Università degli Studi della Repubblica di San Marino, Salita alla Rocca 44, 47890 San Marino città, San Marino and DIEF — Dipartimento di Ingegneria "Enzo Ferrari", Università di Modena e Reggio Emilia, Via Vignolese 905, I-41125 Modena, Italy

ANDREA NOBILI: andrea.nobili@unimore.it
DIEF — Dipartimento di Ingegneria "Enzo Ferrari", Università di Modena e Reggio Emilia, Via Vignolese 905, I-41125 Modena, Italy

ENRICO RADI: enrico.radi@unimore.it
DISMI — Dipartimento di Scienze e Metodi dell'Ingegneria, Università di Modena e Reggio Emilia, Via Amendola 2, I-42122 Reggio Emilia, Italy

ANDREA SORZIA: andrea.sorzia@unimore.it
DISMI — Dipartimento di Scienze e Metodi dell'Ingegneria, Università di Modena e Reggio Emilia, Via Amendola 2, I-42122 Reggio Emilia, Italy

JOURNAL OF MECHANICS OF MATERIALS AND STRUCTURES
Vol. 10, No. 4, 2015
dx.doi.org/10.2140/jomms.2015.10.481

CONTOURS FOR PLANAR CRACKS GROWING IN THREE DIMENSIONS: ILLUSTRATION FOR TRANSVERSELY ISOTROPIC SOLID

LOUIS MILTON BROCK

Three-dimensional dynamic steady state growth of a semi-infinite plane crack in a transversely isotropic solid is considered. Growth takes place on a principal plane with the material symmetry axis as one tangent. Fracture is brittle, and driven by compressive loads that translate on the crack surfaces. Translation speed is constant and subcritical, but direction with respect to the principal axes is arbitrary. An analytical solution is obtained, and examined in light of the dynamic energy release rate criterion for the case of a translating compressive point force. Introduction of quasipolar coordinates leads to a nonlinear first-order differential equation for the distance between force and crack edge. The equation depicts a crack edge that tends to the rectilinear away from the force. An analytical expression for the distance measured parallel to translation direction indicates a marked deviation from the rectilinear near the point force.

Introduction

A major goal of fracture mechanics is the determination of crack edge location. In 2D dynamic fracture, this requires an equation of motion for the crack tip [Freund 1990]. In a 3D study, such an equation must describe the crack contour. This goal has been achieved for semi-infinite crack growth in an unbounded isotropic solid [Brock 2015]. This paper extends the analysis to an unbounded transversely isotropic solid. For simplicity, the crack remains in its original plane, which is a principal plane. Moreover, crack growth is caused by compression loads on the crack surface that translate at constant subcritical speed in a fixed direction, and achieves a dynamic steady state.

Two-dimensional dynamic analyses of transversely isotropic half-spaces in which the material symmetry axis coincides with the surface normal essentially correspond to those for the isotropic case, e.g., [Scott and Miklowitz 1967]. As seen in sliding contact analysis [Brock 2013], elastic properties associated with principal planes other than that on the surface do influence 3D results but the solution forms resemble those for the isotropic case. When the surface normal is not the material symmetry axis, however, 3D solution forms are quite distinctive. Therefore, to enhance the effect of anisotropy, (a) the principal plane in this 3D illustration includes the axis of material symmetry, and (b) the fixed direction is arbitrary with respect to this axis.

Two-dimensional analyses of fracture for the general anisotropic solid in the dynamic steady state exist, of course. Indeed, the semi-infinite interface crack has been examined by Willis [1971]. Principal axes define both in-plane coordinates and interface, and the crack edge exhibits the well-known oscillatory behavior. Nevertheless, as in [Brock 2015] and the present study, a formula for crack extension based on dynamic energy release rate is developed.

Keywords: 3D, dynamic, criteria, analytic solution, crack contour, transverse isotropy, energy release.

Analysis begins by considering the unmixed boundary value problem for a discontinuity in displacement imposed over a semi-infinite plane area A_C contained in an unbounded solid. This is of course a dislocation problem and is a standard [Willis 1971; Barber 1992] first step in fracture analysis. For efficiency in application to the title problem, this study considers a discontinuity that vanishes along area boundary B_C, vanishes at infinite distances from it, and translates with A_C at constant subcritical speed V in a fixed direction. A dynamic steady state ensues and allows use of a translating Cartesian basis. The transform solution is generated, but a quasipolar coordinate system is introduced in the inversion process. Expressions for normal traction on the plane of A_C lead to a classical singular integral equation for the displacement discontinuity produced were A_C a crack subject to a prescribed surface load. Imposition of a fracture criterion leads to a nonlinear first-order differential equation for the distance from a given point in A_C to any point on (now) crack edge B_C.

Displacement discontinuity growth — governing equations

Consider an unbounded, transversely isotropic and linearly elastic solid. Cartesian basis $\boldsymbol{x} = \boldsymbol{x}(x_k)$ defines the principal material axes. The semi-infinite planar region A_C ($x_3 = 0, x_V < 0$) with rectilinear boundary B_C ($x_V = 0$) is subject to discontinuity

$$[\boldsymbol{u}(u_k)] = \boldsymbol{U}(U_k). \tag{1}$$

Here $k = (1, 2, 3)$, [ ] signifies a jump as travel from $x_3 = 0-$ to $x_3 = 0+$ occurs, $\boldsymbol{u}$ is the displacement field and discontinuity components $U_k = U_k(x_1, x_2)$. The x_2-direction defines the axis of material symmetry, and

$$x_V = x_1 \cos\theta + x_2 \sin\theta, \quad |\theta| < \tfrac{\pi}{2}. \tag{2a}$$

The region translates in the positive x_V-direction at constant subcritical speed V. A dynamic steady state is achieved by $(\boldsymbol{U}, A_C)$, and boundary B_C may no longer be rectilinear. Displacement $\boldsymbol{u}(u_k)$ and traction $\boldsymbol{T}(\sigma_{ik})$ do not vary in the moving frame of A_C. Basis $\boldsymbol{x}$ is therefore translated with A_C so that $u_k = u_k(\boldsymbol{x})$, $U_k = U_k(x_1, x_2)$, $\sigma_{ik} = \sigma_{ik}(\boldsymbol{x})$, and the time derivative can be written

$$-V\partial_V, \quad \partial_V = \partial_1 \cos\theta + \partial_2 \sin\theta. \tag{2b}$$

Here ∂_k signifies x_k-differentiation. For convenience, $\boldsymbol{x} = 0$ is located in the region of discontinuity, so that function $\Im(x_1, x_2) = 0$, $\sqrt{x_1^2 + x_2^2} \neq 0$ defines contour B_C and the region can be defined as $(x_1, x_2) \in A_C$. Both $\Im$ and its gradient $\nabla\Im$ are continuous, and any line passing through $\boldsymbol{x} = 0$ in the x_1x_2-plane can cross B_C only once. For $x_3 \neq 0$, governing equations for $\boldsymbol{u}(x_k)$ can be written as [Brock 2013]

$$\nabla \cdot \boldsymbol{T} = C_{44} V^2 \partial_V^2 \boldsymbol{u}, \tag{3a}$$

$$\begin{bmatrix} \sigma_{11} \\ \sigma_{22} \\ \sigma_{33} \end{bmatrix} = \begin{bmatrix} C_{11} & C_{12} & C_{13} \\ C_{12} & C_{22} & C_{12} \\ C_{13} & C_{12} & C_{11} \end{bmatrix} \begin{bmatrix} \partial_1 u_1 \\ \partial_2 u_2 \\ \partial_3 u_3 \end{bmatrix}, \tag{3b}$$

$$\sigma_{2k} = C_{44}(\partial_2 u_k + \partial_k u_2) \quad \text{for } k = 1, 3, \quad \text{and } \sigma_{31} = C_{55}(\partial_3 u_1 + \partial_1 u_3). \tag{3c}$$

Here $(C_{11}, C_{22}, C_{12}, C_{13}, C_{44}, C_{55})$ are the elastic constants, and $C_{13} = C_{11} - 2C_{55}$ [Jones 1999]. As reference quantities, we adopt shear modulus and shear wave speed

$$\mu = C_{44}, \quad V_S = \sqrt{C_{44}/\rho}. \tag{4a}$$

Here ρ is mass density, and (4a) gives the dimensionless terms

$$c = \frac{V}{V_S}, \quad d_1 = \frac{C_{11}}{C_{44}}, \quad d_2 = \frac{C_{22}}{C_{44}}, \quad d_5 = \frac{C_{55}}{C_{44}}, \quad d_{12} = \frac{C_{12}}{C_{44}}, \quad d_{13} = \frac{C_{13}}{C_{44}} = d_1 - 2d_5. \tag{4b}$$

In light of (1), conditions for $x_3 = 0$ are

$$[u_k] = U_k \quad \text{for } (x_1, x_2) \in A_C, \quad [u_k] = 0 \quad \text{for } (x_1, x_2) \notin A_C, \tag{5a}$$

$$[\sigma_{3k}] = 0. \tag{5b}$$

Components U_k are not specified, but must be finite and continuous for $(x_1, x_2) \in A_C$. Therefore $U_k = 0$ for $\Im(x_1, x_2) = 0$, and $(\boldsymbol{u}, \boldsymbol{T})$ should remain finite for $|\boldsymbol{x}| \to \infty$, $x_3 \neq 0$.

General transform solution

A double bilateral transform [Sneddon 1972] can be defined as

$$\hat{F} = \iint F(x_1, x_2) \exp(-p_1 x_1 - p_2 x_2)\, dx_1\, dx_2. \tag{6}$$

Integration is along the entire $\mathrm{Re}(x_1)$- and $\mathrm{Re}(x_2)$-axes. Application of (6) to (3) gives

$$\hat{\boldsymbol{u}} = \hat{\boldsymbol{u}}_5 + \hat{\boldsymbol{u}}_+ + \hat{\boldsymbol{u}}_-, \tag{7a}$$

$$\hat{\boldsymbol{u}}_5 = \boldsymbol{U}_5^{(\pm)} \exp(-B_5|x_3|), \quad \hat{\boldsymbol{u}}_\pm = \boldsymbol{U}_\pm^{(\pm)} \exp(-A_\pm|x_3|). \tag{7b}$$

In (7b) superscript $(\pm)$ signifies $x_3 \geq 0$ and $x_3 \leq 0$, respectively, and

$$(U_5)_1^{(\pm)} = (\pm) B_5 V_5^{(\pm)}, \quad (U_5)_2^{\pm} = 0, \quad (U_5)_3^{(\pm)} = p_1 V_5^{(\pm)}, \tag{8a}$$

$$(U_\pm)_1^{(\pm)} = -(1 + d_{12}) p_1 p_2 V_\pm^{(\pm)}, \quad (U_2)_2^{(\pm)} = d_1 (A_\pm^2 + \Gamma_1) V_\pm^{(\pm)}, \tag{8b}$$

$$(U_\pm)_3^{(\pm)} = (\pm)(1 + d_{12}) p_2 A_\pm V_\pm^{(\pm)}. \tag{8c}$$

Here $(V_5^{(\pm)}, V_\pm^{(\pm)})$ are arbitrary functions of (p_1, p_2) and

$$B_5 = \sqrt{-p_1^2 - \Gamma_0/d_5}, \qquad T_5 = d_5(p_1^2 - B_5^2), \tag{9a}$$

$$\Gamma_0 = p_2^2 - c^2 p_V^2, \qquad p_V = p_1 \cos\theta + p_2 \sin\theta, \tag{9b}$$

$$A_\pm = \sqrt{-p_1^2 - \Gamma_\pm/d_1}, \qquad \Gamma_\pm = \tfrac{1}{2}\big(M \pm \sqrt{M^2 - 4d_1\Gamma_2\Gamma_0}\big), \tag{9c}$$

$$M = d_1\Gamma_2 + \Gamma_0 - (1 + d_{12})^2 p_2^2, \quad \Gamma_1 = p_1^2 + \Gamma_0/d_1, \quad \Gamma_2 = d_2 p_2^2 - c^2 p_V^2. \tag{9d}$$

For bounded behavior as $|x_3| \to \infty$, (7b) requires that $\mathrm{Re}(B_5, A_\pm) \geq 0$ in the cut complex (p_1, p_2)-planes. Application of (6) to (3b), (3c) and (5) and substitution of (8) and (9) gives equations for $(V_5^{(\pm)}, V_+^{(\pm)}, V_-^{(\pm)})$ in terms of transforms $\widehat{U}_k$. The solutions are then used to generate expression (A.1)

for $(\hat\sigma_{33}, \hat\sigma_{31}, \hat\sigma_{32})$ in plane $x_3 = 0$. That the x_3-direction does not correspond to the material symmetry axis is clear from the different forms for (A.1b) and (A.1c).

Transform inversion — general formulas

In (5), inhomogeneous terms (U_1, U_2, U_3) arise only for $(x_1, x_2) \in A_C$. In light of (A.1), therefore, the inversion operation corresponding to (6) gives $(\sigma_{33}, \sigma_{31}, \sigma_{32})$ for $x_3 = 0$ as linear combinations of expressions

$$\iint U_k \, d\xi_1 \, d\xi_2 \, \frac{1}{2\pi i} \int dp_1 \, \frac{1}{2\pi i} \int P_k \, dp_2 \, \exp[p_1(x_1 - \xi_1) + p_2(x_2 - \xi_2)]. \tag{10}$$

Here $U_k = U_k(\xi_1, \xi_2)$ and $P_k = P_k(p_1, p_2)$ is the corresponding coefficient. Double integration is over A_C, and single integration is over the entire $\mathrm{Im}(p_1)$- and $\mathrm{Im}(p_2)$-axes. After [Brock 2013; 2015], transformations are introduced:

$$p_1 = p\cos\psi, \quad p_2 = p\sin\psi, \tag{11a}$$

$$\begin{bmatrix} x \\ y \end{bmatrix} = \begin{bmatrix} \cos\psi & \sin\psi \\ -\sin\psi & \cos\psi \end{bmatrix} \begin{bmatrix} x_1 \\ x_2 \end{bmatrix}, \quad \begin{bmatrix} \xi \\ \eta \end{bmatrix} = \begin{bmatrix} \cos\psi & \sin\psi \\ -\sin\psi & \cos\psi \end{bmatrix} \begin{bmatrix} \xi_1 \\ \xi_2 \end{bmatrix}. \tag{11b}$$

In (11a) and (11b), $\mathrm{Re}(p) = 0+$, $|\mathrm{Im}(p), x, y, \xi, \eta| < \infty$ and $|\psi - \theta| < \frac{\pi}{2}$. Parameters (p, ψ), $(x, \psi; y = 0)$ and $(\xi, \psi; \eta = 0)$ resemble quasipolar coordinate systems, i.e.,

$$d\xi_1 \, d\xi_2 = |\xi| \, d\xi \, d\psi, \quad dp_1 \, dp_2 = |p| \, dp \, d\psi. \tag{11c}$$

Use of (11) in (9) give

$$\Gamma_0 = p^2 C_0, \qquad \Gamma_1 = p^2 C_1, \qquad \Gamma_2 = p^2 C_2, \quad T_5 = p^2 T_5, \tag{12a}$$

$$\Gamma_\pm = p^2 C_\pm, \qquad M = p^2 M, \tag{12b}$$

$$A_\pm = A_\pm \sqrt{p}\sqrt{-p}, \quad B_5 = B_5 \sqrt{p}\sqrt{-p}. \tag{12c}$$

Equation (12) is based on parameters that depend on (c, ψ, θ):

$$C_0 = \sin^2\psi - c_V^2, \qquad C_1 = \cos^2\psi + C_0/d_1, \qquad C_2 = d_2 \sin^2\psi - c_V^2, \tag{13a}$$

$$T_5 = 2d_5 \cos^2\psi + C_0, \qquad c_V = c\cos(\psi - \theta), \tag{13b}$$

$$M = d_1 C_2 + C_0 - (1 + d_{12})^2 \sin^2\psi, \quad C_\pm = \tfrac{1}{2}\big(M \pm \sqrt{M^2 - 4d_1 C_2 C_0}\big), \tag{13c}$$

$$B_5 = \sqrt{\cos^2\psi + C_0/d_5}, \qquad A_\pm = \sqrt{\cos^2\psi + C_\pm/d_1}. \tag{13d}$$

If $\mathrm{Re}(B_5, A_\pm) \geq 0$, terms in (7) are bounded when branches $\mathrm{Im}(p) = 0$, $\mathrm{Re}(p) < 0$ and $\mathrm{Im}(p) = 0$, $\mathrm{Re}(p) > 0$ are introduced for $\sqrt{\pm p}$, respectively, such that $\mathrm{Re}(\sqrt{\pm p}) > 0$ in the cut p-plane. Behavior of $(B_5, A_\pm)$ therefore helps to define allowable speed for a particular solid.

Transform inversion — transversely isotropic solid, allowable speed

In view of [Payton 1983] and (4b), transversely isotropic solids can be categorized as follows, where we define $\gamma = 1 + d_1 d_2 - (1 + d_{12})^2$:

θ	0°	30°	45°	60°	90°
$c_+(\theta)$	2.0564	1.9502	1.8149	1.6673	1.2762
$c_-(\theta)$	1.0	0.8805	0.7967	0.7061	1.0
$c_5(\theta)$	1.2823	1.2178	1.1498	1.0775	1.0

Table 1. Dimensionless speeds for x_V-direction in x_1x_2-principal plane (zinc).

$$\text{I:}\quad \begin{cases} 2\sqrt{d_1d_2} \le \gamma \le 1+d_1d_2 & \text{for } 1<d_1<d_2,\\ d_1+d_2 \le \gamma \le 1+d_1d_2 & \text{for } 1<d_2<d_1,\\ 2d \le \gamma \le 1+d^2 & \text{for } 1<d_1=d_2=d; \end{cases}$$

$$\text{II:}\quad 1+d_1<\gamma<d_1+d_2 \quad \text{for } \gamma^2-4d_1d_2<0;$$

$$\text{III:}\quad \gamma<1+d_1 \quad \text{for } \gamma^2-4d_1d_2<0.$$

For $|\psi-\theta|<\pi/2$ and $M^2-4d_1C_2C_0\ge 0$ Equations (13c) and (13d) hold, and $A_\pm$ is real and nonnegative. For $M^2-4d_1C_2C_0\le 0$ however, the complex conjugates arise:

$$A_\pm = \Omega_C \pm i\Omega_S, \tag{14a}$$

$$\Omega_C = \tfrac{1}{\sqrt{2}}\sqrt{A_\Psi^2+\cos^2\psi+M/2d_1}\ge 0, \quad \Omega_S = \tfrac{1}{\sqrt{2}}\sqrt{A_\Psi^2-\cos^2\psi-M/2d_1}\ge 0, \tag{14b}$$

$$A_\Psi = \left[\cos^4\psi+(M\cos^2\psi+C_2C_0)/d_1\right]^{1/4}, \tag{14c}$$

$$A_+ + A_- = 2\Omega_C, \quad A_+A_- = A_\Psi^2. \tag{14d}$$

For $|\psi-\theta|<\frac{\pi}{2}$, $c_V<c$ so that allowable speed for a given translation direction is defined by branch points of $(A_\pm, B_5)$ on the positive Re(c)-axis for $\left(\psi=\theta, |\theta|<\frac{\pi}{2}\right)$:

$$c_\pm(\theta) = \sqrt{D_2\pm\sqrt{D_2^2-D_4}}, \quad c_5(\theta)=\sqrt{d_5\cos^2\theta+\sin^2\theta}, \tag{15a}$$

$$D_2 = \tfrac{1}{2}\left(1+d_1\cos^2\theta+d_2\sin^2\theta\right), \tag{15b}$$

$$D_4 = d_1\cos^4\theta+d_2\sin^4\theta+\gamma\sin^2\theta\cos^2\theta. \tag{15c}$$

As an illustration, consider materials [Payton 1979]

III (zinc): $d_1=4.2286$, $d_2=1.6286$, $d_5=1.6442$, $d_{12}=1.3195$, $d_{13}=0.9403$.

I (beryl): $d_1=4.11$, $d_2=3.62$, $d_5=2.0$, $d_{12}=1.017$, $d_{13}=1.055$.

Calculations of (15a) are presented in Tables 1 and 2 for values of θ. Table 1 for zinc demonstrates that $c_+(\theta)>c_5(\theta)\ge c_-(\theta)$. Table 2, however, shows that the relation between $c_5(\theta)$ and $c_-(\theta)$ is itself θ-dependent. Although these are examples, the present study will focus on category III materials and, in particular, those which, like zinc, restrict speed for translation direction $|\theta-\psi|<\frac{\pi}{2}$ to the range $0<c<c_-(\theta)$.

In view of this, and conditions on contour function $\Im$, (10) assumes the form

$$\frac{1}{i\pi}\int_\Psi P_k\,d\psi\int_N d\eta\,\frac{\partial}{\partial x}\int_X d\xi\,\frac{\partial U_k}{\partial\xi}(\xi,\eta)\frac{1}{2\pi i}\int\frac{|p|}{p}\frac{\sqrt{-p}}{\sqrt{p}}\,dp\exp(p(x-\xi)). \tag{16}$$

θ	0°	30°	45°	60°	90°
$c_+(\theta)$	2.0278	1.9428	1.857	1.8514	1.9026
$c_-(\theta)$	1.0	1.1326	1.1902	1.1469	1.0
$c_5(\theta)$	$\sqrt{2}$	1.3229	1.2247	1.118	1.0

Table 2. Dimensionless speeds for x_V-direction in x_1x_2-principal plane (beryl).

Symbols (N, X, Ψ) signify integration over ranges $|\psi - \theta| < \frac{\pi}{2}$, $N^- < \eta < N^+$ and $X_- < \xi < X_+$, respectively. In light of (A.1), (13d) and (14d), term $P_k = P_k(\psi, \theta)$ is real-valued. The p-integration is along the positive side of the entire imaginary axis, and can be performed by use of Appendix B. Then, because U_k vanishes continuously on C, (16) gives

$$\frac{1}{\pi}\int_\Psi P_k\, d\psi \frac{\partial}{\partial x}\int_N d\eta \frac{1}{\pi}\int_X \frac{\partial U_k}{\partial \xi}(\xi,\eta)\frac{d\xi}{\xi - x}. \tag{17}$$

Limits $N^\pm(\psi)$ in (17) are defined by

$$\Im(\xi_1(\xi, N^\pm), \xi_2(\xi, N^\pm)) = 0, \quad \frac{dN^\pm}{d\xi} = 0. \tag{18}$$

That is, for given ψ, limits $N^\pm$ are the maximum and minimum values of η on B_C, and for given η, limits $X_\pm(\psi, \eta)$ locate the ends of lines that run parallel to the ξ-axis and that span A_C. Conditions on B_C imply that these limits exist, are single-valued, and vary continuously in ψ. Figure 1 gives a generic sketch for A_C and it is seen that, for semi-infinite A_C, $N^\pm(\psi) \to \pm\infty$ and $|X_-(\psi, \eta)| \to \infty$ for certain ranges of ψ.

In light of (7)–(12), traction in A_C itself, i.e., $x_3 = 0$, $(x_1, x_2) \in A_C$, is

$$\sigma_{3k} = -\frac{1}{\pi}\int_\Psi d\psi \int_N d\eta \frac{\partial}{\partial x}\int_X d\xi\, \delta(\xi,\eta)\sigma_{3k}(x_1(\xi,\eta), x_2(\xi,\eta)). \tag{19}$$

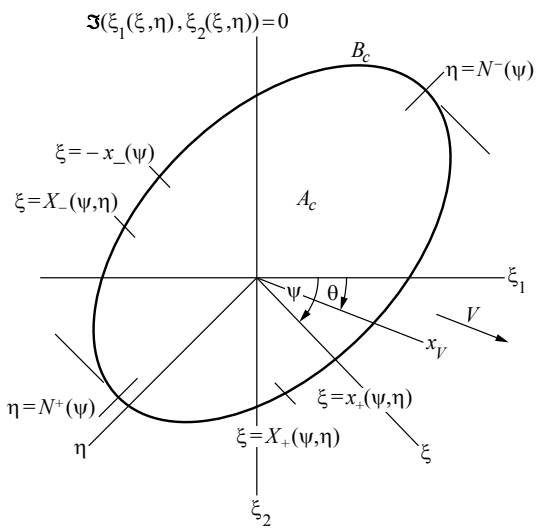

Figure 1. Schematic of area A_C and contour B_C.

In (19), δ is the Dirac function. Therefore, expressions for traction in A_C can be obtained by matching the integrands of (ψ, η)-integration in (19) with combinations of those in (17). Moreover, ξ in (17) and (19) is an integration variable representing parameter x that itself depends on (x_1, x_2) and ψ. As noted in connection with (11), coordinates (x_1, x_2) can be replaced by (x, ψ) for $y = 0$. Thus, every point $(x_1, x_2) \in A_C$ lies on an integration path $\eta = 0$ that passes through both limit points of the ξ-integral. Results of matching (17) and (19) give, therefore, expression (C.3).

Related crack growth problem: Basic results

Region A_C is now a semi-infinite crack, i.e., translation speed V is the crack growth speed, and $\Im(x_1, x_2) = 0$ is such that B_C in Figure 1 is an arc of infinite length. The two crack surfaces are subjected to equal compressive stress $\sigma_{32} = \sigma_{31} = 0$, $\sigma_{33} = -\sigma_{33}^C$, where, for $(x_1, x_2) \in A_C$, σ_{33}^C is nonnegative, finite, piecewise continuous and

$$\sigma_{33}^C \approx O((x_1^2 + x_2^2)^{-\chi}), \quad \sqrt{x_1^2 + x_2^2} \to \infty \quad \text{for } \chi > 1. \tag{20}$$

Coupled singular integral equations for the x-derivatives of (U_1, U_2, U_3) are provided by (C.3), with $(\sigma_{32}, \sigma_{31}) = 0$ and $\sigma_{33} = -\sigma_{3k}^C$. Solution gives the derivatives and the functions themselves. If σ_{33}^C-values are largest near $(x_1, x_2) = 0$, it is reasonable to assume that any curvature of crack edge B_C will produce an essentially concave profile with respect to this point. In view of the original conditions on B_C then, $(U_1, U_2) = 0$ and two cases arise for U_3. Case $X_+ = x_+(\psi) > 0$, $X_- = -x_-(\psi)$ gives

$$\frac{\partial U_3}{\partial x} = \frac{1}{\sqrt{x_+ - x}\sqrt{x + x_-}} \frac{(vp)}{\pi} \int_X \frac{g_3\, d\xi}{\xi - x} \sqrt{x_+ - \xi}\sqrt{\xi + x_-}, \tag{21a}$$

$$U_3 = \frac{1}{\pi} \int_X g_3\, d\xi \ln \left| \frac{\sqrt{x_+ - x}\sqrt{\xi + x_-} - \sqrt{x + x_-}\sqrt{x_+ - \xi}}{\sqrt{x_+ - x}\sqrt{\xi + x_-} + \sqrt{x + x_-}\sqrt{x_+ - \xi}} \right|, \tag{21b}$$

$$g_3 = -\frac{2C_0}{\mu G_3} \sigma_{33}^C. \tag{21c}$$

Continuity of B_C requires $x_\pm\left(\frac{\pi}{2} - \theta\right) = x_\mp\left(-\frac{\pi}{2} - \theta\right)$. For $X_+ = x_+(\psi)$, $X_- \to -\infty$,

$$\frac{\partial U_3}{\partial x} = \frac{1}{\sqrt{x_+ - x}} \frac{(vp)}{\pi} \int_X \frac{g_3\, d\xi}{\xi - x} \sqrt{x_+ - \xi}, \tag{22a}$$

$$U_3 = \frac{1}{\pi} \int_X g_3\, d\xi \ln \left| \frac{\sqrt{x_+ - \xi} - \sqrt{x_+ - x}}{\sqrt{x_+ - \xi} + \sqrt{x_+ - x}} \right|. \tag{22b}$$

Continuity of B_C now requires that $x_+\left(\theta \pm \frac{\pi}{2}\right) \to \infty$. Equations (21b) and (22b), as is appropriate, vanish continuously on B_C. Substitution of (21a) and (22a) into (17) and performing the ξ-integration for $x \notin X$ leads to, respectively, expressions for traction on plane $x_3 = 0$, $(x, \psi) \notin A_C$:

$$\sigma_{33} = \frac{1}{\pi\sqrt{x_+ - x}\sqrt{x_- + x}} \int_X \frac{\sigma_{33}^C\, d\xi}{\xi - x} \sqrt{x_+ - \xi}\sqrt{\xi + x_-}, \tag{23a}$$

$$\sigma_{33} = \frac{1}{\pi\sqrt{x_+ - x}} \int_X \frac{\sigma_{33}^C\, d\xi}{\xi - x} \sqrt{x_+ - \xi}. \tag{23b}$$

Critical speed: Illustration

Restriction $0 < c < c_-(\theta)$ guarantees a bounded solution. In addition, (21b) and (22b) define crack surface separation, which should be nonnegative. Thus term C_0/G_3 in (21c) should be negative and finite. The same condition arises in the isotropic limit

$$d_1 = d_2 = d, \quad d_4 = d_5 = 1, \quad d_{12} = d_{13} = d - 2, \quad d = 2\frac{1-\nu}{1-2\nu}.$$

Here υ is Poisson's ratio, and it can be shown that

$$c_+(\theta) = \sqrt{d}, \qquad c_-(\theta) = c_5(\theta) = 1, \tag{24a}$$

$$A_+ = A = \sqrt{1 - c_V^2/d}, \qquad A_- = B_5 = B = \sqrt{1 - c_V^2}, \tag{24b}$$

$$G_3/C_0 = -R/c_V^2 A, \qquad R = 4AB - (1 + B^2)^2. \tag{24c}$$

In (24c), $R \to 0+$ ($c_V \to 0$) and $R = -1$ ($c_V \to 1$), which implies that $R = 0$ ($c_V V = c_R$, $0 < c_R < 1$). Thus, R is a Rayleigh function, V_R is the Rayleigh speed, and crack growth rate is restricted by $0 < c < c_R$.

The situation is more complicated for the transversely isotropic solid: for $\psi = \theta = 0$, G_3/C_0 is negative for $c < c_-$ and vanishes when

$$4A_1A_5 - (1 + A_5^2)^2 = 0, \tag{25a}$$

$$A_1 = \sqrt{1 - c^2/d_1}, \quad A_5 = \sqrt{1 - c^2/d_5}. \tag{25b}$$

For the category III solid, in particular, G_3/C_0 vanishes for $\psi = \theta = \frac{\pi}{2}$ when

$$\left[1 + (1 + d_{12})^2 - \sqrt{d_1 d_2}A_2 B\right]B^2 + \sqrt{d_1 d_2}\left(1 - \sqrt{d_1 d_2}B^2\right)A_2^2 = 0, \tag{26a}$$

$$A_2 = \sqrt{1 - c^2/d_2}, \quad B = \sqrt{1 - c^2}. \tag{26b}$$

Calculations for zinc give the roots of (25a) and (26a) as $c_R \approx 1.16$ and $c_R \approx 0.26$, respectively. However, Table 1 shows that the first root exceeds $c_-(0)$. A similar result arose for sliding contact [Brock 2013]. That is, G_3/C_0 plays the role of a Rayleigh function (cf. (25a) and (24c)) but its roots c_R may not give the minimum critical speed.

Brittle fracture parameter: Energy release (rate)

After [Griffith 1921] crack growth occurs when the rate of dynamic energy release matches that of potential energy decrease. For the 2D brittle crack, this criterion equates the rate per unit length (of crack edge) of energy release and negative of power per unit length generated in the crack plane [Willis 1971; Achenbach 1973; Freund 1990]. Here, total release rate $\dot{D}_3$ and total power are considered. Affixed subscript "3" signifies the possibility that release rate in an anisotropic material depends on orientation of the fracture surface, e.g., here the surface normal aligns with the x_3-principal direction. Use of (8) for the dynamic steady state gives

$$\dot{D}_3 = -V\int_\Psi d\psi\left[\left(\int_{-\infty}^{\infty} - \int_X\right)dx\,\sigma_{33}\partial_V U_3 + \int_X |x|\,dx\,\sigma_{33}^C\partial_V U_3\right], \tag{27a}$$

$$\partial_V = \cos(\psi-\theta)\frac{\partial}{\partial x} - \frac{\sin(\psi-\theta)}{|x|}\frac{\partial}{\partial \psi}. \tag{27b}$$

To illustrate the form of $\dot{D}_3$ the ∂_V-operator is applied to case (23b):

$$\partial_V U_3 = -\frac{(vp)}{\pi\sqrt{x_+ - x}}\int_X g_3\, d\xi\left[\frac{\sqrt{x_+-\xi}}{\xi - x}\cos(\psi-\theta) - \frac{\sin(\psi-\theta)}{|x|\sqrt{x_+-\psi}}\frac{dx_+}{d\psi}\right] + \frac{\sin(\psi-\theta)}{\pi|x|}\int_X d\xi \ln\left|\frac{\sqrt{x_+-\xi}+\sqrt{x_+-x}}{\sqrt{x_+-\xi}-\sqrt{x_+-x}}\right|\frac{\partial g_3}{\partial\psi}. \tag{28}$$

Equations (5a), (23b) and (28) imply that $\dot{D}_3 = 0$ in (27a). However (23b) and (28) are square-root singular for $x \to x_+ + 0$ and $x \to x_+ - 0$ respectively and, in the sense of a distribution [Achenbach and Brock 1973],

$$\frac{H(x_+-x)}{\sqrt{x_+-x}}\frac{H(x-x_+)}{\sqrt{x-x_+}} = \frac{\pi}{2}\delta(x-x_+). \tag{29}$$

Here H is the step function. Also, $\dot{D}_3$ is assumed invariant in (27a) with respect to its integrand. Singular behavior guarantees invariance in terms of x, so that the integrand need only be constant in terms of ψ. Therefore, for $|\psi-\theta| < \frac{\pi}{2}$,

$$\frac{\dot{D}_3}{\mu V_S} = -\frac{cC_0}{G_3}\left(\frac{G}{\mu}\right)^2\frac{d}{d\psi}[x_+\sin(\psi-\theta)], \quad G = \int_X \frac{\sigma_{33}^C\, dt}{\sqrt{x_+ - t}}. \tag{30}$$

Equation (30) is a nonlinear differential equation for $x_+(\psi)$ based on (23), i.e., semi-infinite A_C.

Illustration: Point force

Consider compressive point force loading

$$\sigma_{31}^C = \sigma_{32}^C = 0, \quad \sigma_{33}^C = \frac{P\delta(r_0)}{2\pi r_0}, \quad r_0 = \sqrt{x_1^2 + x_2^2}. \tag{31}$$

Here P is a force, so that traction σ_{33}^C is the axially symmetric Dirac function in standard polar coordinates. Function G in (30) for (31) is given in Appendix D. The right-hand side of (30) must be finite for $|\psi-\theta| \to \frac{\pi}{2}$, and use of (13a), (C.2d) and (D.4b) gives

$$x_+ \approx \sqrt{\frac{c}{2S}\frac{\mu V_S}{\dot{D}_3}}\frac{P}{2\pi\mu}\frac{1}{\sqrt{\cos(\psi-\theta)}} \quad \text{as } |\psi-\theta| \to \tfrac{\pi}{2}. \tag{32}$$

Terms in (32) are given by

$$S = 4d_5c_5'\tan^2\theta + \frac{Q}{\Omega}\sqrt{d_1}\cos^2\theta + T'^2\left(\frac{Q}{\Omega}\sqrt{d_1} - \frac{\Omega}{D_4}\right), \tag{33a}$$

$$c_5' = \sqrt{d_5\sin^2\theta + \cos^2\theta}, \tag{33b}$$

$$Q = 1 + \frac{1}{D_4}\left(\sqrt{d_1}\sin^2\theta + \frac{\cos^2\theta}{\sqrt{d_1}}\right), \quad T' = \frac{2c_5'^2}{\cos\theta} - \cos\theta, \tag{33c}$$

$$\Omega = \sqrt{\gamma \cos^2\theta + 2\sqrt{d_1}\big(\sqrt{d_1}\sin^2\theta + D_4\big)}, \tag{33d}$$

$$D_4 = \sqrt{d_1 \sin^4\theta + d_2 \cos^4\theta + \gamma \sin^2\theta \cos^2\theta}. \tag{33e}$$

Equation (30) involves only $x_+(\theta)$ itself for $\psi = \theta$, i.e., the distance between point forces and crack edge measured in the direction of translation. In light of Appendix D, (30) can be solved algebraically as

$$x_+(\theta) = F(c,\theta)L, \tag{34a}$$

$$F(c,\theta) = \sqrt{-cC_0/G_3}, \quad L = (P/2\pi)\sqrt{V_S/\mu \dot{D}_3}. \tag{34b}$$

Reference length L depends on a force/energy ratio. Term $F(c,\theta)$ is dimensionless. Quantities (C_0, G_3) come from (13), (14), (C.2d) and (C.3b) upon setting $\psi = \theta$, $c_V = c$. In view of (34) and invariance, (30) can be rewritten for $|x - \theta| < \frac{\pi}{2}$ as

$$-\frac{2C_0}{G_3 x_+^3}\frac{d}{d\psi}[\sin(\psi - \theta)x_+] = \frac{F^2(c,\theta)}{c x_+^2(\theta)}. \tag{35}$$

On the left-hand side of (35) we temporarily introduce $z = x_+ \sin(\psi - \theta)$, which allows separation of variables. Integration in view of the asymptotic behavior noted above then gives x_+ when $\psi \neq \theta$:

$$\frac{x_+^2(\theta)}{x_+^2(\psi)} = \frac{1}{c}F^2(c,\theta)\sin^2(\psi - \theta)\int_- \frac{G_3\, d\phi}{C_0 \sin^3(\phi - \theta)} \quad \text{for } -\tfrac{\pi}{2} < \psi - \theta < 0, \tag{36a}$$

$$\frac{x_+^2(\theta)}{x_+^2(\psi)} = -\frac{1}{c}F^2(c,\theta)\sin^2(\psi - \theta)\int_+ \frac{G_3\, d\phi}{C_0 \sin^3(\phi - \theta)} \quad \text{for } 0 < \psi - \theta < \tfrac{\pi}{2}. \tag{36b}$$

Symbols $\pm$ affixed to integral operators in (36) signify, respectively, integration ranges $\psi < \phi < \theta + \frac{\pi}{2}$ and $\theta - \frac{\pi}{2} < \phi < \psi$. Differentiation of (36) shows that $dx_+/d\psi = 0$ for $\psi = \theta$, i.e., crack edge and direction of point force translation are perpendicular directly ahead of the forces.

Calculations

Equation (36) and the asymptotic behavior noted for (32) indicate that, as in the isotropic case [Brock 2015], the crack edge B_C resembles those in Figure 2, where "×" denotes point force location. That is, it is a straight line at right angles to the translation/growth direction that is deformed by a bulge near the location $\boldsymbol{x} = 0$ of the translating point forces. Bulge size is characterized somewhat by the distance $x_+(\theta)$ in (34). Therefore, values of dimensionless ratio $F(c,\theta)$ are displayed in Table 3 for $\theta = (0°, 30°, 45°, 60°, 90°)$ respectively, and subcritical values of c. Entries in Table 3 show that the bulge effect is enhanced by increase in extension speed (c) and by deviation (θ) in force translation direction from the x_1-principal direction. Perhaps the latter behavior arises because $d_2 < d_1$ $(C_{22} < C_{11})$.

Some observations for more general loading

Consider in place of (31) a finite, simply connected region $A_0 \in A_C$ subjected to a finite and piecewise continuous pressure p_0. The Green's function for this case is obtained by replacing $(P, |x|)$ in (D.2)

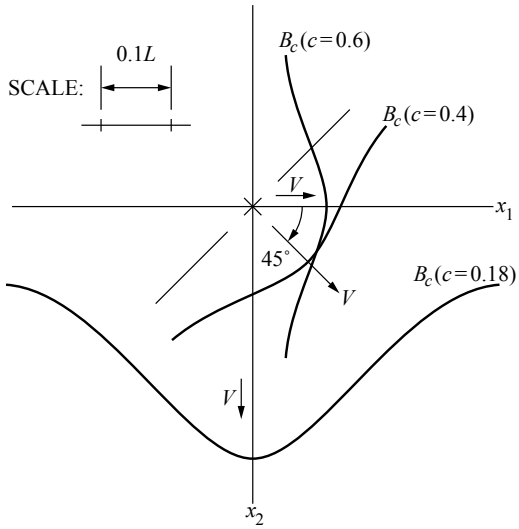

Figure 2. Sketches of crack edge contour B_C.

with, respectively,

$$\iint_{A_0} p_0(u,\phi)|u|\,du\,d\phi, \tag{37a}$$

$$X = \sqrt{x^2+u^2-2ux\cos(\phi-\psi)}. \tag{37b}$$

Quasipolar coordinates (u,ϕ) lie in A_0 and, in consequence, the right-hand side of (D.3) is

$$\frac{1}{\sqrt{z-x_+}Z}\frac{1}{Z^2+\epsilon^2}, \qquad Z=\sqrt{z^2+u^2-2uz\cos(\phi-\psi)}. \tag{38a}$$

Now $F_G(z)$ has three nonintersecting branch cuts, and the right-hand side of (D.4b) is

$$\iint_{A_0}\frac{d\phi}{\pi\sqrt{2}}\frac{p_0(u,\phi)|u|\,du}{Z_+\sqrt{Z_++x_+-u\cos(\phi-\psi)}} \quad \text{as } \epsilon\to 0, \tag{38b}$$

$$Z_+=\sqrt{x_+^2+u^2-2ux_+\cos(\phi-\psi)}. \tag{38c}$$

Use of (38b) gives an equation for $x_+(\theta)$ that in general does not yield a closed-form result such as (34a). The result for x_+ when $|\psi-\theta|\to\frac{\pi}{2}$, however, is given by (32) with P replaced by (37a). That is, asymptotic behavior of the crack edge depends only on total compressive load, not how that load may be distributed over a finite area.

	$c=0.1$	$c=0.2$	$c=0.3$	$c=0.4$
$\theta=0°$	0.03559	0.05069	0.06286	0.07394
$\theta=30°$	0.04288	0.06169	0.07773	0.09402
$\theta=45°$	0.02526	0.0687	0.0883	0.112
$\theta=60°$	0.0538	0.07902	0.1043	0.14
$\theta=90°$	0.1439	0.2473	$c>c_R$	$c>c_R$

Table 3. Crack edge location parameter $F(c,\theta)$ (zinc).

Some comments

This study extends a dynamic steady-state 3D analysis for an isotropic solid [Brock 2015] by illustrating semi-infinite crack growth in the principal plane of a transversely isotropic solid. Fracture is driven by compressive traction applied to the crack surfaces. An exact solution is possible and, upon introduction of a quasipolar coordinate system, gives a nonlinear first-order differential equation for the distance between a point on the crack plane and the crack edge. The distance function therefore defines the crack contour. The equation is studied for point force loading, so that distance can be chosen as that between forces and crack edge. Calculations show that the crack edge is rectilinear away from the point forces, and translates with them. Near the point forces, however, a bulge forms about them. Force-crack edge distance now increases with force translation speed, and increases are even more prominent as the translation direction aligns with the principal axis associated with the smaller elastic modulus.

These results are consistent with those of [Brock 2015]. Calculations of the distance (contour) function, however, require numerical evaluation of first integrals in (36); in [Brock 2015] analytical evaluation is possible. In addition these results are illustrations for a particular category of transversely isotropic solids [Payton 1983]. Nevertheless, general effects of transverse isotropy are emphasized, because the axis of material symmetry lies in the crack plane. These results are also consistent with those for sliding indentation on a half-space whose surface is the same principal plane [Brock 2013]: minimum critical growth rate may not be a Rayleigh speed. In closing, however, it should be mentioned that the possibility of energy release (rate) dependence on crack surface orientation was not exploited here.

Appendix A

For $x_3 = 0$:

$$\frac{\Gamma_0}{\mu}\hat{\sigma}_{33} = \widehat{U}_3\left[2d_5^2 p_1^2 B_5 + \frac{(\Gamma_1 - A_+A_-)}{2A_+A_-(A_+ + A_-)}\left(\tfrac{1}{2}T_5^2 + \Gamma_0 p_2^2\right) + \tfrac{1}{2}T_5^2\left(\frac{1}{A_+} + \frac{1}{A_-}\right)\right], \tag{A.1a}$$

$$\frac{\Gamma_0}{\mu}\hat{\sigma}_{31} = \frac{T_5}{2B_5}(T_5\widehat{U}_1 + p_1p_2\widehat{U}_2) + \frac{d_5p_1}{A_+ + A_-}\left[(\Gamma_1 - A_+A_-)(2p_1\widehat{U}_1 - p_2\widehat{U}_2) - \frac{\Gamma_0 p_2\widehat{U}_2}{d_1(1+d_{12})}\right], \tag{A.1b}$$

$$\begin{aligned}\frac{\Gamma_0}{\mu}\hat{\sigma}_{32} = {} & \frac{p_1p_2}{2B_5}(T_5\widehat{U}_1 + p_1p_2\widehat{U}_2) - \Gamma_0\left[\frac{d_5(1+d_{12})p_1p_2}{A_+ + A_-}\widehat{U}_1 + \tfrac{1}{2}\widehat{U}_2(A_+ + A_-)\right] \\ & - \frac{\Gamma_1 - A_+A_-}{A_+ + A_-}\left[d_5p_1p_2\widehat{U}_1 + (p_2^2 + \Gamma_0)\tfrac{1}{2}\widehat{U}_2\right].\end{aligned} \tag{A.1c}$$

Appendix B

Consider the integral over the entire $\mathrm{Im}(p)$-axis:

$$\frac{1}{2\pi i}\int |p|\frac{\sqrt{-p}}{\sqrt{p}}(A_R \mp iA_I)\exp\left(pX - (Y_R \mp iY_I)\sqrt{-p}\sqrt{p}\right)\frac{dp}{p}. \tag{B.1}$$

Here (A_R, A_I, X, Y_R, Y_I) are real constants, with $(X, Y_R, Y_I) \geq 0$, and $\mp$ signifies, respectively, $\mathrm{Im}(p) > 0$ and $\mathrm{Im}(p) < 0$. As noted in connection with (11) and (12), $\mathrm{Re}(\sqrt{\pm p}) \geq 0$ in the p-plane with branch cuts $\mathrm{Im}(p) = 0,\ \mathrm{Re}(p) < 0$ and $\mathrm{Im}(p) = 0,\ \mathrm{Re}(p) > 0$, respectively. In particular, for $\mathrm{Re}(p) = 0+$ and,

respectively, $\mathrm{Im}(p) = q > 0$ and $\mathrm{Im}(p) = q < 0$, we have

$$\sqrt{-p} = \left|\frac{q}{2}\right|^{1/2}(1 \mp i), \quad \sqrt{p} = \left|\frac{q}{2}\right|^{1/2}(1 \pm i). \tag{B.2}$$

Use of (B.2) reduces (B.1) to

$$\frac{1}{i\pi}\int_0^\infty \exp(-Y_R q)\big[A_R \cos(X + Y_I)q - A_I \sin(X + Y_I)q\big]\,dq. \tag{B.3}$$

Performing the integration gives

$$\frac{1}{i\pi}\left[A_R \frac{X + Y_I}{(X + Y_I)^2 + Y_R^2} - A_I \frac{Y_R}{(X + Y_I)^2 + Y_R^2}\right]. \tag{B.4a}$$

If factor $\sqrt{-p}/\sqrt{p}$ in (B.1) is replaced by unity, the result becomes

$$\frac{1}{i\pi}\left[A_R \frac{Y_R}{(X + Y_I)^2 + Y_R^2} + A_I \frac{X + Y_I}{(X + Y_I)^2 + Y_R^2}\right]. \tag{B.4b}$$

It is noted that

$$\frac{1}{\pi}\frac{Y_R}{(X + Y_I)^2 + Y_R^2} \to \delta(X + Y_I) \quad \text{as } Y_R \to 0+. \tag{B.5}$$

Here δ is the Dirac function.

Appendix C

For $x_3 = 0,\ X_- < x < X_+,\ \psi \in \Psi$, i.e., $x_3 = 0,\ (x_1, x_2) \in C$, we have

$$\sigma_{33} = -\frac{\mu}{2\pi C_0}(vp)\int_X \frac{\partial U_3}{\partial x}\frac{G_3\,d\xi}{\xi - x}, \tag{C.1a}$$

$$\sigma_{31} = -\frac{\mu}{2\pi C_0}(vp)\int_X \frac{\partial U_1}{\partial x}\frac{G_1\,d\xi}{\xi - x} - \frac{\mu}{2\pi C_0}(vp)\int_X \frac{\partial U_2}{\partial x}\sin 2\psi\,\frac{G_{12}\,d\xi}{\xi - x}, \tag{C.1b}$$

$$\sigma_{32} = -\frac{\mu}{2\pi C_0}(vp)\int_X \frac{\partial U_1}{\partial x}\sin 2\psi\,\frac{G_{21}\,d\xi}{\xi - x} - \frac{\mu}{2\pi C_0}(vp)\int_X \frac{\partial U_2}{\partial x}\frac{G_2\,d\xi}{\xi - x}. \tag{C.1c}$$

Here $U_k = U_k(\xi, \psi)$, (vp) signifies the principal value, and for $M^2 - 4d_1C_2C_0 > 0$ we have

$$G_1 = -\frac{T_5^2}{B_5} - 4d_5\frac{A_+A_- + C_1}{A_+ + A_-}\cos^2\psi, \tag{C.2a}$$

$$G_2 = -\frac{\sin^2 2\psi}{2B_5} - C_0(A_+ + A_-) + \frac{A_+A_- + C_1}{A_+ + A_-}(\sin^2\psi - C_0), \tag{C.2b}$$

$$G_{12} = G_{21} = -\frac{T_5}{2B_5} + \frac{2d_5}{A_+ + A_-}\left[A_+A_- + C_1 + (1+d_{12})\frac{C_0}{d_1}\right], \tag{C.2c}$$

$$G_3 = 4d_5^2 B_5 \cos^2\psi + \left(1 + \frac{C_1}{A_+A_-}\right)\frac{T_5^2 + C_0\sin^2\psi}{A_+ + A_-} - \frac{T_5^2}{A_+A_-}(A_+ + A_-). \tag{C.2d}$$

For $M^2 - 4d_1C_2C_0 < 0$ we have

$$G_1 = -\frac{T_5^2}{B_5} - \frac{2d_5}{\Omega_C}(A_\psi^2 + C_1)\cos^2\psi, \tag{C.3a}$$

$$G_2 = -\frac{\sin^2 2\psi}{2B_5} - 2C_0\Omega_C + \frac{1}{2\Omega_C}(A_\Psi^2 + C_1)(\sin^2\psi - C_0), \tag{C.3b}$$

$$G_{12} = G_{21} = -\frac{T_5}{2B_5} + \frac{d_5}{\Omega_C}\left[A_\Psi^2 + C_1 + (1+d_{12})\frac{C_0}{d_1}\right], \tag{C.3c}$$

$$G_3 = 4d_5^2 B_5\cos^2\psi + \frac{1}{2\Omega_C}\left(1 + \frac{C_1}{A_\Psi^2}\right)(T_5^2 + C_0\sin^2\psi) - \frac{2\Omega_C}{A_\Psi^2}T_5^2. \tag{C.3d}$$

Equations (13) and (14) govern equations (C.2) and (C.3), respectively. Term C_0 defined by (13a) may vanish for subcritical V, but ratios of $(G_1, G_2, G_{12}, G_{21}, G_3)$ with C_0 remain finite, e.g., for $c_V^2 \to \sin^2\psi$

$$\frac{G_3}{C_0} = 2d_5\cos^2\psi + \frac{1}{M_C}(4d_5^2\cos^2\psi + \sin^2\psi) + 4d_5^2\cos^2\psi\left[\frac{\cos\psi}{d_1M_C(M_C+\cos\psi)} - \frac{1}{M_C} - \frac{1}{\cos\psi}\right]$$
$$- \frac{d_5^2}{d_1M_C}\cos^3\psi(m_+\cos\psi + m_-M_C)\left[1 + \frac{1+\cos\psi}{M_C(M_C+\cos\psi)}\right], \tag{C.4a}$$

$$m_+ = 1 + d_1 + (1+d_{12})^2, \quad m_- = \sin^2\psi - \frac{2d_1(d_2-1)}{\gamma - 1 - d_1}, \tag{C.4b}$$

$$M_C = \sqrt{\cos^2\psi + \left[\tfrac{1}{d_1}(\gamma-1) - 1\right]\sin^2\psi}, \tag{C.4c}$$

$$\gamma = 1 + d_1d_2 - (1+d_{12})^2. \tag{C.4d}$$

Appendix D

In terms of quasipolar coordinates (x, ψ), (31) gives

$$\sigma_{33}^C = P\frac{\delta(x)}{\pi|x|}, \quad |\psi| < \tfrac{\pi}{2}. \tag{D.1}$$

Evaluation of G in (30) is obtained in terms of representation

$$\sigma_{33}^C = P\frac{\epsilon}{\pi^2|x|(x^2+\epsilon^2)} \quad \text{as } \epsilon \to 0. \tag{D.2}$$

Function $F_G(z)$ in the complex z-plane, where $x = \mathrm{Re}(z)$, is defined as

$$F_G(z) = \frac{1}{\sqrt{z^2 - \epsilon_0^2}(z^2+\epsilon^2)\sqrt{z - x_+}} \quad \text{for } \epsilon_0 \approx 0. \tag{D.3}$$

Here $F_G \approx O(z^{-3})$, $|z| \to \infty$ and exhibits branch cuts on the $\mathrm{Re}(z)$-axis with branch points $z = (\pm\epsilon_0, x_+)$, and poles $z = \pm i\epsilon$. Thus integration over a closed contour that includes a portion $|z| \to \infty$, but excludes the poles and branch cuts, can be performed by residue theory. Setting $\epsilon_0 = 0$ then leads to the following expressions for G:

$$G = \frac{P}{\pi\alpha\sqrt{2(1+\alpha)}}\frac{1}{x_+^{3/2}}, \quad \alpha = \sqrt{1+\epsilon^2/x_+^2}, \tag{D.4a}$$

$$G = \frac{P}{2\pi x_+^{3/2}} \quad \text{as } \epsilon \to 0. \tag{D.4b}$$

References

[Achenbach 1973] J. D. Achenbach, *Wave propagation in elastic solids*, Applied Mathematics and Mechanics **16**, North-Holland, Amsterdam, 1973.

[Achenbach and Brock 1973] J. D. Achenbach and L. M. Brock, "On quasistatic and dynamic fracture", pp. 529–541 in *Proceedings of an international conference on dynamic crack propagation*, edited by G. C. Sih, Springer, Netherlands, 1973.

[Barber 1992] J. R. Barber, *Elasticity*, Solid Mechanics and its Applications **12**, Kluwer, Dordrecht, 1992.

[Brock 2013] L. M. Brock, "Rapid sliding contact in three-dimensional by an ellipsoidal die on transversely isotropic half-spaces with surfaces on different principal planes", *J. Appl. Mech.* (*ASME*) **81**:3 (2013), Art. ID #031005.

[Brock 2015] L. M. Brock, "Contours for planar cracks in three dimensions", *J. Mech. Mater. Struct.* **10**:1 (2015), 63–77.

[Freund 1990] L. B. Freund, *Dynamic fracture mechanics*, Cambridge University Press, 1990.

[Griffith 1921] A. A. Griffith, "The phenomena of rupture and flow in solids", *Phil. Trans. R. Soc. A* **221**:582–593 (1921), 163–198.

[Jones 1999] R. M. Jones, *Mechanics of composite materials*, 2nd ed., Taylor & Francis, New York, 1999.

[Payton 1979] R. G. Payton, "Epicenter motion of a transversely isotropic elastic half-space due to a suddenly applied buried point source", *Int. J. Eng. Sci.* **17**:7 (1979), 879–887.

[Payton 1983] R. G. Payton, *Elastic wave propagation in transversely isotropic media*, Mechanics of elastic and inelastic solids **4**, Kluwer, The Hague, 1983.

[Scott and Miklowitz 1967] R. A. Scott and J. Miklowitz, "Transient elastic waves in anisotropic plates", *J. Appl. Mech.* (*ASME*) **34**:1 (1967), 104–110.

[Sneddon 1972] I. N. Sneddon, *The use of integral transforms*, McGraw-Hill, New York, 1972.

[Willis 1971] J. R. Willis, "Fracture mechanics of interfacial cracks", *J. Mech. Phys. Solids* **19**:6 (1971), 353–368.

Received 29 Mar 2015. Revised 12 Jul 2015. Accepted 17 Jul 2015.

LOUIS MILTON BROCK: louis.brock@uky.edu
Department of Mechanical Engineering, College of Engineering, University of Kentucky, 265 RGAN, Lexington, KY 40506-0503, United States

JOURNAL OF MECHANICS OF MATERIALS AND STRUCTURES
Vol. 10, No. 4, 2015
dx.doi.org/10.2140/jomms.2015.10.497

ON CESÀRO MEANS OF ENERGY IN MICROPOLAR THERMOELASTIC DIFFUSION THEORY

MARIN MARIN AND SAMY REFAHY MAHMOUD

This paper is dedicated to the theory of thermoelasticity of micropolar diffusion. For the mixed initial boundary value problem defined in this context, we prove that the Cesàro means of the kinetic and strain energies of a solution with finite energy become asymptotically equal as time tends to infinity.

1. Introduction

Eringen [2003] has developed a continuum theory for a mixture of a micropolar elastic solid and a micropolar viscous fluid. All materials, whether natural or synthetic, possess microstructures.

In the micropolar continuum theory, the rotational degrees of freedom play a central role. The material points of porous solids and dirty fluids undergo translation and rotations. Thus, we have six degrees of freedom, instead of the three degrees of freedom considered in classical elasticity and fluid mechanics (see [Eringen 1999; 2001]). A large class of engineering materials, as well as soils, rocks, granular materials, sand and underground water mixtures may be modeled more realistically by means the theory proposed in [Eringen 2003]. Consolidation problems in the building industry and oil exploration problems fall into the domain of this theory.

In the last decade of time, the micropolar theory was extended to include thermal effects in many studies. One can refer to [Ieşan 2004; Marin and Florea 2014; Marin et al. 2013a; 2013b; Sharma and Marin 2014; Dhaliwal and Singh 1987] for a review on the micropolar thermoelasticity and a historical survey of the subject, as well as to [Eringen 1999] in the Continuum Physics series, in which the general theory of micromorphic media has been summed up.

Aouadi [2008] extended the micropolar theory to include thermal and diffusion effects. In fact, the development of high technologies in the years before, during, and after the second world war pronouncedly affected the investigations in which the fields of temperature and diffusion in solids cannot be neglected. At elevated and low temperatures, the processes of heat and mass transfer play the decisive role in many problems of satellites, returning space vehicles, and landing on water or land. These days, oil companies are interested in the process of thermodiffusion for more efficient extraction of oil from oil deposits. Diffusion can be defined as the random walk of an ensemble of particles from regions of high concentration to regions of lower concentration. Thermodiffusion in an elastic solid is due to coupling of the fields of temperature, mass diffusion and that of strain.

The earliest results concerning energy equipartition were dedicated to the abstract differential equations and to the abstract wave equation. The result established in [Levine 1977] using the Lagrange identity, represents a simplified proof that asymptotic equipartition occurs between the Cesàro means of

Keywords: Cesàro mean, micropolar, thermoelastic diffusion, equipartition, kinetic energy, strain energy.

the kinetic and potential energies. The asymptotic equipartition between the mean kinetic and strain energies in the context of linear elastodynamics was studied in [Day 1980]. Also, we can refer to [Dassios and Galanis 1980; Goldstein and Sandefur 1976] and, in specific cases, [Marin and Stan 2013; Teodorescu-Draghicescu and Vlase 2011; Vlase et al. 2012].

In the present paper we consider the linear theory of micropolar thermoelastic diffusion and we formulate the basic initial-boundary value problem in the framework of the linearized theory developed in [Aouadi 2008]. Then we study the asymptotic partition of the energy associated with the solution of this problem. In this aim we introduce the Cesàro mean of various parts of the total energy and use the methods deduced in [Levine 1977; Day 1980; Rionero and Chirita 1987; Marin 2009] to establish the relations that describe the asymptotic behavior of the mean energies. Thus, we use some Lagrange–Brun identities to prove that the mean thermal energy tends to zero as time goes to infinity and the asymptotic equipartition occurs between the Cesàro means of the kinetic and internal energies.

The asymptotic equipartition property is a familiar notion in differential equations field. This means that the kinetic and potential energy of a classical solution with finite energy become asymptotic equal in means as time tends to infinite. Such a property is presented in various papers for physical systems governed by nondissipative hyperbolic partial differential equations or systems of such equations.

But the system of equations governing our mixed initial boundary value problem consists of hyperbolic equations with dissipation and, therefore, does not belong to one of the categories considered previously in literature of subject. By using the dissipation mechanism of the system, we can prove that equipartition occurs between the mean kinetic and strain energies. Instead of abstracted version of this question, we prefer to emphasize the technique itself in the context of micropolar thermoelastic diffusion.

We want to outline that there are many papers which employ the various refinements of the Lagrange identity. One can refer to [Levine 1977; Day 1980; Rionero and Chirita 1987; Gurtin 1993].

The plan of our study is the following one. We first write down the mixed initial boundary value problem defined in the above context. Then we shall establish some Lagrange type identities and, also, we introduce the Cesàro means of various parts of the total energy associated to the solutions. Based on these estimations, at last, we establish the relations that describe the asymptotic behavior of the mean energies.

2. Basic equations and conditions

We assume that a bounded region B of three-dimensional Euclidean space $\mathbb{R}^3$ is occupied by a microstretch thermoelastic body, referred to the reference configuration and a fixed system of rectangular Cartesian axes. Let $\bar{B}$ denote the closure of B and call ∂B the boundary of the domain B. We consider ∂B be a piecewise smooth surface and designate by n_i the components of the outward unit normal to the surface ∂B. Letters in boldface stand for vector fields. We use the notation v_i to designate the components of the vector $\boldsymbol{v}$ in the underlying rectangular Cartesian coordinates frame. Superposed dots stand for the material time derivative. We shall employ the usual summation and differentiation conventions: the subscripts are understood to range over integers $(1, 2, 3)$. Summation over repeated subscripts is implied and subscripts preceded by a comma denote partial differentiation with respect to the corresponding Cartesian coordinate.

The spatial argument and time argument of a function will be omitted when there is no likelihood of confusion. We refer the motion of the body to a fixed system of rectangular Cartesian axes Ox_i, $i = 1, 2, 3$.

Let us denote by u_i the components of the displacement vector and by ϕ_i the components of the microrotation vector. Also, we denote by C the concentration of the diffusive material in the micropolar body and by T the temperature measured from the constant absolute temperature T_0 of the body in its reference state.

As usual, we denote by σ_{ij} the components of the stress tensor and by μ_{ij} the components of the couple stress tensor over B.

In the absence of body force, body couple force and heat supply fields, the field of basic equations for micropolar thermoelastic diffusion are the following (see [Aouadi 2008]):

- the equation of motion

$$\begin{aligned} \rho\ddot{u}_i &= \sigma_{ji,\,j}, \\ \epsilon_{ijk}\sigma_{jk} + \mu_{ji,\,j} &= \rho J_{ij}\ddot{\phi}_j; \end{aligned} \tag{1}$$

- the equation of energy

$$q_{i,\,i} = \rho T_0 \dot{S}; \tag{2}$$

- the equation of conservation of mass

$$\eta_{i,\,i} = \dot{C}. \tag{3}$$

In these equations we have used the following notation:

- ρ is the reference constant mass density;
- $J_{ij} = J_{ji}$ are the coefficients of microinertia;
- σ_{ij}, μ_{ij} are the components of the stress;
- S is the entropy per unit mass;
- q_i are the components of heat flux vector;
- η_i are the components of the flow of diffusing mass vector.

Let us denote by θ the temperature, where $\theta = T - T_0$. Here T_0 is the temperature of the medium in its natural state.

If we suppose that the micropolar body, in the reference state, has a center of symmetry at each point, but is otherwise nonisotropic, we have the following constitutive equations:

$$\begin{aligned} \sigma_{ij} &= c_{ijkl}\varepsilon_{kl} + p_{ijkl}\phi_{kl} + a_{ij}\theta + b_{ij}C, \\ \mu_{ij} &= p_{ijkl}\varepsilon_{kl} + d_{ijkl}\phi_{kl} + p_{ij}\theta + q_{ij}C, \\ \rho S &= -a_{ij}\varepsilon_{ij} - p_{ij}\phi_{ij} + \frac{\rho c_E}{T_0}\theta + \varpi C, \\ P &= b_{ij}\varepsilon_{ij} + q_{ij}\phi_{ij} - \varpi\theta + \varrho C, \\ q_i &= \kappa_{ij}\theta_{,\,j} \\ \eta_i &= d_{ij}P_{,\,j} \end{aligned} \tag{4}$$

In the above relations P is the chemical potential per unit mass, c_E is the specific heat at constant strain, c_{ijkl} is the tensor of elastic constants. Also, the equations $(4)_5$ and $(4)_6$ are know as Fourier's law and Fick's law, respectively. The constants ϖ and ϱ are measures of thermodiffusion effects and diffusive effects, respectively. The rest of parameters are material constants.

The characteristic quantities of the strain ε_{ij} and ϕ_{ij} used in the above equations, are defined by means of the geometric equations

$$\varepsilon_{ji} = u_{i,\,j} - \epsilon_{kji}\phi_k, \quad \phi_{ji} = \phi_{i,\,j}, \tag{5}$$

where ϵ_{ijk} is the alternating tensor.

The functions c_{ijkl}, p_{ijkl}, d_{ijmn}, a_{ij}, b_{ij}, p_{ij}, q_{ij}, κ_{ij}, d_{ij} and ϱ are the characteristic constitutive coefficients. Regarding these coefficients, the conductivity tensor κ_{ij} and the diffusion tensor d_{ij} we have the symmetry relations

$$c_{ijkl} = c_{klij}, \quad d_{ijkl} = d_{klij}, \quad p_{ijkl} = p_{klij}, \quad \kappa_{ij} = \kappa_{ji}, \quad d_{ij} = d_{ji}. \tag{6}$$

The density ρ, the coefficients of inertia J_{ij} and the temperature θ_0 are given constants which satisfy the conditions

$$\rho > 0, \quad J_{ij} > 0, \quad \theta_0 > 0. \tag{7}$$

In accordance with entropy production inequality we must assume that c_{ijmn}, p_{ijmn}, d_{ijmn}, a_{ij}, b_{ij} and κ_{ij} are positive definite tensors, i.e.,

$$\begin{aligned}
c_{ijkl}\xi_{ij}\xi_{mn} &\geq k_0\xi_{ij}\xi_{ij}, \quad k_0 > 0, \quad \text{for all } \xi_{ij} = \xi_{ji},\\
p_{ijkl}\xi_{ij}\xi_{mn} &\geq k_1\xi_{ij}\xi_{ij}, \quad k_1 > 0, \quad \text{for all } \xi_{ij},\\
d_{ijkl}\xi_{ij}\xi_{mn} &\geq k_2\xi_{ij}\xi_{ij}, \quad k_2 > 0, \quad \text{for all } \xi_{ij} = \xi_{ji},\\
a_{ij}\xi_i\xi_j &\geq k_3\xi_i\xi_i, \quad k_3 > 0, \quad \text{for all } \xi_i,\\
b_{ij}\xi_i\xi_j &\geq k_4\xi_i\xi_i, \quad k_4 > 0, \quad \text{for all } \xi_i,\\
\kappa_{ij}\xi_i\xi_j &\geq k_5\xi_i\xi_i, \quad k_5 > 0, \quad \text{for all } \xi_i.
\end{aligned} \tag{8}$$

The components of the surface traction t_i, the surface couple m_i, the heat flux q and the diffusion flux η, at regular points of ∂B, are given by

$$t_i = \sigma_{ji}n_j, \quad m_i = \mu_{ji}n_j, \quad q = q_in_i, \quad \eta = \eta_in_i,$$

respectively. By n_i we denoted the components of the outward unit normal of surface ∂B. Now, we admit the following prescribed boundary conditions:

$$\begin{aligned}
u_i &= 0 \quad \text{on } \partial B_1 \times [0,\infty), \qquad t_i = 0 \quad \text{on } \partial B_1^c \times [0,\infty),\\
\phi_i &= 0 \quad \text{on } \partial B_2 \times [0,\infty), \qquad m_i = 0 \quad \text{on } \partial B_2^c \times [0,\infty),\\
\theta &= 0 \quad \text{on } \partial B_3 \times [0,\infty), \qquad q = 0 \quad \text{on } \partial B_3^c \times [0,\infty),\\
P &= 0 \quad \text{on } \partial B_4 \times [0,\infty), \qquad \eta = 0 \quad \text{on } \partial B_4^c \times [0,\infty).
\end{aligned} \tag{9}$$

Here ∂B_1, ∂B_2, ∂B_3 and ∂B_4 with respective complements ∂B_1^c, ∂B_2^c, ∂B_3^c and ∂B_4^c are subsets of the surface ∂B such that

$$\begin{aligned}
&\partial B_1 \cap \partial B_1^c = \partial B_2 \cap \partial B_2^c = \partial B_3 \cap \partial B_3^c = \partial B_4 \cap \partial B_4^c = \varnothing,\\
&\partial B_1 \cup \partial B_1^c = \partial B_2 \cup \partial B_2^c = \partial B_3 \cup \partial B_3^c = \partial B_4 \cup \partial B_4^c = \partial B.
\end{aligned}$$

Introducing the constitutive equations (4) into equations (1)–(3) we obtain the system of equations

$$\begin{aligned}
\rho\ddot{u}_i &= c_{ijkl}\varepsilon_{kl,\,i} + p_{ijkl}\phi_{kl,\,j} + a_{ij}\theta_{,\,j} + b_{ij}C_{,\,j},\\
\rho J_{ij}\ddot{\phi}_j &= p_{ijkl}\varepsilon_{kl,\,j} + d_{ijkl}\phi_{kl,\,j} + p_{ij}\theta_{,\,j} + q_{ij}C_{,\,j}\\
&\quad + \epsilon_{ijk}[c_{jkml}\varepsilon_{ml} + p_{jkml}\phi_{ml} + a_{jk}\theta + \beta_{jk}C],\\
\kappa_{ij}\theta_{,\,ij} &= \varrho c_E\dot{\theta} - T_0 a_{ij}\dot{\varepsilon}_{ij} - T_0 p_{ij}\dot{\phi}_{ij} + T_0\varpi\dot{C}\\
\dot{C} &= d_{ij}(\varrho C + b_{ij}\varepsilon_{ij} + q_{ij}\phi_{ij} - \varpi\theta)_{,\,ij},
\end{aligned} \tag{10}$$

To this system of equations we adjoin the initial conditions

$$\begin{aligned}
&u_i(x,0) = u_i^0(x), \qquad \dot{u}_i(x,0) = u_i^1(x), \qquad \phi_i(x,0) = \phi_i^0(x), \qquad \dot{\phi}_i(x,0) = \phi_i^1(x),\\
&\theta(x,0) = \theta^0(x), \qquad \dot{\theta}(x,0) = \theta^1(x), \qquad C(x,0) = C^0(x), \qquad x \in B.
\end{aligned} \tag{11}$$

By a solution of the mixed initial boundary value problem of micropolar thermoelastic diffusion in the cylinder $\Omega_0 = B \times [0,\infty)$ we mean an ordered array $(u_i,\ \phi_i,\ \theta,\ C)$ which satisfies the system of equations (10) for all $(x,t) \in \Omega_0$, the boundary conditions (9) and the initial conditions (11).

Let us observe that if $\mathrm{meas}(\partial B_1) = 0$ and $\mathrm{meas}(\partial B_2) = 0$ then there exists a family of rigid motions and null temperature and null diffusion which satisfy the equations (10) and null boundary conditions. In this way we can decompose the initial data (u_i^0, u_i^1) and (ϕ_i^0, ϕ_i^1) as

$$u_i^0 = u_i^* + U_i^0, \quad u_i^1 = \dot{u}_i^* + U_i^1, \quad \phi_i^0 = \phi_i^* + \Phi_i^0, \quad \phi_i^1 = \dot{\phi}_i^* + \Phi_i^1, \tag{12}$$

where $(u_i^*, \dot{u}_i^*)$ are rigid displacements and $(\phi_i^*, \dot{\phi}_i^*)$ are rigid microrotations determined such that (U_i^0, U_i^1) and (Φ_i^0, Φ_i^1) satisfy the restrictions

$$\begin{aligned}
&\int_B (\rho U_i^0 + \rho J_{ij}\Phi_j^0)\,dV = 0, \qquad \int_B \rho\epsilon_{ijk}x_j(U_k^0 + J_{lk}\Phi_l^0)\,dV = 0,\\
&\int_B (\rho U_i^1 + \rho J_{ij}\Phi_j^1)\,dV = 0, \qquad \int_B \rho\epsilon_{ijk}x_j(U_k^1 + J_{lk}\Phi_l^1)\,dV = 0,
\end{aligned} \tag{13}$$

where ϵ_{ijk} is Ricci's tensor.

Similarly, if $\mathrm{meas}(\partial B_3) = 0$ then there exists a family of constant temperatures, null displacements, null microrotations and null diffusion which satisfy the equations (10) and null boundary conditions. Thus, we can decompose the initial data θ^0 and θ^1 in the form

$$\theta^0 = \theta^* + T^0, \quad \theta^1 = \dot{\theta}^* + T^1, \tag{14}$$

where θ^* and $\dot{\theta}^*$ are constants temperatures determined such that T^0 and T^1 satisfy the restrictions

$$\int_B T^0 dV = 0, \qquad \int_B T^1 dV = 0. \tag{15}$$

3. Specific notations

We denote by $C^m(B)$ the class of scalar functions possessing derivatives up to the m-th order in the domain B which are continuous on B.

For $f \in C^m(B)$ we define the norm

$$\|f\|_{C^m(B)} = \sum_{k=1}^{m} \sum_{i_1,i_2,\dots,i_k} \max |f_{,\, i_1 i_2 \dots i_k}|.$$

By $\boldsymbol{C}^m(B)$ we denote the class of vector fields with six components $C^m(B)$.

For $\boldsymbol{w} \in \boldsymbol{C}^m(B)$ we define the norm

$$\|\boldsymbol{w}\|_{\boldsymbol{C}^m(B)} = \sum_{i=1}^{6} \|w_i\|_{C^m(B)}.$$

By $W_m(B)$ we denote the Hilbert space obtained as the completion of the space $C^m(B)$ by means of the norm $\|\cdot\|_{W_m(B)}$ induced by the inner product

$$(f, g)_{W_m(B)} = \sum_{k=1}^{m} \sum_{i_1,i_2,\dots,i_k} \int_B f_{,\, i_1 i_2 \dots i_k} g_{,\, i_1 i_2 \dots i_k}\, dV.$$

Finally, we will denote by $\boldsymbol{W}_m(B)$ the space obtained as the completion of the space $\boldsymbol{C}^m(B)$ by means of the norm $\|\cdot\|_{\boldsymbol{W}_m(B)}$ induced by the inner product

$$(\boldsymbol{u}, \boldsymbol{v})_{\boldsymbol{W}_m(B)} = \sum_{i=1}^{6} (u_i, v_i)_{W_m(B)}.$$

We will use as norm in Cartesian product of the normed spaces the sum of the norms of the factor spaces. Let us introduce the notation

$$\widehat{C}^1(B) = \big\{\chi \in C^1(B) : \chi = 0 \text{ on } \partial B_3 \text{ or } \chi = 0 \text{ on } \partial B_4; \quad \text{if } \operatorname{meas}(\partial B_3) = 0 \text{ or } \operatorname{meas}(\partial B_4) = 0 \text{ then } \textstyle\int_B \chi\, dV = 0\big\},$$

$$\widehat{\boldsymbol{C}}^1(B) = \big\{(v_i, \psi_i) \in \boldsymbol{C}^1(B) : v_i = 0 \text{ on } \partial B_1,\ \psi_i = 0 \text{ on } \partial B_2; \quad \text{if } \operatorname{meas}(\partial B_1) = \operatorname{meas}(\partial B_2) = 0 \text{ then } \textstyle\int_B (\rho v_i + \rho J_{ij} \psi_j)\, dV = 0\big\},$$

$\widehat{W}_1(B)$ = the completion of $\widehat{C}^1(B)$ by means of the norm $\|\cdot\|_{W_1(B)}$,

$\widehat{\boldsymbol{W}}_1(B)$ = the completion of $\widehat{\boldsymbol{C}}^1(B)$ by means of the norm $\|\cdot\|_{\boldsymbol{W}_1(B)}$.

In this notation $W_m(B)$ represents the familiar Sobolev space (see [Adams 1975]) and $\boldsymbol{W}_m(B)$ is the Cartesian product $\boldsymbol{W}_m(B) = [W_m(B)]^6$.

The hypothesis (11) assures that the following (Korn's inequality) holds (see [Hlaváček and Nečas 1970a; 1970b]):

$$\int_B [c_{ijkl}\varepsilon_{kl}(\boldsymbol{u})\varepsilon_{ij}(\boldsymbol{u}) + 2p_{klij}\varepsilon_{kl}(\boldsymbol{u})\phi_{ij}(\boldsymbol{u}) + d_{klij}\phi_{kl}(\boldsymbol{u})\phi_{ij}(\boldsymbol{u})] \geq m_1 \int_B (u_i u_i + u_{i,j}u_{i,j} + \phi_i\phi_i + \phi_{i,j}\phi_{i,j})\, dV, \quad (16)$$

for all $\boldsymbol{u} = (u_i, \phi_i) \in \boldsymbol{W}_1(B)$, where m_1 is a constant, $m_1 > 0$, and

$$\varepsilon_{ji}(\boldsymbol{u}) = u_{i,\,j} - \varepsilon_{kji}\phi_k, \quad \phi_{ji}(\boldsymbol{u}) = \phi_{i,\,j}.$$

Also, using the hypothesis (8), the following (Poincaré's inequality) holds for all $(\chi, \pi) \in \widehat{W}_1(B) \times \widehat{W}_1(B)$:

$$\int_B (\kappa_{ij}\chi_{,i}\chi_{,j} + d_{ij}\pi_{,i}\pi_{,j})\,dV \geq m_2 \int_B (\chi^2 + \pi^2)\,dV, \tag{17}$$

where m_2 is a constant, $m_2 > 0$.

If $\operatorname{meas}(\partial B_1) = \operatorname{meas}(\partial B_2) = 0$ then we can decompose the solution $((u_i, \phi_i), \theta, C)$ in the form

$$u_i = u_i^* + t\dot{u}_i^* + v_i, \quad \phi_i = \phi_i^* + t\dot{\phi}_i^* + \psi_i, \quad \theta = \chi, \quad C = \pi, \tag{18}$$

where $((v_i, \psi_i), \chi, \pi) \in \widehat{\boldsymbol{W}}_1(B) \times \widehat{W}_1(B) \times \widehat{W}_1(B)$ represents the solution of the system of equations (10) with the boundary conditions (9) and the initial conditions

$$\begin{aligned} &v_i(x,0) = U_i^0(x), \quad \dot{v}_i(x,0) = U_i^1(x), \quad \psi_i(x,0) = \Phi_i^0(x), \quad \dot{\psi}_i(x,0) = \Phi_i^1(x), \\ &\chi(x,0) = \theta^0(x), \quad \dot{\chi}(x,0) = \theta^1(x), \quad P(x,0) = \mathcal{P}^0(x), \quad \text{for all } x \in B. \end{aligned}$$

Now, we consider that $\operatorname{meas}(\partial B_4) = 0$.

Then we can decompose the solution $((u_i, \phi_i), \theta, C)$ in the form

$$u_i = v_i, \phi_i = \psi_i, \theta = \theta^* + \chi, C = \pi \tag{19}$$

where $((v_i, \psi_i), \chi, \pi) \in \widehat{\boldsymbol{W}}_1(B) \times \widehat{W}_1(B) \times \widehat{W}_1(B)$ represents the solution of the system of equations (10) with the boundary conditions initial conditions

$$\begin{aligned} &v_i(x,0) = u_i^0(x), \quad \dot{v}_i(x,0) = u_i^1(x), \quad \psi_i(x,0) = \varphi_i^0(x), \quad \dot{\psi}_i(x,0) = \varphi_i^1(x), \\ &\chi(x,0) = T^0(x), \quad \dot{\chi}(x,0) = T^1(x), \quad \pi(x,0) = C^0(x), \quad \text{for all } x \in B. \end{aligned} \tag{20}$$

4. Preliminary results

In this section we shall establish some evolutionary integral identities which form the basis in proving the relations that express the asymptotic partition of energy. In the first next theorem we prove a conservation law of total energy.

Theorem 1. *Let $((u_i, \phi_i), \theta, C)$ be a solution of the mixed initial boundary value problem defined by the equations (10), the boundary conditions (9) and the initial conditions (11). If we suppose that*

$$(u_i^0, \phi_i^0) \in \boldsymbol{W}_1(B), \quad (u_i^1, \phi_i^1) \in \boldsymbol{W}_0(B), \quad (\theta^0, C^0) \in W_1(B) \times W_1(B), \quad \theta^1 \in W_0(B),$$

then the following energy conservation law holds:

$$\mathscr{E}(t) + \frac{1}{T_0}\int_0^t \int_B \kappa_{ij}\theta_{,i}(s)\theta_{,j}(s)\,dV\,ds + \int_0^t \int_B C(s)\dot{P}(s)\,dV\,ds = \mathscr{E}(0) \tag{21}$$

for any $t \in [0, \infty)$, where

$$\begin{aligned} \mathscr{E}(t) = \frac{1}{2}\int_B [\rho\dot{u}_i(t)\dot{u}_i(t) + \rho J_{ij}\dot{\phi}_i(t)\dot{\phi}_j(t) + \frac{\rho c_E}{T_0}\theta^2(t) + 2\varpi C(t)\theta(t) - \varrho C^2(t)]\,dV \\ + \frac{1}{2}\int_B [c_{ijkl}\varepsilon_{ij}(t)\varepsilon_{kl}(t) + 2p_{ijkl}\varepsilon_{ij}(t)\phi_{kl}(t) + d_{ijkl}\phi_{ij}(t)\phi_{kl}(t)]\,dV. \end{aligned}$$

Proof. In view of equations of motion $(10)_1$, we get

$$\begin{aligned}\frac{1}{2}\frac{d}{ds}[\rho\dot{u}_i(s)\dot{u}_i(s)] &= \rho\dot{u}_i(s)\ddot{u}_i(s) = \dot{u}_i(s)\sigma_{ij,\,j}(s)\\ &= \dot{u}_i(s)[c_{ijkl}\varepsilon_{kl}(s) + p_{ijkl}\phi_{kl}(s) + a_{ij}\theta(s) + b_{ij}C(s)]_{,\,j}\\ &= \{\dot{u}_i(s)[c_{ijkl}\varepsilon_{kl}(s) + p_{ijkl}\phi_{kl}(s) + a_{ij}\theta(s) + b_{ij}C(s)]\}_{,\,j}\\ &\quad - [c_{ijkl}\varepsilon_{kl}(s) + p_{ijkl}\phi_{kl}(s) + a_{ij}\theta(s) + b_{ij}C(s)]\dot{u}_{i,\,j}(s). \end{aligned} \tag{22}$$

Taking into account the equation $(10)_2$, we obtain

$$\begin{aligned}&\frac{1}{2}\frac{d}{ds}[\rho J_{ij}\dot{\phi}_i(s)\dot{\phi}_j(s)]\\ &\quad = \rho J_{ij}\dot{\phi}_i(s)\ddot{\phi}_j(s) = \dot{\phi}_i(s)[\mu_{ij,\,j}(s) + \epsilon_{ijk}\sigma_{jk}(s)]\\ &\quad = \dot{\phi}_i(s)\{[p_{ijkl}\varepsilon_{kl}(s) + d_{ijkl}\phi_{kl}(s) + p_{ij}\theta(s) + q_{ij}C(s)]_{,\,j} + \epsilon_{ijk}\sigma_{jk}(s)\}\\ &\quad = \{\dot{\phi}_i(s)[p_{ijkl}\varepsilon_{kl}(s) + d_{ijkl}\phi_{kl}(s) + p_{ij}\theta(s) + q_{ij}C(s)]\}_{,\,j}\\ &\qquad - [p_{ijkl}\varepsilon_{kl}(s) + d_{ijkl}\phi_{kl}(s) + p_{ij}\theta(s) + q_{ij}C(s)]\dot{\phi}_{ij}(s)\\ &\qquad + \epsilon_{ijk}[c_{jkmn}\varepsilon_{mn}(s) + d_{jkmn}\phi_{mn}(s) + a_{jk}\theta(s) + b_{jk}C(s)]\dot{\phi}_i(s). \end{aligned} \tag{23}$$

Now we are adding equalities (22) and (23) member by member:

$$\begin{aligned}&\frac{1}{2}\frac{d}{ds}[\rho\dot{u}_i(s)\dot{u}_i(s) + \rho J_{ij}\dot{\phi}_i(s)\dot{\phi}_j(s)]\\ &\quad = \{\dot{u}_i(s)[c_{ijkl}\varepsilon_{kl}(s) + p_{ijkl}\phi_{kl}(s) + a_{ij}\theta(s) + b_{ij}C(s)]\}_{,\,j}\\ &\qquad + \{\dot{\phi}_i(s)[p_{ijkl}\varepsilon_{kl}(s) + d_{ijkl}\phi_{kl}(s) + p_{ij}\theta(s) + q_{ij}C(s)]\}_{,\,j}\\ &\qquad - c_{ijkl}\varepsilon_{kl}(s)\dot{\varepsilon}_{ij}(s) - p_{ijkl}(\phi_{kl}(s)\dot{\varepsilon}_{ij}(s) + \dot{\phi}_{kl}(s)\varepsilon_{ij}(s)) - d_{ijkl}\phi_{kl}(s)\dot{\phi}_{ij}(s)\\ &\qquad - \theta(s)[a_{ij}\dot{\varepsilon}_{ij}(s) + p_{ij}\dot{\phi}_{ij}(s)] - C(s)[b_{ij}\dot{\varepsilon}_{ij}(s) + q_{ij}\dot{\phi}_{ij}(s)]. \end{aligned} \tag{24}$$

On the other hand, by using the equations $(10)_4$ and $(10)_5$, we get

$$\begin{aligned}&\theta(s)[a_{ij}\dot{\varepsilon}_{ij}(s) + p_{ij}\dot{\phi}_{ij}(s)] + C(s)[b_{ij}\dot{\varepsilon}_{ij}(s) + q_{ij}\dot{\phi}_{ij}(s)]\\ &\qquad = \frac{1}{2}\frac{d}{ds}[\frac{\rho c_E}{T_0}\theta^2(s) + 2\varpi C(s)\theta(s) - \varrho C^2(s)] + C(s)\dot{P}(s) - \frac{1}{T_0}\kappa_{ij}\theta_{,\,ij}(s)\theta(s). \end{aligned} \tag{25}$$

From (24) and (25) we deduce

$$\begin{aligned}&\frac{1}{2}\frac{d}{ds}[\rho\dot{u}_i(s)\dot{u}_i(s) + \rho J_{ij}\dot{\phi}_i(s)\dot{\phi}_j(s) + \frac{\rho c_E}{T_0}\theta^2(s) + 2\varpi C(s)\theta(s) - \varrho C^2(s)]\\ &\quad = \{\dot{u}_i(s)[c_{ijkl}\varepsilon_{kl}(s) + p_{ijkl}\phi_{kl}(s) + a_{ij}\theta(s) + b_{ij}C(s)]\}_{,\,j}\\ &\qquad + \{\dot{\phi}_i(s)[p_{ijkl}\varepsilon_{kl}(s) + d_{ijkl}\phi_{kl}(s) + p_{ij}\theta(s) + q_{ij}C(s)]\}_{,\,j}\\ &\qquad - c_{ijkl}\varepsilon_{kl}(s)\dot{\varepsilon}_{ij}(s) - p_{ijkl}(\phi_{kl}(s)\dot{\varepsilon}_{ij}(s) + \dot{\phi}_{kl}(s)\varepsilon_{ij}(s))\\ &\qquad - d_{ijkl}\phi_{kl}(s)\dot{\phi}_{ij}(s) - C(s)\dot{P}(s) + \frac{1}{T_0}\kappa_{ij}\theta_{,\,ij}(s)\theta(s), \end{aligned}$$

and this equality can be restated in the form

$$\begin{aligned}
&\frac{1}{2}\frac{d}{ds}\Big[\rho\dot{u}_i(s)\dot{u}_i(s)+\rho J_{ij}\dot{\phi}_i(s)\dot{\phi}_j(s)+\frac{\rho c_E}{T_0}\theta^2(s)+2\varpi C(s)\theta(s)-\varrho C^2(s)\Big]\\
&\quad+\frac{1}{2}\frac{d}{ds}[\cdot c_{ijkl}\varepsilon_{kl}(s)\varepsilon_{ij}(s)+2p_{ijkl}\varepsilon_{ij}(s)\phi_{kl}(s)+d_{ijkl}\phi_{kl}(s)\phi_{ij}(s)]\\
&\quad+\frac{1}{T_0}\kappa_{ij}\theta_{,\,i}(s)\theta_{,\,j}(s)-C(s)\dot{P}(s)\\
&=\{\dot{u}_i(s)[c_{ijkl}\varepsilon_{kl}(s)+p_{ijkl}\phi_{kl}(s)+a_{ij}\theta(s)+b_{ij}C(s)]\}_{,\,j}\\
&\quad+\{\dot{\phi}_i(s)[p_{ijkl}\varepsilon_{kl}(s)+d_{ijkl}\phi_{kl}(s)+p_{ij}\theta(s)+q_{ij}C(s)]\}_{,\,j}+\Big(\frac{1}{T_0}\kappa_{ij}\theta_{,\,i}(s)\theta(s)\Big)_{,\,j}. \qquad (26)
\end{aligned}$$

Now, we integrate the relation (26) over $B\times(0,t)$ and use the divergence theorem, the symmetry relations (6), the boundary conditions (9) and the initial conditions (11) so that we arrive at the desired result (21) and Theorem 1 is concluded. □

Theorem 2. *Consider $((u_i,\phi_i),\theta,C)$ a solution of the mixed initial boundary value problem defined by the equations (10), the boundary conditions (9) and the initial conditions (11). If we suppose that*

$$(u_i^0,\phi_i^0)\in \boldsymbol{W}_1(B),\ (u_i^1,\phi_i^1)\in \boldsymbol{W}_0(B),\ (\theta^0,C^0)\in W_1(B)\times W_1(B),\ \theta^1\in W_0(B),$$

then the following identity holds:

$$\begin{aligned}
&2\int_B[\rho u_i(t)\dot{u}_i(t)+\rho J_{ij}\phi_i(t)\dot{\phi}_j(t)]\,dV\\
&\quad+\int_B\frac{1}{T_0}k_{ij}\Big(\int_0^t\theta_{,i}(s)\,ds\Big)\Big(\int_0^t\theta_{,\,j}(s)\,ds\Big)\,dV+\int_B d_{ij}\Big(\int_0^t P_{,i}(s)\,ds\Big)\Big(\int_0^t P_{,j}(s)\,ds\Big)\,dV\\
&=2\int_0^t\int_B[\rho\dot{u}_i(s)\dot{u}_i(s)+\rho J_{ij}\dot{\phi}_i(s)\dot{\phi}_j(s)]\,dV\,ds\\
&\quad-\int_0^t\int_B[c_{ijkl}\varepsilon_{kl}(s)\varepsilon_{ij}(s)+2p_{ijkl}\phi_{kl}(s)\varepsilon_{ij}(s)+d_{ijkl}\phi_{kl}(s)\phi_{ij}(s)]\,dV\,ds\\
&\quad-\int_0^t\int_B[\frac{\rho c_E}{T_0}\theta^2(s)+2\varpi C(s)\theta(s)-\varrho C^2(s)]\,dV\,ds+2\int_0^t\int_B[\rho S^0\theta(s)-P^0C(s)]\,dV\,ds\\
&\quad+2\int_B[\rho u_i^0\dot{u}_i^1+\rho J_{ij}\phi_i^0\dot{\phi}_j^1]\,dV, \qquad (27)
\end{aligned}$$

where

$$\begin{aligned}
\rho S^0&=\frac{\rho c_E}{T_0}\theta^0-a_{ij}\varepsilon_{ij}^0-p_{ij}\phi_{ij}^0+\varpi C^0,\\
P^0&=b_{ij}\varepsilon_{ij}^0+q_{ij}\phi_{ij}^0-\varpi\theta^0+\varrho C^0\\
\varepsilon_{ji}^0&=u_{i,\,j}^0-\epsilon_{kji}\phi_k^0,\\
\phi_{ji}^0&=\phi_{i,\,j}^0.
\end{aligned} \qquad (28)$$

Proof. In view of equations of motion $(10)_1$, we get

$$\begin{aligned}\frac{d}{ds}[\rho u_i(s)\dot{u}_i(s)] &= \rho\dot{u}_i(s)\dot{u}_i(s)+\rho u_i(s)\ddot{u}_i(s)=\rho\dot{u}_i(s)\dot{u}_i(s)+u_i(s)\sigma_{ij,\,j}(s)\\ &=\rho\dot{u}_i(s)\dot{u}_i(s)+u_i(s)[c_{ijkl}\varepsilon_{kl}(s)+p_{ijkl}\phi_{kl}(s)+a_{ij}\theta(s)+b_{ij}C(s)]_{,\,j}\\ &=\rho\dot{u}_i(s)\dot{u}_i(s)+\{u_i(s)[c_{ijkl}\varepsilon_{kl}(s)+p_{ijkl}\phi_{kl}(s)+a_{ij}\theta(s)+b_{ij}C(s)]\}_{,\,j}\\ &\quad-u_{i,\,j}(s)[c_{ijkl}\varepsilon_{kl}(s)+p_{ijkl}\phi_{kl}(s)+a_{ij}\theta(s)+b_{ij}C(s)]\\ &=\rho\dot{u}_i(s)\dot{u}_i(s)-[c_{ijkl}\varepsilon_{kl}(s)+p_{ijkl}\phi_{kl}(s)+a_{ij}\theta(s)+b_{ij}C(s)]u_{i,\,j}(s)\\ &\quad+\{u_i(s)[c_{ijkl}\varepsilon_{kl}(s)+p_{ijkl}\phi_{kl}(s)+a_{ij}\theta(s)+b_{ij}C(s)]\}_{,\,j}. \end{aligned}\tag{29}$$

Taking into account the equations of motion $(10)_2$, we obtain

$$\begin{aligned}\frac{d}{ds}[\rho J_{ij}\phi_i(s)\dot{\phi}_j(s)] &= \rho J_{ij}\dot{\phi}_i(s)\dot{\phi}_j(s)+\rho J_{ij}\phi_i(s)\ddot{\phi}_j(s)\\ &=\rho J_{ij}\dot{\phi}_i(s)\dot{\phi}_j(s)+\phi_i(s)[p_{ijkl}\varepsilon_{kl}(s)+d_{ijkl}\phi_{kl}(s)+p_{ij}\theta(s)+q_{ij}C(s)]_{,\,j}\\ &\quad+\epsilon_{ijk}[c_{jkmn}\varepsilon_{mn}(s)+d_{jkmn}\phi_{mn}(s)+a_{jk}\theta(s)+b_{jk}C(s)]\phi_i\\ &=\rho J_{ij}\dot{\phi}_i(s)\dot{\phi}_j(s)+\{\phi_i(s)[p_{ijkl}\varepsilon_{kl}(s)+d_{ijkl}\phi_{kl}(s)+a_{ij}\theta(s)+b_{ij}C(s)]\}_{,\,j}\\ &\quad-[p_{ijkl}\varepsilon_{kl}(s)+d_{ijkl}\phi_{kl}(s)+p_{ij}\theta(s)+q_{ij}C(s)]\phi_{i,\,j}(s)\\ &\quad+\epsilon_{ijk}[c_{jkmn}\varepsilon_{mn}(s)+p_{jkmn}\phi_{mn}(s)+a_{jk}\theta(s)+b_{jk}C(s)]\phi_i. \end{aligned}\tag{30}$$

Now we are adding equalities (29) and (30) member by member:

$$\begin{aligned}\frac{d}{ds}[\rho u_i(s)\dot{u}_i(s)+\rho J_{ij}\phi_i(s)\dot{\phi}_j(s)] &= \rho\dot{u}_i(s)\dot{u}_i(s)+\rho J_{ij}\dot{\phi}_i(s)\dot{\phi}_j(s)\\ &\quad+\{u_i(s)[c_{ijkl}\varepsilon_{kl}(s)+p_{ijkl}\phi_{kl}(s)+a_{ij}\theta(s)+b_{ij}C(s)]\}_{,\,j}\\ &\quad+\{\phi_i(s)[p_{ijkl}\varepsilon_{kl}(s)+d_{ijkl}\phi_{kl}(s)+p_{ij}\theta(s)+q_{ij}C(s)]\}_{,\,j}\\ &\quad-c_{ijkl}\varepsilon_{kl}(s)\varepsilon_{ij}(s)-2p_{ijkl}\varepsilon_{ij}(s)\phi_{kl}(s)-d_{ijkl}\phi_{kl}(s)\phi_{ij}(s)\\ &\quad-[a_{ij}\varepsilon_{ij}(s)+p_{ij}\phi_{ij}(s)]\theta(s)-[b_{ij}\varepsilon_{ij}(s)+q_{ij}\phi_{ij}(s)]C(s). \end{aligned}\tag{31}$$

By an integration with respect to time variable in the equation $(10)_3$ and then by using the initial conditions (11) we deduce

$$\begin{aligned}&-[a_{ij}\varepsilon_{ij}(s)+p_{ij}\phi_{ij}(s)]\\ &\qquad=\frac{1}{T_0}\left(\int_0^s\kappa_{ij}\theta_{,\,i}(z)\,dz\right)_{,\,j}-\frac{\rho c_E}{T_0}\theta(s)-\varpi C(s)+\frac{\rho c_E}{T_0}\theta^0+\varpi C^0-a_{ij}\varepsilon_{ij}^0-p_{ij}\phi_{ij}^0.\end{aligned}$$

Here we multiply by $\theta(s)$ and obtain

$$\begin{aligned}-[a_{ij}\varepsilon_{ij}(s)+p_{ij}\phi_{ij}(s)]\theta(s) &= \frac{1}{T_0}\left(\int_0^s\kappa_{ij}\theta_{,\,i}(z)\,dz\right)_{,\,j}\theta(s)\\ &\quad-\frac{\rho c_E}{T_0}\theta^2(s)-\varpi C(s)\theta(s)+\left(\frac{\rho c_E}{T_0}\theta^0-a_{ij}\varepsilon_{ij}^0-p_{ij}\phi_{ij}^0+\varpi C^0\right)\theta(s). \end{aligned}\tag{32}$$

Also, by integrating with respect to the time variable, from Fick's law and the initial conditions (11) we deduce

$$b_{ij}\varepsilon_{ij}(s)+q_{ij}\phi_{ij}(s)=\left(\int_0^s d_{ij}P_{,i}(z)\,dz\right)_{,j}+\varpi\theta(s)-\varrho C(s)+b_{ij}\varepsilon_{ij}^0+q_{ij}\phi_{ij}^0-\varpi\theta^0+\varrho C^0.$$

Here we multiply by $C(s)$ so that we are led to

$$\begin{aligned}-[b_{ij}\varepsilon_{ij}(s)+q_{ij}\phi_{ij}(s)]C(s)=&-\left(\int_0^s d_{ij}\ P_{,i}(z)\,dz\right)_{,j}C(s)\\&-\varpi\theta(s)C(s)+\varrho C^2(s)-(b_{ij}\varepsilon_{ij}^0+q_{ij}\phi_{ij}^0-\varpi\theta^0+\varrho C^0)C(s).\end{aligned}\tag{33}$$

By adding relations (32) and (33) member by member one obtains

$$\begin{aligned}&-[a_{ij}\varepsilon_{ij}(s)+p_{ij}\phi_{ij}(s)]\theta(s)-[b_{ij}\varepsilon_{ij}(s)+q_{ij}\phi_{ij}(s)]C(s)\\&\quad=\frac{1}{T_0}\left(\int_0^s\kappa_{ij}\theta_{,i}(z)\,dz\right)_{,j}\theta(s)-\frac{\rho c_E}{T_0}\theta^2(s)-\varpi C(s)\theta(s)\\&\qquad+\left(\frac{\rho c_E}{T_0}\theta^0-a_{ij}\varepsilon_{ij}^0-p_{ij}\phi_{ij}^0+\varpi C^0\right)\theta(s)\\&\qquad-\left(\int_0^s d_{ij}P_{,i}(z)\,dz\right)_{,j}C(s)-\varpi\theta(s)C(s)+\varrho C^2(s)\\&\qquad-(b_{ij}\varepsilon_{ij}^0+q_{ij}\phi_{ij}^0-\varpi\theta^0+\varrho C^0)C(s).\end{aligned}\tag{34}$$

We introduce in (34) into (31) so that we get the equality

$$\begin{aligned}&\frac{d}{ds}[\rho u_i(s)\dot u_i(s)+\rho J_{ij}\phi_i(s)\dot\phi_j(s)]\\&\quad=\rho\dot u_i(s)\dot u_i(s)+\rho J_{ij}\dot\phi_i(s)\dot\phi_j(s)\\&\qquad+\{u_i(s)[c_{ijkl}\varepsilon_{kl}(s)+p_{ijkl}\phi_{kl}(s)+a_{ij}\theta(s)+b_{ij}C(s)]\}_{,j}\\&\qquad+\{\phi_i(s)[p_{ijkl}\varepsilon_{kl}(s)+d_{ijkl}\phi_{kl}(s)+p_{ij}\theta(s)+q_{ij}C(s)]\}_{,j}\\&\qquad-c_{ijkl}\varepsilon_{kl}(s)\varepsilon_{ij}(s)-2p_{ijkl}\phi_{kl}(s)\varepsilon_{ij}(s)-d_{ijkl}\phi_{kl}(s)\phi_{ij}(s)\\&\qquad+\frac{1}{T_0}\left(\int_0^s\kappa_{ij}\theta_{,i}(z)\,dz\right)_{,j}\theta(s)-\frac{\rho c_E}{T_0}\theta^2(s)-\varpi C(s)\theta(s)\\&\qquad+\left(\frac{\rho c_E}{T_0}\theta^0-a_{ij}\varepsilon_{ij}^0-p_{ij}\phi_{ij}^0+\varpi C^0\right)\theta(s)\\&\qquad-\left(\int_0^s d_{ij}P_{,i}(z)\,dz\right)_{,j}C(s)-\varpi\theta(s)C(s)+\varrho C^2(s)\\&\qquad-(b_{ij}\varepsilon_{ij}^0+q_{ij}\phi_{ij}^0-\varpi\theta^0+\varrho C^0)C(s).\end{aligned}$$

This relation can be restated in the form

$$\begin{aligned}
&\frac{d}{ds}[\rho u_i(s)\dot{u}_i(s)+\rho J_{ij}\phi_i(s)\dot{\phi}_j(s)]\\
&\quad=\rho\dot{u}_i(s)\dot{u}_i(s)+\rho J_{ij}\dot{\phi}_i(s)\dot{\phi}_j(s)\\
&\qquad+\{u_i(s)[c_{ijkl}\varepsilon_{kl}(s)+p_{ijkl}\phi_{kl}(s)+a_{ij}\theta(s)+b_{ij}C(s)]\}_{,\,j}\\
&\qquad+\{\phi_i(s)[p_{ijkl}\varepsilon_{kl}(s)+d_{ijkl}\phi_{kl}(s)+p_{ij}\theta(s)+q_{ij}C(s)]\}_{,\,j}\\
&\qquad-c_{ijkl}\varepsilon_{kl}(s)\varepsilon_{ij}(s)-2p_{ijkl}\phi_{kl}(s)\varepsilon_{ij}(s)-d_{ijkl}\phi_{kl}(s)\phi_{ij}(s)\\
&\qquad+\rho S^0\theta(s)-P^0C(s)-\frac{\rho c_E}{T_0}\theta^2(s)-2\varpi C(s)\theta(s)+\varrho C^2\\
&\qquad+\frac{1}{T_0}(\kappa_{ij}\theta(s)\int_0^s\theta_{,\,i}(z)\,dz)_{,\,j}-\frac{1}{T_0}\kappa_{ij}\theta_{,\,j}(s)\int_0^s\theta_{,\,i}(z)\,dz\\
&\qquad-(d_{ij}P(s)\int_0^s P_{,\,i}(z)\,dz)_{,\,j}-d_{ij}P_{,\,j}(s)\int_0^s P_{,\,i}(z)\,dz,
\end{aligned}\tag{35}$$

where ρS^0 and P^0 are given in (28).

Integrating by parts, it is easy to obtain

$$\kappa_{ij}\int_0^t\theta_{,\,i}(s)\left(\int_0^s\theta_{,\,j}(z)\,dz\right)ds=k_{ij}\int_0^s\theta_{,\,j}(z)\,dz\int_0^s\theta_{,\,i}(z)\,dz\Big|_{s=0}^{s=t}-k_{ij}\int_0^t\theta_{,\,j}(s)\left(\int_0^s\theta_{,\,i}(z)\,dz\right)ds.$$

On the basis of symmetry of tensor κ_{ij}, from the above equality we deduce that

$$2\kappa_{ij}\int_0^t\theta_{,\,i}(s)\left(\int_0^s\theta_{,\,j}(z)\,dz\right)ds=\kappa_{ij}\left(\int_0^t\theta_{,\,i}(s)\,ds\right)\left(\int_0^t\theta_{,\,j}(s)\,ds\right).\tag{36}$$

Analogous, on the basis of symmetry of tensor d_{ij}, we obtain the equality

$$2d_{ij}\int_0^t P_{,\,i}(s)\left(\int_0^s P_{,\,j}(z)\,dz\right)ds=d_{ij}\left(\int_0^t P_{,\,i}(s)\,ds\right)\left(\int_0^t P_{,\,j}(s)\,ds\right).\tag{37}$$

Now we integrate the identity (35) over $B\times(0,t)$, then we employ the divergence theorem, the boundary conditions (9), the initial conditions (11), the symmetry relations (6) and relations (36)–(37) so that we are led to the desired identity (27).

This concludes Theorem 2. □

Theorem 3. *Consider $((u_i,\phi_i),\theta,C)$ a solution of the mixed initial boundary value problem defined by the equations (10), the boundary conditions (9) and the initial conditions (11). If we suppose that*

$$(u_i^0,\varphi_i^0)\in\boldsymbol{W}_1(B),\quad (u_i^1,\varphi_i^1)\in\boldsymbol{W}_0(B),\quad (\theta^0,C^0)\in W_1(B)\times W_1(B),\quad \theta^1\in W_0(B),$$

then we have the identity

$$2\int_B [\rho u_i(t)\dot{u}_i(t) + \rho J_{ij}\phi_i(t)\dot{\phi}_j(t)]\,dV + \int_B \kappa_{ij}\left[\left(\int_0^t \theta_{,\,i}(z)\,dz\right)\left(\int_0^t \theta_{,\,j}(z)\,dz\right)\right]dV + \int_B d_{ij}\left[\left(\int_0^t P_{,\,i}(z)\,dz\right)\left(\int_0^t P_{,\,j}(z)\,dz\right)\right]dV$$
$$= \int_B \{\varrho[u_i^0\dot{u}_i(2t) + u_i^1 u_i(2t)] + \rho J_{ij}[\phi_i^0\dot{\phi}_j(2t) + \phi_i^1\phi_j(2t)]\}\,dV + \int_0^t\int_B \{\rho S^0[\theta(t+s) - \theta(t-s)] + P^0[C(t+s) - C(t-s)]\}\,dV\,ds, \quad (38)$$

where ϱS^0 and P^0 are defined by relations (28).

Proof. It is not difficult to prove the identity

$$\frac{d}{ds}\{\rho[f_i(s)\dot{g}_i(s) - \dot{f}_i(s)g_i(s)]\} = \rho[f_i(s)\ddot{g}_i(s) - \ddot{f}_i(s)g_i(s)],$$

where $f_i(x, s)$ and $g_i(x, s)$ are twice continuously differentiable functions with respect to time variable s. By integrating the above identity over $B \times (0, t)$ one obtains

$$\int_B \varrho[f_i(s)\dot{g}_i(s) - \dot{f}_i(s)g_i(s)]\,dV = \int_0^t\int_B \varrho[f_i(s)\ddot{g}_i(s) - \ddot{f}_i(s)g_i(s)]\,dV\,ds + \int_B \varrho[f_i(0)\dot{g}_i(0) - \dot{f}_i(0)g_i(0)]\,dV. \quad (39)$$

Now, we set in (46) the functions f_i and g_i as follows:

$$f_i(x, s) = u_i(x, t-s), \quad g_i(x, s) = u_i(x, t+s) \quad \text{for } s \in [0, t],\ t \in (0, \infty),$$

so that one obtains the identity

$$2\int_B \rho u_i(t)\dot{u}_i(t)\,dV = \int_B \varrho[u_i^0\dot{u}_i(2t) + u_i^1 u_i(2t)]\,dV + \int_0^t\int_B \rho[u_i(t+s)\ddot{u}_i(t-s) - u_i(t-s)\ddot{u}_i(t+s)]\,dV\,ds, \quad t \in [0, \infty). \quad (40)$$

Similarly, if we substitute in (46) the functions f_i and g_i defined by

$$f_i(x, s) = \phi_i(x, t-s), \quad g_i(x, s) = \phi_i(x, t+s) \quad \text{for } s \in [0, t],\ t \in (0, \infty),$$

then we are led to the identity

$$2\int_B \rho J_{ij}\phi_i(t)\dot{\phi}_j(t)\,dV = \int_B \rho J_{ij}[\phi_i^0\dot{\phi}_j(2t) + \phi_i^1\phi_j(2t)]\,dV + \int_0^t\int_B \rho J_{ij}[\phi_i(t+s)\ddot{\phi}_j(t-s) - \phi_i(t-s)\ddot{\phi}_j(t+s)]\,dV\,ds, \quad t \in [0, \infty). \quad (41)$$

We add the equalities (40) and (41) member by member and obtain

$$
\begin{aligned}
&2\int_B [\rho u_i(t)\dot{u}_i(t) + \rho J_{ij}\phi_i(t)\dot{\phi}_j(t)]\,dV \\
&\quad = \int_B \varrho[u_i^0\dot{u}_i(2t) + u_i^1 u_i(2t)]\,dV + \int_B \rho J_{ij}[\phi_i^0\dot{\phi}_j(2t) + \phi_i^1\phi_j(2t)]\,dV \\
&\qquad + \int_0^t \int_B \rho[u_i(t+s)\ddot{u}_i(t-s) - u_i(t-s)\ddot{u}_i(t+s)]\,dV\,ds \\
&\qquad + \int_0^t \int_B \rho J_{ij}[\phi_i(t+s)\ddot{\phi}_j(t-s) - \phi_i(t-s)\ddot{\phi}_j(t+s)]\,dV\,ds
\end{aligned} \tag{42}
$$

for any $t \in [0, \infty)$.

The last two integrals in (42) contain some inertial terms which will be eliminated in the following. First, taking into account the equations $(10)_1$ one obtains

$$
\begin{aligned}
&\rho[u_i(t+s)\ddot{u}_i(t-s) - u_i(t-s)\ddot{u}_i(t+s)] \\
&\quad = u_i(t+s)\rho\ddot{u}_i(t-s) - u_i(t-s)\rho\ddot{u}_i(t+s) \\
&\quad = u_i(t+s)[c_{ijkl}\varepsilon_{kl}(t-s) + p_{ijkl}\phi_{kl}(t-s) + a_{ij}\theta(t-s) + b_{ij}\,C(t-s)]_{,\,j} \\
&\qquad - u_i(t-s)[c_{ijkl}\varepsilon_{kl}(t+s) + p_{ijkl}\phi_{kl}(t+s) + a_{ij}\theta(t+s) + b_{ij}\,C(t+s)]_{,\,j} \\
&\quad = \{u_i(t+s)[c_{ijkl}\varepsilon_{kl}(t-s) + p_{ijkl}\phi_{kl}(t-s) + a_{ij}\theta(t-s) + b_{ij}\,C(t-s)]\}_{,\,j} \\
&\qquad - u_{i,\,j}(t+s)[c_{ijkl}\varepsilon_{kl}(t-s) + p_{ijkl}\phi_{kl}(t-s) + a_{ij}\theta(t-s) + b_{ij}\,C(t-s)] \\
&\qquad - \{u_i(t-s)[c_{ijkl}\varepsilon_{kl}(t+s) + p_{ijkl}\phi_{kl}(t+s) + a_{ij}\theta(t+s) + b_{ij}\,C(t+s)]\}_{,\,j} \\
&\qquad + u_{i,\,j}(t-s)[c_{ijkl}\varepsilon_{kl}(t+s) + p_{ijkl}\phi_{kl}(t+s) + a_{ij}\theta(t+s) + b_{ij}\,C(t+s)].
\end{aligned} \tag{43}
$$

In view of equations $(10)_2$ we get

$$
\begin{aligned}
&\rho J_{ij}[\phi_i(t+s)\ddot{\phi}_j(t-s) - \phi_i(t-s)\ddot{\phi}_j(t+s)] \\
&\quad = \phi_i(t+s)\rho J_{ij}\ddot{\phi}_j(t-s) - \phi_i(t-s)\rho J_{ij}\ddot{\phi}_i(t+s) \\
&\quad = \phi_i(t+s)[p_{ijkl}\varepsilon_{kl}(t-s) + d_{ijkl}\phi_{kl}(t-s) + p_{ij}\theta(t-s) + q_{ij}\,C(t-s)]_{,\,j} \\
&\qquad + \epsilon_{ijk}\phi_i(t+s)[a_{jkmn}\varepsilon_{mn}(t-s) + p_{jkmn}\phi_{mn}(t-s) + a_{jk}\theta(t-s) + b_{jk}C(t-s)] \\
&\qquad - \phi_i(t-s)[p_{ijkl}\varepsilon_{kl}(t+s) + d_{ijkl}\phi_{kl}(t+s) + p_{ij}\theta(t+s) + q_{ij}\,C(t+s)]_{,\,j} \\
&\qquad - \epsilon_{ijk}\phi_i(t-s)[a_{jkmn}\varepsilon_{mn}(t+s) + p_{jkmn}\phi_{kl}(t+s) + a_{jk}\theta(t+s) + b_{jk}C(t+s)] \\
&\quad = \{\phi_i(t+s)[p_{ijkl}\varepsilon_{kl}(t-s) + d_{ijkl}\phi_{kl}(t-s) + p_{ij}\theta(t-s) + q_{ij}\,C(t-s)]\}_{,\,j} \\
&\qquad - \phi_{i,\,j}(t+s)[p_{ijkl}\varepsilon_{kl}(t-s) + d_{ijkl}\phi_{kl}(t-s) + p_{ij}\theta(t-s) + q_{ij}\,C(t-s)] \\
&\qquad + \epsilon_{ijk}\phi_i(t+s)[a_{jkmn}\varepsilon_{mn}(t-s) + p_{jkmn}\phi_{mn}(t-s) + a_{jk}\theta(t-s) + b_{jk}C(t-s)] \\
&\qquad - \{\phi_i(t-s)[p_{ijkl}\varepsilon_{kl}(t+s) + d_{ijkl}\phi_{kl}(t+s) + p_{ij}\theta(t+s) + q_{ij}\,C(t+s)]\}_{,\,j} \\
&\qquad + \phi_{i,\,j}(t-s)[p_{ijkl}\varepsilon_{kl}(t+s) + d_{ijkl}\phi_{kl}(t+s) + p_{ij}\theta(t+s) + q_{ij}\,C(t+s)] \\
&\qquad - \epsilon_{ijk}\phi_i(t-s)[a_{jkmn}\varepsilon_{mn}(t+s) + p_{jkmn}\phi_{kl}(t+s) + a_{jk}\theta(t+s) + b_{jk}\,C(t+s)].
\end{aligned} \tag{44}
$$

If we add the equalities (43) and (44) together, then we are led to

$$\begin{aligned}
&\rho[u_i(t+s)\ddot{u}_i(t-s)-u_i(t-s)\ddot{u}_i(t+s)]+\rho J_{ij}[\phi_i(t+s)\ddot{\phi}_j(t-s)-\phi_i(t-s)\ddot{\phi}_j(t+s)]\\
&\quad=\{u_i(t+s)[c_{ijkl}\varepsilon_{kl}(t-s)+p_{ijkl}\phi_{kl}(t-s)+a_{ij}\theta(t-s)+b_{ij}C(t-s)]\}_{,\,j}\\
&\qquad-\{u_i(t-s)[c_{ijkl}\varepsilon_{kl}(t+s)+p_{ijkl}\phi_{kl}(t+s)+a_{ij}\theta(t+s)+b_{ij}C(t+s)]\}_{,\,j}\\
&\qquad+\{\phi_i(t+s)[p_{ijkl}\varepsilon_{kl}(t-s)+d_{ijkl}\phi_{kl}(t-s)+p_{ij}\theta(t-s)+q_{ij}C(t-s)]\}_{,\,j}\\
&\qquad-\{\phi_i(t-s)[p_{ijkl}\varepsilon_{kl}(t+s)+d_{ijkl}\phi_{kl}(t+s)+p_{ij}\theta(t+s)+q_{ij}C(t+s)]\}_{,\,j}\\
&\qquad-[a_{ij}\varepsilon_{ij}(t+s)+p_{ij}\phi_{ij}(t+s)]\theta(t-s)+[a_{ij}\varepsilon_{ij}(t-s)+p_{ij}\phi_{ij}(t-s)]\theta(t+s)\\
&\qquad-[b_{ij}\varepsilon_{ij}(t+s)+q_{ij}\phi_{ij}(t+s)]C(t-s)+[b_{ij}\varepsilon_{ij}(t-s)+q_{ij}\phi_{ij}(t-s)]C(t+s). \qquad (45)
\end{aligned}$$

For the last two rows of right-hand side of equality (45) we get the equivalent expressions using the energy equation and the equation of mass diffusion, respectively.

So, by an integration with respect to time variable, from the energy equation $(10)_3$ and the initial conditions (11) we deduce

$$\begin{aligned}
-[a_{ij}\varepsilon_{ij}(t+s)+p_{ij}\phi_{ij}(t+s)]\theta(t-s)&=\frac{1}{T_0}\left(\int_0^{t+s}\kappa_{ij}\theta_{,\,i}(z)\,dz\right)_{,\,j}\theta(t-s)\\
&\quad-\frac{\rho c_E}{T_0}\theta(t-s)\theta(t+s)-\varpi\theta(t-s)C(t-s)+\rho S^0\theta(t-s), \qquad (46)
\end{aligned}$$

where ρS^0 is defined in (28).

Similarly, we have

$$\begin{aligned}
[a_{ij}\varepsilon_{ij}(t-s)+p_{ij}\phi_{ij}(t-s)]\theta(t+s)&=-\frac{1}{T_0}\left(\int_0^{t-s}\kappa_{ij}\theta_{,\,i}(z)\,dz\right)_{,\,j}\theta(t+s)\\
&\quad+\frac{\rho c_E}{T_0}\theta(t+s)\theta(t-s)+\varpi\theta(t-s)C(t+s)-\rho S^0\theta(t+s). \qquad (47)
\end{aligned}$$

From (46) and (47) we deduce

$$\begin{aligned}
&-[a_{ij}\varepsilon_{ij}(t+s)+p_{ij}\phi_{ij}(t+s)]\theta(t-s)+[a_{ij}\varepsilon_{ij}(t-s)+p_{ij}\phi_{ij}(t-s)]\theta(t+s)\\
&\quad=\varpi[\theta(t+s)C(t-s)-\theta(t-s)C(t+s)]+\rho S^0[\theta(t+s)-\theta(t-s)]\\
&\qquad+\frac{1}{T_0}\kappa_{ij}\left[\theta(t-s)\left(\int_0^{t+s}\theta_{,\,i}(z)\,dz\right)_{,\,j}-\theta(t+s)\left(\int_0^{t-s}\theta_{,\,i}(z)\,dz\right)_{,\,j}\right]. \qquad (48)
\end{aligned}$$

The equality (48) can be restated in the form

$$\begin{aligned}
&-[a_{ij}\varepsilon_{ij}(t+s)+p_{ij}\phi_{ij}(t+s)]\theta(t-s)+[a_{ij}\varepsilon_{ij}(t-s)+p_{ij}\phi_{ij}(t-s)]\theta(t+s)\\
&\quad=\varpi[\theta(t+s)C(t-s)-\theta(t-s)C(t+s)]+\rho S^0[\theta(t+s)-\theta(t-s)]\\
&\qquad+\left[\frac{1}{T_0}\kappa_{ij}\theta(t-s)\int_0^{t+s}\theta_{,\,i}(z)\,dz-\frac{1}{T_0}\kappa_{ij}\theta(t+s)\int_0^{t-s}\theta_{,\,i}(z)\,dz\right]_{,\,j}\\
&\qquad+\frac{1}{T_0}\kappa_{ij}\left[\theta_{,\,j}(t+s)\int_0^{t-s}\theta_{,\,i}(z)\,dz-\theta_{,\,i}(t-s)\int_0^{t+s}\theta_{,\,i}(z)\,dz\right]. \qquad (49)
\end{aligned}$$

It is easy to deduce that the last row in (49) can be written in the form

$$\frac{1}{T_0}\kappa_{ij}\left[\theta_{,\,j}(t+s)\int_0^{t-s}\theta_{,\,i}(z)\,dz-\theta_{,\,i}(t-s)\int_0^{t+s}\theta_{,\,i}(z)\,dz\right]$$
$$=\frac{1}{T_0}\kappa_{ij}\frac{d}{ds}\left[\left(\int_0^{t+s}\theta_{,\,i}(z)\,dz\right)\left(\int_0^{t-s}\theta_{,\,j}(z)\,dz\right)\right],$$

so that (49) receives the form

$$\begin{aligned}
&-[a_{ij}\varepsilon_{ij}(t+s)+p_{ij}\phi_{ij}(t+s)]\theta(t-s)+[a_{ij}\varepsilon_{ij}(t-s)+p_{ij}\phi_{ij}(t-s)]\theta(t+s)\\
&\quad=\varpi[\theta(t+s)C(t-s)-\theta(t-s)C(t+s)]+\rho S^0[\theta(t+s)-\theta(t-s)]\\
&\qquad+\left[\frac{1}{T_0}\kappa_{ij}\theta(t-s)\int_0^{t+s}\theta_{,\,i}(z)\,dz-\frac{1}{T_0}\kappa_{ij}\theta(t+s)\int_0^{t-s}\theta_{,\,i}(z)\,dz\right]_{,\,j}\\
&\qquad+\frac{1}{T_0}\kappa_{ij}\frac{d}{ds}\left[\left(\int_0^{t+s}\theta_{,\,i}(z)\,dz\right)\left(\int_0^{t-s}\theta_{,\,j}(z)\,dz\right)\right].
\end{aligned}\tag{50}$$

Now, by an integration with respect to time variable, from the equation (3), Fick's law and the initial conditions (11) we deduce

$$\begin{aligned}
&-[b_{ij}\varepsilon_{ij}(t+s)+q_{ij}\phi_{ij}(t+s)]C(t-s)\\
&\quad=-\left(\int_0^{t+s}d_{ij}P_{,\,i}(z)\,dz\right)_{,\,j}C(t-s)-\varpi\theta(t+s)C(t-s)+\varrho C(t+s)C(t-s)-P^0C(t-s),
\end{aligned}\tag{51}$$

where P^0 is defined in (28).

Similarly, we have

$$\begin{aligned}
&[b_{ij}\varepsilon_{ij}(t-s)+q_{ij}\phi_{ij}(t-s)]C(t+s)\\
&\quad=\left(\int_0^{t-s}d_{ij}P_{,\,i}(z)\,dz\right)_{,\,j}C(t+s)+\varpi\theta(t-s)C(t+s)-\varrho C(t-s)C(t+s)+P^0C(t+s),
\end{aligned}\tag{52}$$

so that from (51) and (52) we are led to

$$\begin{aligned}
&-[b_{ij}\varepsilon_{ij}(t+s)+q_{ij}\phi_{ij}(t+s)]C(t-s)+[b_{ij}\varepsilon_{ij}(t-s)+q_{ij}\phi_{ij}(t-s)]C(t+s)\\
&\quad=\varpi[\theta(t-s)C(t+s)-\theta(t+s)C(t-s)]+P^0[C(t+s)-C(t-s)]\\
&\qquad-\left(\int_0^{t-s}d_{ij}P_{,\,i}(z)\,dz\right)_{,\,j}C(t+s)+\left(\int_0^{t+s}d_{ij}P_{,\,i}(z)\,dz\right)_{,\,j}C(t-s).
\end{aligned}\tag{53}$$

The equality (53) can be restated in the form

$$\begin{aligned}
&-[b_{ij}\varepsilon_{ij}(t+s)+q_{ij}\phi_{ij}(t+s)]C(t-s)+[b_{ij}\varepsilon_{ij}(t-s)+q_{ij}\phi_{ij}(t-s)]C(t+s)\\
&\quad=\varpi[\theta(t-s)C(t+s)-\theta(t+s)C(t-s)]+P^0[C(t+s)-C(t-s)]\\
&\qquad+\left[d_{ij}(P(t+s)\int_0^{t-s}P_{,\,i}(z)\,dz-P(t-s)\int_0^{t+s}P_{,\,i}(z)\,dz)\right]_{,\,j}\\
&\qquad-d_{ij}\left[P_{,\,j}(t+s)\int_0^{t-s}P_{,\,i}(z)\,dz-P_{,\,j}(t-s)\int_0^{t+s}P_{,\,i}(z)\,dz\right].
\end{aligned}\tag{54}$$

It is easy to deduce that the last row in (54) can be written in the form

$$d_{ij}\left[P_{,\,j}(t+s)\int_0^{t-s}P_{,\,i}(z)\,dz-P_{,\,j}(t-s)\int_0^{t+s}P_{,\,i}(z)\,dz\right]=d_{ij}\frac{d}{ds}\left[\left(\int_0^{t+s}P_{,\,i}(z)\,dz\right)\left(\int_0^{t-s}P_{,\,j}(z)\,dz\right)\right],$$

so that (54) receives the form

$$\begin{aligned}
&-[b_{ij}\varepsilon_{ij}(t+s)+q_{ij}\phi_{ij}(t+s)]C(t-s)+[b_{ij}\varepsilon_{ij}(t-s)+q_{ij}\phi_{ij}(t-s)]C(t+s)\\
&\quad=\varpi[\theta(t-s)\,C(t+s)-\theta(t+s)\,C(t-s)]+P^0[C(t+s)-P(t-s)]\\
&\qquad+\left[d_{ij}(P(t+s)\int_0^{t-s}P_{,\,i}(z)\,dz-P(t-s)\int_0^{t+s}P_{,\,i}(z)\,dz)\right]_{,\,j}\\
&\qquad+d_{ij}\frac{d}{ds}\left[\left(\int_0^{t+s}P_{,\,i}(z)\,dz\right)\left(\int_0^{t-s}P_{,\,j}(z)\,dz\right)\right].
\end{aligned}\tag{55}$$

We now introduce the expressions (50) and (55) into equality (45) and we are led to

$$\begin{aligned}
&\rho[u_i(t+s)\ddot{u}_i(t-s)-u_i(t-s)\ddot{u}_i(t+s)]+\rho J_{ij}[\phi_i(t+s)\ddot{\phi}_j(t-s)-\phi_i(t-s)\ddot{\phi}_j(t+s)]\\
&\quad=\{u_i(t+s)[c_{ijkl}\varepsilon_{kl}(t-s)+p_{ijkl}\phi_{kl}(t-s)+a_{ij}(\theta(t-s)+\alpha\dot{\theta}(t-s))+b_{ij}\,P(t-s)]\}_{,\,j}\\
&\qquad-\{u_i(t-s)[c_{ijkl}\varepsilon_{kl}(t+s)+p_{ijkl}\phi_{kl}(t+s)+a_{ij}(\theta(t+s)+\alpha\dot{\theta}(t+s))+b_{ij}\,P(t+s)]\}_{,\,j}\\
&\qquad+\{\phi_i(t+s)[p_{ijkl}\varepsilon_{kl}(t-s)+d_{ijkl}\phi_{kl}(t-s)+\kappa_{ij}(\theta(t-s)+\alpha\dot{\theta}(t-s))+q_{ij}P(t-s)]\}_{,\,j}\\
&\qquad-\{\phi_i(t-s)[p_{ijkl}\varepsilon_{kl}(t+s)+d_{ijkl}\phi_{kl}(t+s)+\kappa_{ij}(\theta(t+s)+\alpha\dot{\theta}(t+s))+q_{ij}P(t+s)]\}_{,\,j}\\
&\qquad+\rho S^0[\theta(t+s)-\theta(t-s)]+P^0[C(t+s)-C(t-s)]\\
&\qquad+\left[\frac{1}{T_0}\kappa_{ij}\theta(t-s)\int_0^{t+s}\theta_{,\,i}(z)\,dz-\frac{1}{T_0}\kappa_{ij}\theta(t+s)\int_0^{t-s}\theta_{,\,i}(z)\,dz\right]_{,\,j}\\
&\qquad+\left[d_{ij}\left(P(t+s)\int_0^{t-s}P_{,\,i}(z)\,dz-P(t-s)\int_0^{t+s}P_{,\,i}(z)\,dz\right)\right]_{,\,j}\\
&\qquad+\frac{1}{T_0}\kappa_{ij}\frac{d}{ds}\left[\left(\int_0^{t+s}\theta_{,\,i}(z)\,dz\right)\left(\int_0^{t-s}\theta_{,\,j}(z)\,dz\right)\right]\\
&\qquad+d_{ij}\frac{d}{ds}\left[\left(\int_0^{t+s}P_{,\,i}(z)\,dz\right)\left(\int_0^{t-s}P_{,\,j}(z)\,dz\right)\right].
\end{aligned}\tag{56}$$

We now substitute the relation (56) into (42) and we use the divergence theorem and the boundary conditions (9) in order to obtain

$$\begin{aligned}
&2\int_B[\rho u_i(t)\dot{u}_i(t)+\rho J_{ij}\phi_i(t)\dot{\phi}_j(t)]\,dV\\
&\quad=\int_B\varrho[u_i^0\dot{u}_i(2t)+u_i^1u_i(2t)]\,dV+\int_B\rho J_{ij}[\phi_i^0\dot{\phi}_j(2t)+\phi_i^1\phi_j(2t)]\,dV\\
&\qquad+\int_0^t\int_B\{\rho S^0[\theta(t+s)-\theta(t-s)]+P^0[C(t+s)-C(t-s)]\}\,dV\,ds\\
&\qquad+\int_0^t\int_B\frac{1}{T_0}\kappa_{ij}\frac{d}{ds}\left[\left(\int_0^{t+s}\theta_{,\,i}(z)\,dz\right)\left(\int_0^{t-s}\theta_{,\,j}(z)\,dz\right)\right]dV\,ds
\end{aligned}$$

$$+\int_0^t\int_B d_{ij}\frac{d}{ds}\left[\left(\int_0^{t+s}P_{,\,i}(z)\,dz\right)\left(\int_0^{t-s}P_{,\,j}(z)\,dz\right)\right]dV\,ds. \tag{57}$$

It is not difficult to observe that

$$\int_0^t\frac{d}{ds}\left[\left(\int_0^{t+s}\theta_{,\,i}(z)\,dz\right)\left(\int_0^{t-s}\theta_{,\,j}(z)\,dz\right)\right]ds=-\left(\int_0^t\theta_{,\,i}(z)\,dz\right)\left(\int_0^t\theta_{,\,j}(z)\,dz\right),$$

and, analogously,

$$\int_0^t\frac{d}{ds}\left[\left(\int_0^{t+s}P_{,\,i}(z)\,dz\right)\left(\int_0^{t-s}P_{,\,j}(z)\,dz\right)\right]ds=-\left(\int_0^t P_{,\,i}(z)\,dz\right)\left(\int_0^t P_{,\,j}(z)\,dz\right).$$

Finally, by using the last two relations in (57), one obtains the desired equality (38) so that Theorem 3 is proved. □

5. Equipartition of energy

In this section we shall use the identities (21), (27) and (38) such that by using the hypotheses made in Section 2 we establish the asymptotic partition of total energy.

Let us introduce the Cesàro means of all energies contained in the identity (21). So, we have Cesàro means of kinetic energy, strain energy, thermal energy and energy of dissipation, respectively:

$$\begin{aligned}
\mathcal{K}_C(t)&\equiv\frac{1}{2t}\int_0^t\int_B[\rho\dot{u}_i(s)\dot{u}_i(s)+\rho J_{ij}\dot{\phi}_i(s)\dot{\phi}_j(s)]\,dV\,ds,\\
\mathcal{S}_C(t)&\equiv\frac{1}{2t}\int_0^t\int_B[c_{ijkl}\varepsilon_{ij}(t)\varepsilon_{kl}(t)+2p_{ijkl}(t)\varepsilon_{ij}(t)\phi_{kl}+d_{ijkl}\phi_{ij}(t)\phi_{kl}]\,dV\,ds,\\
\mathcal{T}_C(t)&\equiv\frac{1}{2t}\int_0^t\int_B\frac{\rho c_E}{T_0}\theta^2(s)\,dV\,ds,\\
\Gamma_C(t)&\equiv\frac{1}{t}\int_0^t\int_0^s\int_B[\frac{1}{T_0}\kappa_{ij}\theta_{,\,i}(\xi)\theta_{,\,j}(\xi)+C(\xi)\dot{P}(\xi)]\,dV\,d\xi\,ds.
\end{aligned} \tag{58}$$

In the following theorem we state and prove the main result of our study.

Theorem 4. *Consider $((u_i,\phi_i),\theta,C)$ a solution of the mixed initial boundary value problem defined by equations (10), the boundary conditions (9) and the initial conditions (11). We assume that the hypotheses from Section 2 are satisfied. Then, for all initial data*

$$(u_i^0,\phi_i^0)\in\boldsymbol{W}_1(B),\quad (u_i^1,\phi_i^1)\in\boldsymbol{W}_0(B),\quad (\theta^0,C^0)\in W_1(B)\times W_1(B),\quad \theta^1\in W_0(B),$$

we have the following relations:

(i) *If* $\operatorname{meas}(\partial B_3)\neq 0$, *then*

$$\lim_{t\to\infty}\mathcal{T}_C(t)=0. \tag{59}$$

(ii) *If* $\operatorname{meas}(\partial B_1)\neq 0$, $\operatorname{meas}(\partial B_2)\neq 0$ *and* $\operatorname{meas}(\partial B_4)\neq 0$, *then*

$$\lim_{t\to\infty}\mathcal{K}_C(t)=\lim_{t\to\infty}\mathcal{S}_C(t), \tag{60}$$

$$\lim_{t\to\infty}\Gamma_C(t)=\mathcal{E}(0)-2\lim_{t\to\infty}\mathcal{K}_C(t)=\mathcal{E}(0)-2\lim_{t\to\infty}\mathcal{S}_C(t). \tag{61}$$

(iii) *If* $\operatorname{meas}(\partial B_1) = 0$ *or* $\operatorname{meas}(\partial B_2) = 0$ *or* $\operatorname{meas}(\partial B_3) = 0$ *or* $\operatorname{meas}(\partial B_4) = 0$, *then*

$$\lim_{t\to\infty} \mathcal{H}_C(t) = \lim_{t\to\infty} \mathcal{S}_C(t) + \frac{1}{2}\int_B [\rho \dot{u}_i^* \dot{u}_i^* + \rho J_{ij}\dot{\phi}_i^*\dot{\phi}_j^*]\,dV, \tag{62}$$

$$\begin{aligned}\lim_{t\to\infty} \Gamma_C(t) &= \mathcal{E}(0) - 2\lim_{t\to\infty} \mathcal{H}_C(t) + \frac{1}{2}\int_B [\rho \dot{u}_i^* \dot{u}_i^* + \rho J_{ij}\dot{\phi}_i^*\dot{\phi}_j^*]\,dV \\ &= \mathcal{E}(0) - 2\lim_{t\to\infty} \mathcal{S}_C(t) - \frac{1}{2}\int_B [\rho \dot{u}_i^* \dot{u}_i^* + \rho J_{ij}\dot{\phi}_i^*\dot{\phi}_j^*]\,dV.\end{aligned} \tag{63}$$

Proof. (i) Suppose that $\operatorname{meas}(\partial B_3) \neq 0$. It is easy to prove that $\theta \in \widehat{W}_1(B)$. Therefore, we can apply the Poincaré inequality (17) so that from the identity (21) one obtains

$$\int_0^t \int_B \frac{\rho c_E}{T_0}\theta^2(s)\,dV\,ds \le \frac{1}{m_2}\int_0^t \int_B \kappa_{ij}\theta_{,i}(s)\theta_{,j}(s)\,dV\,ds \le \frac{1}{m_2}\mathcal{E}(0). \tag{64}$$

From relation (64), taking into account (58), we obtain the conclusion (59).

(ii) We first use the energy conservation law (21) and the hypotheses of Section 2 in order to obtain the following estimates:

$$\int_B \frac{\rho c_E}{T_0}\theta^2(t)\,dV \le \mathcal{E}(0), \qquad t \in [0,\infty), \tag{65}$$

$$\int_B [\rho \dot{u}_i(t)\dot{u}_i(t) + \rho J_{ij}\dot{\phi}_i(t)\dot{\phi}_j(t)]\,dV \le 2\mathcal{E}(0), \qquad t \in [0,\infty), \tag{66}$$

$$\int_0^t \int_B \left[\frac{\rho c_E}{T_0}\kappa_{ij}\theta_{,i}(s)\theta_{,j}(s) + C(s)\dot{P}(s)\right] dV\,ds \le \mathcal{E}(0), \quad t \in [0,\infty). \tag{67}$$

On the basis of identities (27) and (38) we will find some relationships between the types of energy. So, from (27) we find

$$\begin{aligned}&\frac{1}{2t}\int_0^t \int_B [\rho \dot{u}_i(s)\dot{u}_i(s) + \rho J_{ij}\dot{\phi}_i(s)\dot{\phi}_j(s)]\,dV\,ds \\ &\quad - \frac{1}{2t}\int_0^t \int_B [c_{ijkl}\varepsilon_{ij}(s)\varepsilon_{kl}(s) + 2p_{ijkl}\phi_{ij}(s)\varepsilon_{kl}(s) + d_{ijkl}\phi_{ij}(s)\phi_{kl}(s)]\,dV\,ds \\ &= \frac{1}{2t}\int_0^t \int_B \left[\frac{\rho c_E}{T_0}\theta^2(s) + 2\varpi C(s)\theta(s) - \varrho C^2(s)\right] dV\,ds - \frac{1}{2t}\int_B [\rho u_i^0 u_i^1 + \rho J_{ij}\phi_i^0\phi_i^1]\,dV \\ &\quad - \frac{1}{4t}\int_0^t \int_B [\rho S^0\theta(s) - P^0 C(s)]\,dV\,ds + \frac{1}{2t}\int_B [\rho u_i(t)\dot{u}_i(t) + \rho J_{ij}\phi_i(t)\dot{\phi}_j(t)]\,dV \\ &\quad + \frac{1}{4t}\int_B \frac{1}{T_0}\kappa_{ij}\left(\int_0^t \theta_{,i}(\xi)d\xi\right)\left(\int_0^t \theta_{,j}(\xi)d\xi\right) dV \\ &\quad + \frac{1}{4t}\int_B d_{ij}\left(\int_0^t P_{,i}(\xi)d\xi\right)\left(\int_0^t P_{,j}(\xi)d\xi\right) dV.\end{aligned} \tag{68}$$

By using (38), from (68) one obtains

$$\begin{aligned}
&\frac{1}{2t}\int_0^t\int_B[\rho\dot{u}_i(s)\dot{u}_i(s)+\rho J_{ij}\dot{\phi}_i(s)\dot{\phi}_j(s)]\,dV\,ds\\
&\quad-\frac{1}{2t}\int_0^t\int_B[c_{ijkl}\varepsilon_{ij}(s)\varepsilon_{kl}(s)+2p_{ijkl}\phi_{ij}(s)\varepsilon_{kl}(s)+d_{ijkl}\phi_{ij}(s)\phi_{kl}(s)]\,dV\,ds\\
&=\frac{1}{2t}\int_0^t\int_B\left[\frac{\rho c_E}{T_0}\theta^2(s)+2\varpi C(s)\theta(s)-\varrho C^2(s)\right]dV\,ds\\
&\quad-\frac{1}{2t}\int_B[\rho u_i^0u_i^1+\rho J_{ij}\phi_i^0\phi_i^1]\,dV-\frac{1}{4t}\int_0^t\int_B[\rho S^0\theta(s)-P^0C(s)]\,dV\,ds\\
&\quad+\frac{1}{4t}\int_B\{\varrho[u_i^0\dot{u}_i(2t)+u_i^1u_i(2t)]+\rho J_{ij}[\phi_i^0\dot{\phi}_j(2t)+\phi_i^1\phi_j(2t)]\}\,dV\\
&\quad+\frac{1}{4t}\int_0^t\int_B\{\rho S^0[\theta(t+s)-\theta(t-s)]+P^0[C(t+s)-C(t-s)]\}\,dV\,ds.
\end{aligned}\tag{69}$$

Taking into account the notations (58) and using the initial conditions (11), from the identity (69) we deduce

$$\begin{aligned}
&\mathcal{H}_C(t)-\mathcal{S}_C(t)\\
&\quad=-\frac{1}{2t}\int_B[\rho u_i^0u_i^1+\rho J_{ij}\phi_i^0\phi_i^1]\,dV\\
&\qquad+\frac{1}{2t}\int_B[\rho u_i^0\dot{u}_i(2t)+\rho J_{ij}\phi_i^0\dot{\phi}_j(2t)]\,dV+\frac{1}{2t}\int_B[\rho u_i^1u_i(2t)+\rho J_{ij}\phi_i^1\phi_j(2t)]\,dV\\
&\qquad+\frac{1}{4t}\int_0^t\int_B[2\varpi C(s)\theta(s)-\varrho C(s)]\,dV\,ds-\frac{1}{4t}\int_0^t\int_B[\rho S^0\theta(s)-P^0C(s)]\,dV\,ds\\
&\qquad+\frac{1}{4t}\int_0^t\int_B\{\rho S^0[\theta(t+s)-\theta(t-s)]+P^0[C(t+s)-C(t-s)]\}\,dV\,ds+\mathcal{T}_C(t).
\end{aligned}\tag{70}$$

Now we will use the Schwarz and Cauchy inequalities on the right-hand side of (70). Then, by using the relations (64)–(67) we get

$$\begin{aligned}
&\left|-\frac{1}{2t}\int_B[\rho u_i^0u_i^1+\rho J_{ij}\phi_i^0\phi_j^1]\,dV\right|\le\frac{1}{4t}\int_B[\rho(u_i^0u_i^0+u_i^1u_i^1)+\rho J_{ij}(\phi_i^0\phi_j^0+\phi_i^1\phi_j^1)]\,dV;\\
&\left|\frac{1}{4t}\int_B[\rho u_i^0\dot{u}_i(2t)+\rho J_{ij}\phi_i^0\dot{\phi}_j(2t)]\,dV\right|\le\frac{1}{8t}\int_B[\rho u_i^0u_i^0+\rho J_{ij}\phi_i^0\phi_j^0]\,dV+\frac{1}{4t}\,\mathcal{E}(0).
\end{aligned}\tag{71}$$

Since $(u_i,\phi_i)\in\widehat{W}_1(B)$, and $P\in\widehat{W}_1(B)$ by using the conditions (7), the Korn's inequality (16), the identity (21) and the inequalities (8) one obtains

$$\begin{aligned}
&\int_B[\rho u_i(s)u_i(s)+\rho J_{ij}\phi_i(s)\phi_j(s)]\,dV\\
&\le\frac{\rho}{m_1}\int_B[c_{ijkl}\varepsilon_{ij}(s)\varepsilon_{kl}(s)+2p_{ijkl}\phi_{ij}(s)\varepsilon_{kl}(s)+d_{ijkl}\phi_{ij}(s)\phi_{kl}(s)]\,dV\le\frac{2\rho}{m_1}\,\mathcal{E}(0),\qquad s\in[0,\infty).
\end{aligned}\tag{72}$$

Thus, by using (72) we are led to

$$\left|\frac{1}{4t}\int_B[\rho u_i^1u_i(2t)+\rho J_{ij}\phi_i^1\phi_j(2t)]\,dV\right|\le\frac{1}{8t}\int_B[\rho u_i^1u_i^1+\rho J_{ij}\phi_i^1\phi_j^1]\,dV+\frac{\rho}{4tm_1}\,\mathcal{E}(0).\tag{73}$$

Taking into account the estimates (71) and (73) and the relation (59), we pass to the limit in (70) as $t \to \infty$ and conclude that the relation (60) holds.

Also, it is not difficult to observe that the relation (61) is obtained from (21) by taking the Cesàro mean and by using the relations (59) and (60).

(iii) We use the decomposition (18) from Section 3, the relation (12), (13) and the fact that $(u_i, \phi_i) \in \widehat{\boldsymbol{W}}_1(B)$ and $P \in \widehat{W}_1(B)$ in order to obtain the identity

$$\frac{1}{4t}\int_B [\rho u_i^0 \dot{u}_i(2t) + \rho J_{ij}\phi_i^0\dot{\phi}_j(2t)]\,dV = \frac{1}{4t}\int_B [\rho u_i^* \dot{u}_i^* + \rho J_{ij}\phi_i^*\dot{\phi}_j^*]\,dV + \frac{1}{2}\int_B [\rho \dot{u}_i^*\dot{u}_i^* + \rho J_{ij}\dot{\phi}_i^*\dot{\phi}_j^*]\,dV + \frac{1}{4t}\int_B [\rho U_i^0 v_i(2t) + \rho J_{ij}\Phi_i^0\psi_j(2t)]\,dV. \quad (74)$$

Also, since $(v_i, \psi_i) \in \widehat{\boldsymbol{W}}_1(B)$, Korn's inequality (16) leads to the relation

$$\begin{aligned}\frac{1}{4t}&\int_B [\rho v_i(s)v_i(s) + \rho J_{ij}\psi_i(s)\psi_j(s)]\,dV \\ &\le \frac{\rho}{m_1}\int_B [c_{ijkl}\bar{\varepsilon}_{ij}(s)\bar{\varepsilon}_{kl}(s) + 2p_{ijkl}\bar{\phi}_{ij}(s)\bar{\varepsilon}_{kl}(s) + d_{ijkl}\bar{\phi}_{ij}(s)\bar{\phi}_{mn}(s)]\,dV \\ &= \frac{\rho}{m_1}\int_B [c_{ijkl}\varepsilon_{ij}(s)\varepsilon_{kl}(s) + 2p_{ijkl}\phi_{ij}(s)\varepsilon_{kl}(s) \\ &\quad + d_{ijkl}\phi_{ij}(s)\phi_{mn}(s)]\,dV \le \frac{2\rho}{m_1}\mathscr{E}(0), \quad s \in [0,\infty), \end{aligned} \quad (75)$$

where $\bar{\varepsilon}_{ji} = v_{i,j} - \epsilon_{kji}\psi_k$, $\bar{\phi}_{ij} = \psi_{j,i}$.

Passing to the limit in (70) as $t \to \infty$ and taking into account the relations (71), (74) and (75) one obtains the conclusion (63). Finally, the relation (63) is obtained on the basis of (21) by taking the Cesàro mean and by using the relations (59), (62) and (71). Thus, the proof of Theorem 4 is complete. □

6. Conclusion

As a concluding remark, we must outline that the relations (60) and (62), restricted to the class of initial data for which $\dot{u}_i^* = \dot{\phi}_i^* = 0$, prove the asymptotic equipartition in mean of the kinetic and strain energies. The presence of other components of total energy does not influence this behavior.

Acknowledgement

The authors are very thankful to the referees for their valuable suggestions, which helped in improvement of the manuscript.

References

[Adams 1975] R. A. Adams, *Sobolev spaces*, Pure and Applied Mathematics **65**, Academic Press, New York, 1975.

[Aouadi 2008] M. Aouadi, "Generalized theory of thermoelasic diffusion for an anisotropic media", *J. Therm. Stresses* **31**:3 (2008), 270–285.

[Dassios and Galanis 1980] G. Dassios and E. Galanis, "Asymptotic equipartition of kinetic and strain energy for elastic waves in anisotropic media", *Quart. Appl. Math.* **38**:1 (1980), 121–128.

[Day 1980] W. A. Day, "Means and autocorrelations in elastodynamics", *Arch. Ration. Mech. Anal.* **73**:3 (1980), 243–256.

[Dhaliwal and Singh 1987] R. S. Dhaliwal and A. Singh, "Micropolar thermoelasticity", pp. 269–328 in *Thermal stresses, II: Mechanics and mathematical methods*, edited by R. B. Hetnarski, North Holland, Amsterdam, 1987.

[Eringen 1999] A. C. Eringen, *Microcontinuum field theories, I: Foundations and solids*, Springer, New York, 1999.

[Eringen 2001] A. C. Eringen, *Microcontinuum field theories, II: Fluent media*, Springer, New York, 2001.

[Eringen 2003] A. C. Eringen, "Micropolar mixture theory of porous media", *J. Appl. Phys.* **94**:6 (2003), 4184–4190.

[Goldstein and Sandefur 1976] J. A. Goldstein and J. T. Sandefur, Jr., "Asymptotic equipartition of energy for differential equations in Hilbert space", *Trans. Amer. Math. Soc.* **219** (1976), 397–406.

[Gurtin 1993] M. E. Gurtin, "The dynamics of solid-solid phase transitions, I: Coherent interfaces", *Arch. Ration. Mech. Anal.* **123**:4 (1993), 305–335.

[Hlaváček and Nečas 1970a] I. Hlaváček and J. Nečas, "On inequalities of Korn's type, I: Boundary-value problems for elliptic system of partial differential equations", *Arch. Ration. Mech. Anal.* **36**:4 (1970), 305–311.

[Hlaváček and Nečas 1970b] I. Hlaváček and J. Nečas, "On inequalities of Korn's type, II: Applications to linear elasticity", *Arch. Ration. Mech. Anal.* **36**:4 (1970), 312–334.

[Ieşan 2004] D. Ieşan, *Thermoelastic models of continua*, Solid Mechanics and its Applications **118**, Kluwer, Dordrecht, 2004.

[Levine 1977] H. A. Levine, "An equipartition of energy theorem for weak solutions of evolutionary equations in Hilbert space: The Lagrange identity method", *J. Differ. Equations* **24**:2 (1977), 197–210.

[Marin 2009] M. Marin, "On the minimum principle for dipolar materials with stretch", *Nonlinear Anal. Real World Appl.* **10**:3 (2009), 1572–1578.

[Marin and Florea 2014] M. Marin and O. Florea, "On temporal behaviour of solutions in thermoelasticity of porous micropolar bodies", *An. St. Univ. Ovidius Constanta, Ser. Mat.* **22**:1 (2014), 169–188.

[Marin and Stan 2013] M. Marin and G. Stan, "Weak solutions in elasticity of dipolar bodies with stretch", *Carpathian J. Math.* **29**:1 (2013), 33–40.

[Marin et al. 2013a] M. Marin, R. P. Agarwal, and S. R. Mahmoud, "Nonsimple material problems addressed by the Lagrange's identity", *Bound. Value Probl.* **2013**:1 (2013), Art. ID 135.

[Marin et al. 2013b] M. Marin, R. P. Agarwal, and S. R. Mahmoud, "Modeling a microstretch thermoelastic body with two temperatures", *Abstr. Appl. Anal.* (2013), Art. ID 583464.

[Rionero and Chirita 1987] S. Rionero and S. Chirita, "The Lagrange identity method in linear thermoelasticity", *Int. J. Eng. Sci.* **25**:7 (1987), 935–947.

[Sharma and Marin 2014] K. Sharma and M. Marin, "Reflection and transmission of waves from imperfect boundary between two heat conducting micropolar thermoelastic solids", *An. St. Univ. Ovidius Constanta, Ser. Mat.* **22**:2 (2014), 151–175.

[Teodorescu-Draghicescu and Vlase 2011] H. Teodorescu-Draghicescu and S. Vlase, "Homogenization and averaging methods to predict elastic properties of pre-impregnated composite materials", *Comput. Mater. Sci.* **50**:4 (2011), 1310–1314.

[Vlase et al. 2012] S. Vlase, H. Teodorescu-Draghicescu, M. R. Calin, and M. L. Scutaru, "Advanced Polylite composite laminate material behavior to tensile stress on weft direction", *J. Opto. Adv. Mater.* **14**:7-8 (2012), 658–663.

Received 8 Apr 2015. Accepted 5 Aug 2015.

MARIN MARIN: m.marin@unitbv.ro
Department of Mathematics and Computer Sciences, Transilvania University of Braşov, Strada Universităţii 1, 500068 Braşov, Romania

SAMY REFAHY MAHMOUD: srhassan@kau.edu.sa
Department of Mathematics, Faculty of Science, King Abdul Azis University, 21589 Jeddah, Saudi Arabia

and

Department of Mathematics, Sohag University, Nasr City Eastern avenue, Sohag, 82524, Egypt

JOURNAL OF MECHANICS OF MATERIALS AND STRUCTURES
Vol. 10, No. 4, 2015
dx.doi.org/10.2140/jomms.2015.10.519

TOPOLOGY OPTIMIZATION OF SPATIAL CONTINUUM STRUCTURES MADE OF NONHOMOGENEOUS MATERIAL OF CUBIC SYMMETRY

RADOSŁAW CZUBACKI AND TOMASZ LEWIŃSKI

The paper deals with the minimum compliance problem of spatial structures made of a nonhomogeneous elastic material of cubic symmetry. The elastic moduli as well as the trajectories of anisotropy directions are design variables. The isoperimetric condition fixes the value of the cost of the design expressed as the integral of the unit cost assumed as a linear combination of the three elastic moduli of the cubic symmetry. The problem has been reduced to the pair of mutually dual auxiliary problems similar to those known from the theory of materials with locking and from the transshipping theory. The auxiliary minimization problem has the integrand of linear growth, which transforms the problem considered to the topology optimization problem in which simultaneously the shape of the structure and its material characteristics are constructed. In contrast to the free material design which in the single load case leads to the optimal Hooke tensor with a single nonzero eigenvalue, the optimal Hooke tensor of cubic symmetry has either three or four nonzero eigenvalues.

1. Introduction

The present paper puts forward a topology optimization method aimed at constructing a stiffest continuum structure transmitting a given load to a given boundary. The problem is specified by assuming that the structure being designed is formed of a nonhomogeneous elastic material of cubic symmetry at each point. All the fields which determine the cubic anisotropy within the whole body are design variables. The isoperimetric condition imposed is viewed as the cost of the design and is expressed by the spatial integral of a linear combination of the eigenvalues of the elastic moduli. This expression encompasses the popular definition of cost, as the integral of the trace of the Hooke tensor of cubic symmetry. Then the weight coefficients in the expression of the unit cost are equal to the multiplicities of the relevant elastic moduli. No *a priori* restrictions on the anisotropy directions are assumed; they are to be determined via the optimization process. The stiffness of the structure is defined as the inverse of the total compliance.

The problem thus formulated is a reformulation of the free material design (FMD) to the case of materials of cubic symmetry. In its original formulation the FMD involves no restrictions on the components of the Hooke tensor, apart from necessary symmetries and positive semidefiniteness conditions; see [Bendsøe et al. 1994] and [Haslinger et al. 2010]. The peculiar feature of the compliance minimizing FMD problem is possible elimination of all design variables, leading to an auxiliary problem of the form

$$\min\Big\{\int_\Omega \|\boldsymbol{\tau}\|\,\mathrm{d}x \mid \boldsymbol{\tau} \in \Sigma(\Omega)\Big\}, \tag{P$_1$}$$

The paper was prepared within the Research Grant no. 2013/11/B/ST8/04436 financed by the National Science Centre (Poland), entitled *Topology optimization of engineering structures. An approach synthesizing the methods of free material design, composite design and Michell-like trusses*.
Keywords: free material design, cubic symmetry, topology optimization.

where $\Sigma(\Omega)$ is the set of statically admissible stress fields $\boldsymbol{\tau} = (\tau_{ij})$ on the given feasible domain Ω; the norm $\|\cdot\|$ being Euclidean one.

The problem dual to (P_1) reads

$$\max\{f(\boldsymbol{v}) \mid \boldsymbol{v} \in V(\Omega),\ \|\boldsymbol{\varepsilon}(\boldsymbol{v}(x))\|^* \le 1 \text{ a.e. in } \Omega\}, \tag{P_1^*}$$

where $f(\boldsymbol{v})$ represents the virtual work of the load on the displacement field $\boldsymbol{v}$; $V(\Omega)$ being the space of kinematically admissible displacement fields; $\boldsymbol{\varepsilon}(\boldsymbol{v})$ is the strain tensor, defined as the symmetric part of the gradient of $\boldsymbol{v}$.

The problems (P_1), (P_1^*) have been derived in [Czarnecki and Lewiński 2012; 2014b; 2014a]. The mathematical structure of these mutually dual problems is similar to the Kantorovich–Rubinstein transshipping problem, while their equivalence can be proved in the manner the Theorem 3.3 in [Bouchitté et al. 2010] was proved; cf. also [Bouchitté et al. 2005]. The inequality involved in (P_1^*) can be written as the inclusion: $\boldsymbol{\varepsilon}(\boldsymbol{v}(x)) \in B$ where B is a locking locus. Here B is the unit ball with respect to the Euclidean norm. The problem (P_1^*) has much in common with the locking material problem, discussed for example in [Demengel and Suquet 1986] and in [Telega and Jemioło 1998].

Mathematically demanding questions concerning the correctness of the problems (P_1), (P_1^*), referring to the contemporary variational calculus and measure theory, are the subject of the contemporary studies, to be published soon. These subtleties will not be discussed in the present paper. Let us yet outline here the most distinguished features of these problems. Note that the minimizer $\boldsymbol{\tau} = \boldsymbol{\sigma}$ of problem (P_1) can vanish on a set Ω_0 of positive measure, being a subset of the feasible domain Ω. In the domain Ω_0 all the components of the optimal elasticity tensor vanish. In the remaining part of the feasible domain the components of Hooke's tensor $\boldsymbol{C}$ are expressed by

$$C_{ijkl}(x) = \lambda_1(x) \overset{1}{\omega}_{ij}(x) \overset{1}{\omega}_{kl}(x), \tag{1-1}$$

where $\lambda_1(x)$ is proportional to $\|\boldsymbol{\sigma}(x)\|$, while $\overset{1}{\boldsymbol{\omega}}(x) = \boldsymbol{\sigma}(x)/\|\boldsymbol{\sigma}(x)\|$.

The optimal Hooke tensor possesses only one positive eigenvalue. The form (1-1) is designed for the given loading; that is why the structure of singular properties (1-1) is capable of transmitting the given load to the given support; cf. [Czarnecki and Lewiński 2014a, §6]. Thus the solution to the problems (P_1) and (P_1^*), or only to the problem (P_1), delivers information of two kinds:

(i) Topology information which determines the shape of the domain $\Omega\backslash\Omega_0$ occupied by the structural material; this domain may be multiconnected

(ii) Information on the nonhomogeneous anisotropy: the values of the elastic moduli C_{ijkl} as well as the anisotropy directions at each point of the body.

The solutions to the problems (P_1) and (P_1^*) do not determine the underlying microstructures possibly producing given anisotropic properties.

The topological information on the shape and connectedness of the structure is crucial. This feature of the FMD method delivers the solution to the topology optimization problem implicitly comprised by the method. The regularity of the optimal shape depends on the regularity of the data.

A natural modification of the FMD is *a priori* imposing certain material symmetries. The strongest assumption is isotropy — this modification has been proposed in [Czarnecki 2015] and [Czarnecki and Wawruch 2015]; it will be called the isotropic material design (IMD). The only design variables are

the bulk $k(x)$ and shear $\mu(x)$ moduli in each point x of the feasible domain. In the spatial setting the collection of the eigenvalues of the Hooke tensor is $(3k, 2\mu, 2\mu, 2\mu, 2\mu, 2\mu)$ and the trace of the Hooke tensor equals $3k + 10\mu$. Let the cost of the design be the integral of the trace of the Hooke tensor. Then the isoperimetric condition assumes the form

$$\int_\Omega (3k + 10\mu)\,\mathrm{d}x = \Lambda, \tag{1-2}$$

where Λ stands for the assumed cost.

Czarnecki [2015] proved that the IMD reduces to an auxiliary problem of a mathematical structure similar to (P_1) with the integrand expressed by the norm

$$|||\boldsymbol{\tau}||| = \alpha|\operatorname{tr}\boldsymbol{\tau}| + \beta\|\operatorname{dev}\boldsymbol{\tau}\|, \tag{1-3}$$

where $\operatorname{tr}\boldsymbol{\tau}$ is the trace of $\boldsymbol{\tau}$ and $\operatorname{dev}\boldsymbol{\tau}$ is the deviator of the stress:

$$\operatorname{dev}\boldsymbol{\tau} = \boldsymbol{\tau} - \tfrac{1}{3}(\operatorname{tr}\boldsymbol{\tau})\overset{2}{\boldsymbol{I}}. \tag{1-4}$$

Here $\overset{2}{\boldsymbol{I}} = (\delta_{ij})$ is a unit tensor in $\mathbb{E}^2_s$, $\mathbb{E}^2_s$ being the set of symmetric tensors of rank 2; positive parameters α, β depend on the dimension of the problem.

The problem dual to (P_1) with the norm (1-3) assumes the form (P_1^*), in which the inequality condition has now the form

$$|||\boldsymbol{\varepsilon}(\boldsymbol{v}(x))|||^* \le 1, \tag{1-5}$$

where $\boldsymbol{\varepsilon} \in \mathbb{E}^2_s$ and the new norm in $\mathbb{E}^2_s$ is defined by

$$|||\boldsymbol{\varepsilon}|||^* = \sup_{\boldsymbol{\tau}\neq 0,\ \boldsymbol{\tau}\in\mathbb{E}^2_s} \frac{\boldsymbol{\tau}\cdot\boldsymbol{\varepsilon}}{|||\boldsymbol{\tau}|||}. \tag{1-6}$$

This is a norm dual to (1-3). In the sequel we shall show the explicit form of the norm (1-6) and the condition (1-5).

Therefore, the IMD problem, as expressed by the mutually dual problems (P_1), (P_1^*) involving the norms (1-3), (1-6), preserves the feature (i): the minimizer of (P_1) determines the domain $\Omega\backslash\Omega_0$ which is its effective domain. The process of designing of a structure made of an isotropic material is thus converted into a topology optimization algorithm admitting all possible topological changes of the initial shape of the feasible domain as far as they do keep the linear form $f(.)$ intact. Indeed, if the load is applied on a part of the boundary, then this part of the boundary cannot undergo changes during the optimization process. If the volume forces are taken into account, then also the domain of their application is kept unchanged. In fact, the method takes care of this condition, since the minimizer $\boldsymbol{\sigma}$ will not vanish in the domains where the loads are present.

The IMD method delivers as a solution: the effective domain of the minimizer, where the material is necessary as well as its isotropic properties: the layouts of the moduli $k(x)$, $\mu(x)$ optimally distributed within the feasible domain. The IMD method does not produce any information on the underlying microstructure. Note that the moduli k and μ determine the values of the Poisson ratio ν. The hitherto experiments show that the optimal Poisson ratio assumes extreme admissible values within some subdomains: in many cases ν approaches values close to -1, which is mathematically justified, while in some subdomains the optimal ν assumes values close to $\frac{1}{2}$. Thus the optimization process makes the Poisson

ratio attain both bounds: $-1 < \nu < \frac{1}{2}$. In the 2D setting the bounds are even broader: $-1 < \nu < 1$. The negative values of ν make the physical interpretation difficult; only very special materials, called auxetic materials, like foams of reentrant microstructure, exhibit such properties; cf. [Friis et al. 1988]. The recent conference Auxetics'14 (Auxetics and other materials and models with "negative" characteristics) was fully devoted to this topic of materials science.

The solution of (P_1) with the norm (1-3) suffices to determine the optimal values of the moduli k and μ. It turns out that the optimal $k(x)$ is proportional to $|\operatorname{tr}\boldsymbol{\sigma}(x)|$, while the optimal $\mu(x)$ is proportional to $\|\operatorname{dev}\boldsymbol{\sigma}(x)\|$.

It is worth indicating here that similar formulae have been reported by Zohdi [2003a] in the paper on the inverse homogenization based on the minimization of the relative distance between the tensor of elastic moduli (of a composite determined by random properties of its *representative volume element* (RVE)) and a reference isotropic tensor. The optimal k occurs to be proportional to $\langle|\operatorname{tr}\boldsymbol{\sigma}|\rangle$, while the optimal μ is proportional to $\langle\|\operatorname{dev}\boldsymbol{\sigma}\|\rangle$, where $\langle\cdot\rangle$ represents averaging over RVE.

In majority of papers on composite materials the isotropy is associated with an ideal mixture of two or several constituents within an RVE. It is easy to show two-dimensional layouts of two materials within a repetitive cell resulting in isotropy of the effective Hooke tensor, see [Grigoliuk and Filshtinskii 1970]. Only recently Łukasiak [2013; 2014] has shown three-dimensional layouts resulting in isotropy of the effective Hooke tensor constructed by the homogenization method. This result has been achieved by a proper choice of RVE compatible with Kelvin's packing; see [Aste and Weaire 2008] and [Weaire 1996]. This result contradicts a remark in [Christensen 1999, p. 95]: "cubic symmetry is the highest order symmetry that can be obtained by a space filling periodic repeating cell pattern".

The composite materials and crystals are usually nonisotropic. Thus it is thought useful to extend the FMD method to the class of designs of lower symmetry. According to Xia [1997] and Ting [2003] there are 8 symmetry classes: triclinic, monoclinic, orthotropic, tetragonal, trigonal, transversely isotropic, cubic and isotropic. In the present paper the material design will be confined to the cubic symmetry case. The aim is to put forward a method to construct — within a given feasible domain — the stiffest structure capable of transmitting a given load to a given supporting surface by appropriate choice of the material characteristics of the cubic symmetry class. In each point of the structure the six parameters: the three elastic moduli and a triplet $(\boldsymbol{n}, \boldsymbol{m}, \boldsymbol{p})$ of mutually orthogonal unit vectors satisfying

$$\begin{gathered}\|\boldsymbol{n}\| = \|\boldsymbol{m}\| = \|\boldsymbol{p}\| = 1,\\ \boldsymbol{n}\cdot\boldsymbol{m} = 0, \quad \boldsymbol{n}\cdot\boldsymbol{p} = 0, \quad \boldsymbol{m}\cdot\boldsymbol{p} = 0\end{gathered} \tag{1-7}$$

are to be determined. The Hooke tensor of a material of cubic symmetry is represented by the celebrated formula by Walpole [1984]:

$$\boldsymbol{C} = a\boldsymbol{J} + b\boldsymbol{L} + c\boldsymbol{M}, \tag{1-8}$$

where a, b, c are elastic moduli while the fourth-rank tensors $\boldsymbol{J}$, $\boldsymbol{L}$, $\boldsymbol{M}$ are expressed as

$$\boldsymbol{J} = \tfrac{1}{3}\overset{2}{\boldsymbol{I}}\otimes\overset{2}{\boldsymbol{I}}, \quad \boldsymbol{L} = \overset{4}{\boldsymbol{I}} - \boldsymbol{S}, \quad \boldsymbol{M} = \boldsymbol{S} - \boldsymbol{J}, \quad \text{and} \tag{1-9}$$

$$\boldsymbol{S} = \boldsymbol{n}\otimes\boldsymbol{n}\otimes\boldsymbol{n}\otimes\boldsymbol{n} + \boldsymbol{m}\otimes\boldsymbol{m}\otimes\boldsymbol{m}\otimes\boldsymbol{m} + \boldsymbol{p}\otimes\boldsymbol{p}\otimes\boldsymbol{p}\otimes\boldsymbol{p}, \tag{1-10}$$

$$\overset{4}{I}_{ijkl} = \tfrac{1}{2}(\delta_{ik}\delta_{jl} + \delta_{il}\delta_{kj}), \tag{1-11}$$

the latter being a unit tensor in $\mathbb{E}_s^4$ or in the space of Hooke tensors obeying usual symmetry rules.

The formula (1-8) is also a spectral representation, since the tensors $\boldsymbol{J}$, $\boldsymbol{L}$, $\boldsymbol{M}$ are projection operators (see [Walpole 1984]):

$$\begin{gathered}\boldsymbol{J}^2=\boldsymbol{J}, \quad \boldsymbol{L}^2=\boldsymbol{L}, \quad \boldsymbol{M}^2=\boldsymbol{M}, \\ \boldsymbol{L}\boldsymbol{J}=\boldsymbol{J}\boldsymbol{L}=\boldsymbol{0}, \quad \boldsymbol{M}\boldsymbol{J}=\boldsymbol{J}\boldsymbol{M}=\boldsymbol{0}, \quad \boldsymbol{M}\boldsymbol{L}=\boldsymbol{L}\boldsymbol{M}=\boldsymbol{0}.\end{gathered} \tag{1-12}$$

The eigenvalues of tensor (1-8) are (a, b, b, b, c, c). Moreover,

$$\operatorname{tr}\boldsymbol{J}=1, \quad \operatorname{tr}\overset{4}{\boldsymbol{I}}=6, \quad \operatorname{tr}\boldsymbol{S}=3 \tag{1-13}$$

or

$$\operatorname{tr}\boldsymbol{C}=a+3b+2c. \tag{1-14}$$

In the optimization problem considered the design variables are the scalar fields $a(x)$, $b(x)$, $c(x)$ and the vector fields $\boldsymbol{n}(x)$, $\boldsymbol{m}(x)$, $\boldsymbol{p}(x)$ satisfying the conditions (1-7).

The spectral representation of the inverse of $\boldsymbol{C}$ reads

$$\boldsymbol{C}^{-1}=\frac{1}{a}\boldsymbol{J}+\frac{1}{b}\boldsymbol{L}+\frac{1}{c}\boldsymbol{M}, \tag{1-15}$$

provided that all the moduli a, b, c are positive. If, for instance, $b=0$, the tensor $\boldsymbol{C}^{-1}$ will be assumed in the form

$$\boldsymbol{C}^{-1}=\frac{1}{a}\boldsymbol{J}+\frac{1}{c}\boldsymbol{M}, \tag{1-16}$$

remembering that then the formula $\boldsymbol{C}^{-1}\boldsymbol{C}=\overset{4}{\boldsymbol{I}}$ is broken.

The cost of the design will be taken as the integral of the linear combination of the elastic moduli:

$$\int_\Omega(\alpha_1 a+\alpha_2 b+\alpha_3 c)\,\mathrm{d}x=\Lambda, \tag{1-17}$$

where $\alpha_i>0$ are fixed. If $\alpha_1=1$, $\alpha_2=3$, $\alpha_3=2$ then the unit cost is equal to $\operatorname{tr}\boldsymbol{C}$; see (1-14). We consider the following problem of optimum design:

> *Find the layout of the elastic moduli a, b, c and the orthogonal trajectories of the vector fields* $(\boldsymbol{m}, \boldsymbol{n}, \boldsymbol{p})$ *at each point of the feasible domain* Ω*, satisfying the isoperimetric condition* (1-17)*, such that the structure made of this nonhomogeneous material (of cubic symmetry at each point) is characterized by the smallest total compliance among all structures designed in the same feasible domain, obeying the same isoperimetric condition and capable of transmitting the same load to the same boundary.*

We shall show that the problem above can be reduced to the two auxiliary problems (P_1), (P_1^*) with norms $|||\cdot|||$, $|||\cdot|||^*$ but with different coefficients α and β than those involved in the auxiliary problems of the IMD method. This result is surprising, since the auxiliary optimization problems for the isotropic and cubic symmetries differ very slightly and preserve their main property: the integrand of (P_1) is still expressed in terms of the two invariants of the stress field. Upon finding the minimizer $\boldsymbol{\tau}=\boldsymbol{\sigma}$ of problem (P_1) one can determine the design variables: the scalars $a(x)$, $b(x)$, $c(x)$ and the vector fields $\boldsymbol{n}(x)$, $\boldsymbol{m}(x)$, $\boldsymbol{p}(x)$ at each point of the domain $\Omega\backslash\Omega_0$ where $\boldsymbol{\sigma}$ does not vanish.

The mentioned similarity between optimized cubic symmetry and isotropy has already been noted previously in a different context of constructing a stationary form of energy density of a material of cubic symmetry; Norris [2006] noted that "the extreme values of the energy for cubic materials have the same form of the energy for an isotropic solid"; see Equations (4.59, 46) therein.

Considered in the present paper the optimal materials of cubic symmetry can be manufactured as cellular foams of small density (see [Christensen 1999]), or the lotus-type porous copper (see [Xie et al. 2004]).

Moreover, the metal matrix composites belong to the class of materials whose cubic symmetry can be tailored by appropriate choice of microstructural parameters determining the physical, topological as well as geometrical properties of second phase particles. Towards this end one should state an inverse problem by appropriate extension of Zohdi's [2001; 2003b] normalizing objective functionals. Although constructed for the isotropic design, they can serve as well for the cubic design provided that the set of design variables is augmented by Euler's angles of particles, following the lines of smooth change of the triplet fields $(\boldsymbol{m}, \boldsymbol{n}, \boldsymbol{p})$. Appropriate liquid state processing makes it possible to align the particles along prescribed directions; see comments in [Zohdi 2001, §2].

Reduction of the optimum design problem to the problem of type (P_1) with the norm $|||\cdot|||$ means that *the method put forward implies simultaneously the topology and the material optimization*. The effective domain $\Omega\backslash\Omega_0$ of the minimizer $\boldsymbol{\tau} = \boldsymbol{\sigma}$ determines the shape of the structure and admits its multiconnectedness. Depending on the shape of the feasible domain Ω and on the type of the surface load applied the method forms the domain $\Omega\backslash\Omega_0$ occupied by the material. We shall prove in the sequel that depending on the sign of $(\alpha_2 - \alpha_3)$ the nonzero optimal moduli are either (a, b) or (a, c). *This means that in all cases exactly one modulus of three* (a, b, c) *vanishes to make the whole structure as stiff as possible*. The optimal cubic material turns out to be degenerated in all cases. Yet the optimal material properties are perfectly suited for the given load and support, thus making the optimal structure fulfill all conditions of equilibrium as well as the boundary conditions. The displacement and strain fields in the optimum structure are not uniquely determined, the constitutive equations being noninvertible, yet the corresponding stress field transmitting the load to the support is unique.

The following conventions are adopted. The feasible domain Ω in $\mathbb{R}^3$ is parametrized by the Cartesian system (x_1, x_2, x_3) of vectors $(\boldsymbol{e}_1, \boldsymbol{e}_2, \boldsymbol{e}_3)$ satisfying $\boldsymbol{e}_i \boldsymbol{e}_j = \delta_{ij}$; the Latin indices $i, j, \ldots$ run over 1, 2, 3. The summation convention over repeated indices is adopted. An arbitrary point x of Ω is identified with its coordinates (x_1, x_2, x_3). The symmetric tensors of rank two form the set $\mathbb{E}^2_s$, while rank-four Hooke tensors of usual symmetries form the set $\mathbb{E}^4_s$. Comma implies partial differentiation: $(\cdot)_{,i} = \partial(\cdot)/\partial x_i$. A symmetric part of the gradient of a vector field $\boldsymbol{v} = (v_1, v_2, v_3)$ is denoted by $\varepsilon_{ij}(\boldsymbol{v}) = \frac{1}{2}(v_{i,j} + v_{j,i})$. The Euclidean norms are defined for vectors by $\|\boldsymbol{v}\| = (v_i v_i)^{1/2}$ for $\boldsymbol{v} \in \mathbb{R}^3$, and for tensors by $\|\boldsymbol{\tau}\| = (\tau_{ij}\tau_{ij})^{1/2}$ for $\boldsymbol{\tau} \in \mathbb{E}^2_s$. The scalar products are defined as

$$\boldsymbol{v} \cdot \boldsymbol{w} = v_i w_i, \quad \boldsymbol{\tau} \cdot \boldsymbol{\varepsilon} = \tau_{ij}\varepsilon_{ij} \quad \text{for } \boldsymbol{v}, \boldsymbol{w} \in \mathbb{R}^3, \ \boldsymbol{\tau}, \boldsymbol{\varepsilon} \in \mathbb{E}^2_s.$$

2. Optimum design problem

The main data is the spatial feasible domain Ω in which the designed structure is to be placed. On a boundary Γ_1 the tractions $\boldsymbol{T} = (T_i)$ are applied. This surface is not subject to optimization. Under the equilibrium problem we understand construction of the stress fields $\boldsymbol{\tau}$ within Ω, transmitting the given load $\boldsymbol{T}$ to the given part Γ_2 of the boundary. Not all points of Γ_2 need to be supporting points — along

some part of the boundary the material can disappear. The vector fields $\boldsymbol{v} = (v_1, v_2, v_3)$ within Ω vanishing on Γ_2 form the space $V(\Omega)$ of kinematically admissible displacements. In this paper we do not formulate the regularity conditions for the fields involved; these conditions can be assumed by analogy with those assumed in [Bouchitté et al. 2005; 2010] concerning the transshipping problem in the scalar version.

The stress field $\boldsymbol{\tau}$ is said to be statically admissible if it satisfies the variational equation

$$\int_\Omega \boldsymbol{\tau} \cdot \boldsymbol{\varepsilon}(\boldsymbol{v})\, \mathrm{d}x = f(\boldsymbol{v}) \quad \text{for all } \boldsymbol{v} \in V(\Omega), \tag{2-1}$$

where the linear form is defined by

$$f(\boldsymbol{v}) = \int_{\Gamma_1} \boldsymbol{T} \cdot \boldsymbol{v}\, \mathrm{d}s. \tag{2-2}$$

The value $f(\boldsymbol{v})$ is the virtual work of the tractions on the field $\boldsymbol{v}$. The set of all stress fields $\boldsymbol{\tau}$ satisfying (2-1), (2-2) forms the linear affine set $\Sigma(\Omega)$.

The body occupying the domain Ω, supported on Γ_2, loaded on Γ_1 of given anisotropy determined by the field of the Hooke tensor $\boldsymbol{C}(x)$ will be called a structure if it is capable of transmitting the given load to the support Γ_2. Its total compliance is expressed by the Castigliano formula:

$$Y = \min_{\boldsymbol{\tau} \in \Sigma(\Omega)} \int_\Omega \boldsymbol{\tau} \cdot (\boldsymbol{C}^{-1}\boldsymbol{\tau})\, \mathrm{d}x. \tag{2-3}$$

Assume that the tensor field $\boldsymbol{C}(x)$ exhibits a cubic symmetry at each point x of the feasible domain. Let the moduli a, b, c and the triplet $(\boldsymbol{m}, \boldsymbol{n}, \boldsymbol{p})$ be design variables. The moduli a, b, c must satisfy the isoperimetric condition (1-17) while the triplet $(\boldsymbol{m}, \boldsymbol{n}, \boldsymbol{p})$ must satisfy the conditions (1-7). The problem of optimum design expressing the compliance minimization is formulated as

$$J = \min_{\substack{(\boldsymbol{m},\boldsymbol{n},\boldsymbol{p}) \\ \text{satisfying (1-7)}}} \; \min_{\substack{(a,b,c) \\ \text{satisfying (1-17)}}} Y \tag{2-4}$$

The fields (a, b, c) and $(\boldsymbol{m}, \boldsymbol{n}, \boldsymbol{p})$ minimizing Y determine the moduli and the trajectories of cubic anisotropy directions. It will be shown in the sequel that minimization over the design variables can be performed analytically, which reduces the problem (2-4) to an auxiliary problem (P_1) with a certain norm of type (1-3).

3. Elimination of design variables

Let us change the sequence of minimization operators in (2-4) and (2-3). We rewrite (2-4) in the form

$$J = \min_{\boldsymbol{\tau} \in \Sigma(\Omega)} Y(\boldsymbol{\tau}), \tag{3-1}$$

where

$$Y(\boldsymbol{\tau}) = \min_{\substack{(\boldsymbol{m},\boldsymbol{n},\boldsymbol{p}) \\ \text{satisfying (1-7)}}} \; \min_{\substack{(a,b,c) \\ \text{satisfying (1-17)}}} \int_\Omega \boldsymbol{\tau} \cdot (\boldsymbol{C}^{-1}\boldsymbol{\tau})\, \mathrm{d}x. \tag{3-2}$$

Let us compute the integrand in (3-2) by using (1-15) and (1-9):

$$\boldsymbol{\tau} \cdot (\boldsymbol{C}^{-1}\boldsymbol{\tau}) = \frac{1}{a}\boldsymbol{\tau} \cdot (\boldsymbol{J}\boldsymbol{\tau}) + \frac{1}{b}(\|\boldsymbol{\tau}\|^2 - \boldsymbol{\tau} \cdot (\boldsymbol{S}\boldsymbol{\tau})) + \frac{1}{c}(\boldsymbol{\tau} \cdot (\boldsymbol{S}\boldsymbol{\tau}) - \boldsymbol{\tau} \cdot (\boldsymbol{J}\boldsymbol{\tau})). \tag{3-3}$$

Let us write

$$\boldsymbol{\tau}\cdot(\boldsymbol{C}^{-1}\boldsymbol{\tau}) = \frac{1}{a}Y_1(\boldsymbol{\tau}) + \frac{1}{b}Y_2(\boldsymbol{\tau}) + \frac{1}{c}Y_3(\boldsymbol{\tau}) \tag{3-4}$$

with

$$\begin{aligned} Y_1(\boldsymbol{\tau}) &= \tfrac{1}{3}(\operatorname{tr}\boldsymbol{\tau})^2, \\ Y_2(\boldsymbol{\tau}) &= \|\boldsymbol{\tau}\|^2 - \boldsymbol{\tau}\cdot(\boldsymbol{S}\boldsymbol{\tau}), \\ Y_3(\boldsymbol{\tau}) &= \boldsymbol{\tau}\cdot(\boldsymbol{S}\boldsymbol{\tau}) - \tfrac{1}{3}(\operatorname{tr}\boldsymbol{\tau})^2. \end{aligned} \tag{3-5}$$

One can prove that for each choice of the triplet $(\boldsymbol{m}, \boldsymbol{n}, \boldsymbol{p})$ satisfying (1-7) the following estimates hold:

$$\tfrac{1}{3}(\operatorname{tr}\boldsymbol{\tau})^2 \le \boldsymbol{\tau}\cdot(\boldsymbol{S}\boldsymbol{\tau}) \le \|\boldsymbol{\tau}\|^2. \tag{3-6}$$

The right inequality becomes sharp if the triplet $(\boldsymbol{m}, \boldsymbol{n}, \boldsymbol{p})$ coincides with principal directions of the stress tensor $\boldsymbol{\tau}$. The left inequality is also attainable, which is much more difficult to prove. It can be inferred from the stationarity criterion of Norris [2006, (4.32)]. The minimizer $(\boldsymbol{m}^*, \boldsymbol{n}^*, \boldsymbol{p}^*)$ of the quadratic form $\boldsymbol{\tau}\cdot(\boldsymbol{S}\boldsymbol{\tau})$, for fixed $\boldsymbol{\tau}$, satisfies the condition

$$\boldsymbol{S}(\boldsymbol{m}^*, \boldsymbol{n}^*, \boldsymbol{p}^*)\boldsymbol{\tau} = \tfrac{1}{3}(\operatorname{tr}\boldsymbol{\tau})\overset{2}{\boldsymbol{I}}, \tag{3-7}$$

which implies

$$\min_{\substack{(\boldsymbol{m},\boldsymbol{n},\boldsymbol{p}) \\ \text{satisfying (1-7)}}} (\boldsymbol{\tau}\cdot(\boldsymbol{S}\boldsymbol{\tau})) = \tfrac{1}{3}(\operatorname{tr}\boldsymbol{\tau})^2. \tag{3-8}$$

We conclude that both $Y_2(\boldsymbol{\tau})$ and $Y_3(\boldsymbol{\tau})$ are nonnegative.

Consider the auxiliary problem

$$W = \min_{\substack{a>0,\, b>0,\, c>0 \\ \text{satisfying (1-17)}}} \int_\Omega \Big(\frac{1}{a}Y_1 + \frac{1}{b}Y_2 + \frac{1}{c}Y_3\Big)\,\mathrm{d}x, \tag{3-9}$$

in which $\boldsymbol{\tau}$ is fixed while the quantities Y_i are positive. Such a problem has been solved in [Czarnecki and Lewiński 2014b, §3.1]. Its solution has the form

$$W = \frac{1}{\Lambda}\bigg[\int_\Omega \big(\sqrt{\alpha_1}\sqrt{Y_1} + \sqrt{\alpha_2}\sqrt{Y_2} + \sqrt{\alpha_3}\sqrt{Y_3}\big)\,\mathrm{d}x\bigg]^2. \tag{3-10}$$

Let us proceed to perform minimization over the triplets $(\boldsymbol{m}, \boldsymbol{n}, \boldsymbol{p})$. Let us introduce the notation

$$z = \boldsymbol{\tau}\cdot(\boldsymbol{S}\boldsymbol{\tau}), \quad z_0 = \tfrac{1}{3}(\operatorname{tr}\boldsymbol{\tau})^2, \quad z_1 = \|\boldsymbol{\tau}\|^2. \tag{3-11}$$

Let us consider the auxiliary problem

$$\min_{z\in[z_0,z_1]} f(z), \tag{3-12}$$

where

$$f(z) = \sqrt{\alpha_2}\sqrt{z_1 - z} + \sqrt{\alpha_3}\sqrt{z - z_0}. \tag{3-13}$$

It is easy to check that $f''(z) < 0$ if $z \in [z_0, z_1]$. Thus the minima of $f(z)$ can only be attained at the ends of the interval $[z_0, z_1]$:

$$\min_{z\in[z_0,z_1]} f(z) = \min(f(z_0), f(z_1)). \tag{3-14}$$

Let us compute

$$f(z_0) = \sqrt{\alpha_2}\sqrt{z_1 - z_0}, \quad f(z_1) = \sqrt{\alpha_3}\sqrt{z_1 - z_0}. \tag{3-15}$$

Thus

$$\min_{z\in[z_0,z_1]} f(z) = \sqrt{z_1 - z_0}\,\min(\sqrt{\alpha_2}, \sqrt{\alpha_3}). \tag{3-16}$$

According to the Norris result (3-7) both the minima are attainable by a certain triplet $(\boldsymbol{m}, \boldsymbol{n}, \boldsymbol{p})$.

The results (3-10), (3-16) solve the problem (3-2):

$$Y(\boldsymbol{\tau}) = \frac{1}{\Lambda}\left(\int_\Omega \left(\sqrt{\alpha_1}\sqrt{Y_1(\boldsymbol{\tau})} + \min(\sqrt{\alpha_2}, \sqrt{\alpha_3})\sqrt{\|\boldsymbol{\tau}\|^2 - Y_1(\boldsymbol{\tau})}\right) \mathrm{d}x\right)^2.$$

Let us note that

$$\sqrt{\|\boldsymbol{\tau}\|^2 - Y_1(\boldsymbol{\tau})} = \|\operatorname{dev}\boldsymbol{\tau}\|. \tag{3-17}$$

The problem (3-7) is thus reduced to the form

$$J = \frac{1}{\Lambda}Z^2, \tag{3-18}$$

where

$$Z = \min\left\{\textstyle\int_\Omega |||\boldsymbol{\tau}||| \,\mathrm{d}x \mid \boldsymbol{\tau} \in \Sigma(\Omega)\right\} \tag{3-19}$$

and

$$|||\boldsymbol{\tau}||| = \sqrt{\alpha_1/3}\,|\operatorname{tr}\boldsymbol{\tau}| + \min(\sqrt{\alpha_2}, \sqrt{\alpha_3})\|\operatorname{dev}\boldsymbol{\tau}\| \tag{3-20}$$

is the norm of type (1-3). Thus the problem (3-20) has almost the same form as that occurring in the similar problem concerning nonhomogeneous isotropy; see [Czarnecki 2015].

Remark 1. The problem (3-19) is the tensorial counterpart of the following problem with a vectorial unknown:

$$Z_s = \min\left\{\textstyle\int_\Omega \|\boldsymbol{p}\| \,\mathrm{d}x \mid \boldsymbol{p} \in \Sigma_s(\Omega)\right\}, \tag{3-21}$$

where $\|\boldsymbol{p}\|$ is a certain norm of the vector $\boldsymbol{p} \in \mathbb{R}^3$; $\Sigma_s(\Omega)$ is the set of vector fields $\boldsymbol{p} = (p_1, p_2, p_3)$ on Ω such that

$$\int_\Omega \boldsymbol{p}\cdot\nabla v \,\mathrm{d}x = \int_{\Gamma_1} T\cdot v \,\mathrm{d}s \quad \text{for all } v \in V_s(\Omega), \tag{3-22}$$

where T is given on $\Gamma_1 \subset \partial\Omega$ while $V_s(\Omega)$ is the set of scalar fields v vanishing on the segment Γ_2 of the boundary. The problem (3-21) appears in the theory of transshipping; cf. [Bouchitté et al. 2010; 2005]. This problem can be rearranged to a well-posed form by completing it with appropriate assumptions concerning the data.

The subtle problems concerning possible well-posedness of the problem (3-19) will be the subject of an independent work. Assume that $\boldsymbol{\tau} = \boldsymbol{\sigma}$ is the minimizer of (3-19). Let $\Omega\backslash\Omega_0$ be the effective domain of $\boldsymbol{\sigma}$. The values of the optimal moduli $a^*(x)$, $b^*(x)$, $c^*(x)$ can be computed by the formulae which follow from minimization of (3-9):

$$a^*(x) = \frac{1}{\sqrt{\lambda\alpha_1}}\sqrt{Y_1(\boldsymbol{\sigma}(x))}, \quad b^*(x) = \frac{1}{\sqrt{\lambda\alpha_2}}\sqrt{Y_2(\boldsymbol{\sigma}(x))}, \quad c^*(x) = \frac{1}{\sqrt{\lambda\alpha_3}}\sqrt{Y_3(\boldsymbol{\sigma}(x))}, \tag{3-23}$$

where the Lagrange multiplier λ is positive and given by the formula

$$\sqrt{\lambda} = \frac{1}{\Lambda}\int_\Omega \left(\sqrt{\alpha_1 Y_1(\boldsymbol{\sigma})} + \sqrt{\alpha_2 Y_2(\boldsymbol{\sigma})} + \sqrt{\alpha_3 Y_3(\boldsymbol{\sigma})}\right) \mathrm{d}x \tag{3-24}$$

and $Y_i(\boldsymbol{\sigma})$ are determined by (3-5), where the triplet $(\boldsymbol{m}^*, \boldsymbol{n}^*, \boldsymbol{p}^*)$ corresponds either to the lower or to the upper bound in (3-6).

In case of $\alpha_2 < \alpha_3$ the minimum in (3-14) is attained if $z = z_0$ then the triplet $(\boldsymbol{m}^*, \boldsymbol{n}^*, \boldsymbol{p}^*)$ makes sharp the left inequality in (3-6). The triplet should be found from the Norris condition (3-7). In case of $\alpha_2 > \alpha_3$ the minimum in (3-14) is attained if $z = z_1$. Then the triplet $(\boldsymbol{m}^*, \boldsymbol{n}^*, \boldsymbol{p}^*)$ makes sharp the right inequality in (3-6). The triplet coincides with eigenvectors of the tensor $\boldsymbol{\tau} = \boldsymbol{\sigma}$.

Let us discuss these two cases in more detail.

Case 1: $\alpha_2 < \alpha_3$. The choice of $(\boldsymbol{m}^*, \boldsymbol{n}^*, \boldsymbol{p}^*)$ by (3-7) implies that $\boldsymbol{\sigma} \cdot (\boldsymbol{S}\boldsymbol{\sigma}) = \frac{1}{3}(\operatorname{tr}\boldsymbol{\sigma})^2$. Thus

$$Y_2(\boldsymbol{\sigma}) = \|\operatorname{dev}\boldsymbol{\sigma}\|^2, \quad Y_3(\boldsymbol{\sigma}) = 0. \tag{3-25}$$

The optimal moduli are expressed as

$$a^*(x) = \frac{1}{\sqrt{\lambda\alpha_1}}\frac{1}{\sqrt{3}}|\operatorname{tr}\boldsymbol{\sigma}(x)|, \quad b^*(x) = \frac{1}{\sqrt{\lambda\alpha_2}}\|\operatorname{dev}\boldsymbol{\sigma}(x)\|, \quad c^*(x) = 0. \tag{3-26}$$

The optimal Hooke tensor $\boldsymbol{C}^*(x)$ is characterized by the eigenvalues $(a^*(x), b^*(x), b^*(x), b^*(x), 0, 0)$. Let us write down its spectral representation:

$$\boldsymbol{C}^*(x) = a^*(x)\boldsymbol{J} + b^*(x)\boldsymbol{L}(x), \tag{3-27}$$

where $\boldsymbol{L}(x) = \overset{4}{\boldsymbol{I}} - \boldsymbol{S}(x)$ and the tensor $\boldsymbol{S}(x)$ is determined by the triplet $(\boldsymbol{m}^*, \boldsymbol{n}^*, \boldsymbol{p}^*)$ satisfying the condition (3-7). Let us write down the formula for the multiplier λ:

$$\sqrt{\lambda} = \frac{1}{\Lambda}\int_\Omega \left(\sqrt{\alpha_1/3}\,|\operatorname{tr}\boldsymbol{\sigma}| + \sqrt{\alpha_2}\,\|\operatorname{dev}\boldsymbol{\sigma}\|\right)\mathrm{d}x, \tag{3-28}$$

which completes the formulae (3-26) for the effective moduli.

Let us write down the constitutive equations of the optimal body taking at the given point x the axes x_i as directed along the triplet $(\boldsymbol{m}^*, \boldsymbol{n}^*, \boldsymbol{p}^*)$ determined by the condition (3-7). The components of the tensor $\boldsymbol{C}$ read

$$C_{ijkl} = \tfrac{1}{3}(a-c)\delta_{ij}\delta_{kl} + \tfrac{1}{2}b(\delta_{ik}\delta_{jl} + \delta_{il}\delta_{jk}) + (c-b)(\delta_{i1}\delta_{j1}\delta_{k1}\delta_{l1} + \delta_{i2}\delta_{j2}\delta_{k2}\delta_{l2} + \delta_{i3}\delta_{j3}\delta_{k3}\delta_{l3}). \tag{3-29}$$

This formula can be inferred from (1-8)–(1-11). The nonzero components C_{ijkl} are

$$\begin{aligned} C_{1111} &= C_{2222} = C_{3333} = \tfrac{1}{3}a + \tfrac{2}{3}c, \\ C_{1122} &= C_{1133} = C_{2233} = \tfrac{1}{3}a - \tfrac{1}{3}c, \\ C_{1212} &= C_{1313} = C_{2323} = \tfrac{1}{2}b. \end{aligned} \tag{3-30}$$

Hence the constitutive equations assume the form

$$\begin{aligned}
\tilde{\sigma}_{11} &= \left(\tfrac{1}{3}a + \tfrac{2}{3}c\right)\tilde{\varepsilon}_{11} + \tfrac{1}{3}(a-c)(\tilde{\varepsilon}_{22} + \tilde{\varepsilon}_{33}),\\
\tilde{\sigma}_{22} &= \left(\tfrac{1}{3}a + \tfrac{2}{3}c\right)\tilde{\varepsilon}_{22} + \tfrac{1}{3}(a-c)(\tilde{\varepsilon}_{11} + \tilde{\varepsilon}_{33}),\\
\tilde{\sigma}_{33} &= \left(\tfrac{1}{3}a + \tfrac{2}{3}c\right)\tilde{\varepsilon}_{33} + \tfrac{1}{3}(a-c)(\tilde{\varepsilon}_{11} + \tilde{\varepsilon}_{22}),\\
\tilde{\sigma}_{12} &= b\tilde{\varepsilon}_{12}, \quad \tilde{\sigma}_{13} = b\tilde{\varepsilon}_{13}, \quad \tilde{\sigma}_{23} = b\tilde{\varepsilon}_{23}
\end{aligned} \tag{3-31}$$

The stresses $\tilde{\sigma}_{ij}$ and strains $\tilde{\varepsilon}_{ij}$ refer to the optimal body. These tensors should not be misled with the solution to the auxiliary problems: (3-19) and the dual to the latter.

In the case discussed $a = a^*$, $b = b^*$, $c = c^* = 0$ the equations (3-31) assume the form

$$\begin{aligned}
&\tilde{\sigma}_{ii} = \tfrac{1}{3}a^*(\tilde{\varepsilon}_{11} + \tilde{\varepsilon}_{22} + \tilde{\varepsilon}_{33}), && \text{(do not sum over } i\text{)},\\
&\tilde{\sigma}_{ij} = b^*\tilde{\varepsilon}_{ij}, && i \neq j.
\end{aligned} \tag{3-32}$$

The principal directions of tensors $\tilde{\boldsymbol{\sigma}}$ and $\boldsymbol{\sigma}$ do not coincide. Consequently, these fields do not coincide.

Case 2: $\alpha_2 > \alpha_3$. The triplet $(\boldsymbol{m}^*, \boldsymbol{n}^*, \boldsymbol{p}^*)$ coincides with eigenvectors of tensor $\boldsymbol{\sigma}$. Thus we have $\boldsymbol{\sigma} \cdot (\boldsymbol{S}\boldsymbol{\sigma}) = \|\boldsymbol{\sigma}\|^2$. Then

$$Y_2(\boldsymbol{\sigma}) = 0, \quad Y_3(\boldsymbol{\sigma}) = \|\operatorname{dev}\boldsymbol{\sigma}\|^2. \tag{3-33}$$

The optimal moduli assume the form

$$a^*(x) = \frac{1}{\sqrt{\lambda\alpha_1}}\frac{1}{\sqrt{3}}|\operatorname{tr}\boldsymbol{\sigma}(x)|, \quad b^*(x) = 0, \quad c^*(x) = \frac{1}{\sqrt{\lambda\alpha_3}}\|\operatorname{dev}\boldsymbol{\sigma}(x)\|. \tag{3-34}$$

The optimal Hooke tensor has the eigenvalues $(a^*(x), 0, 0, 0, c^*(x), c^*(x))$. The spectral representation of the Hooke tensor reads

$$\boldsymbol{C}^*(x) = a^*(x)\boldsymbol{J} + c^*(x)\boldsymbol{M}(x), \tag{3-35}$$

with $\boldsymbol{M}(x) = \boldsymbol{S}(x) - \boldsymbol{J}$ and tensor $\boldsymbol{S}(x)$ is determined by the triplet of eigenvectors of tensor $\boldsymbol{\sigma}$ at point x. Let us write down the expression for the Lagrange multiplier

$$\sqrt{\lambda} = \frac{1}{\Lambda}\int_\Omega \left(\sqrt{\alpha_1/3}\,|\operatorname{tr}\boldsymbol{\sigma}| + \sqrt{\alpha_3}\,\|\operatorname{dev}\boldsymbol{\sigma}\|\right)\mathrm{d}x. \tag{3-36}$$

Thus the formulae for the optimal moduli have been put in their final form.

According to (3-30) the moduli C^*_{1212}, C^*_{1313}, C^*_{2323} vanish. Thus, in the assumed coordinate system the constitutive equations assume the form

$$\tilde{\sigma}_{11} = \left(\tfrac{1}{3}a^* + \tfrac{2}{3}c^*\right)\tilde{\varepsilon}_{11} + \tfrac{1}{3}\left(a^* - c^*\right)\left(\tilde{\varepsilon}_{22} + \tilde{\varepsilon}_{33}\right), \quad \tilde{\sigma}_{12} = 0, \quad \tilde{\sigma}_{13} = 0, \quad \tilde{\sigma}_{23} = 0. \tag{3-37}$$

The remaining equations follow from change of indices. We conclude that the eigendirections of the tensor $\boldsymbol{\sigma}$ (i.e. the minimizer of (3-19)) and of the tensor $\tilde{\boldsymbol{\sigma}}$ (stress field in the optimal structure) coincide. Thus the trajectories of both the fields coincide.

Both the fields $\boldsymbol{\sigma}$ and $\tilde{\boldsymbol{\sigma}}$ are statically admissible and have the same trajectories. Thus, except very specific situations in which the stress field has multiple principal values and undefined eigenvectors, both the stress fields should coincide. Indeed, if writing the equilibrium equations along the trajectories (or — in the curvilinear coordinate system formed by the trajectories) these three equations involve three

unknown fields (principal stresses). This suggests that there is only one solution to this system satisfying the same boundary conditions on the boundary Γ_1. Consequently, the fields $\tilde{\boldsymbol{\sigma}}$ and $\boldsymbol{\sigma}$ must, in general, coincide, except for very specific cases.

The case of $\alpha_2 > \alpha_3$ is particularly important as encompassing the isoperimetric condition expressed in terms of the trace of the Hooke tensor; see (1-14). Then $\alpha_1 = 1$, $\alpha_2 = 3$, $\alpha_3 = 2$ and the norm (3-20) assumes the form

$$|||\boldsymbol{\tau}||| = \tfrac{\sqrt{3}}{3}\,|\operatorname{tr}\boldsymbol{\tau}| + \sqrt{2}\,\|\operatorname{dev}\boldsymbol{\tau}\|, \tag{3-38}$$

the parameters α and β being equal to $\frac{\sqrt{3}}{3}$ and $\sqrt{2}$, respectively.

The algorithm for solving the problem (2-4) with the isoperimetric condition concerning the trace of $\boldsymbol{C}$ can be summarized as below:

(1) Solve the problem (3-19) or construct its minimizer $\boldsymbol{\tau} = \boldsymbol{\sigma}$.

(2) Determine the domain $\Omega\backslash\Omega_0$ where $\boldsymbol{\sigma}$ does not vanish.

(3) Compute by (3-34), (3-36) the moduli a^*, c^* within the domain $\Omega\backslash\Omega_0$.

(4) Find the triplets $(\boldsymbol{m}, \boldsymbol{n}, \boldsymbol{p})$ as eigenvectors of the tensor $\boldsymbol{\sigma}$.

(5) Compute components of $\boldsymbol{C}^*$ by (3-35).

Remark 2. The FMD method in its original version in which no additional conditions are imposed on the structure of the Hooke tensor $\boldsymbol{C}$ leads to the singular optimal solution $\boldsymbol{C}^*$ with only one nonzero eigenvalue. The method proposed in the present paper in which the cubic symmetry is imposed leads to the singular representations (3-27) or (3-35) with two or three vanishing eigenvalues. The method IMD in which the material symmetry is imposed as isotropic leads to the nondegenerate optimal Hooke tensors. This distinguishes the method IMD from other versions of FMD-type, since nonsingular results are obtained even if only one load condition is taken into account.

To make the presented results (3-27) and (3-35) nonsingular one should, e.g., consider multiple load optimization, with the simplest scalarization concept, as used recently in [Czarnecki and Lewiński 2014b] for the classical FMD. This is an open problem to be discussed elsewhere.

4. Formulation dual to the auxiliary minimization problem

As has been stressed in Section 1, the problem dual to the stress-based auxiliary problem of the FMD has the form (P_1^*), which can be expressed as

$$\max\big\{ f(\boldsymbol{v}) \mid \boldsymbol{v} \in V(\Omega),\ \boldsymbol{\varepsilon}(\boldsymbol{v}(x)) \in B \big\}, \tag{4-1}$$

where B is the unit ball in $\mathbb{E}^2_s$ with respect to the Euclidean norm. It is seen that the problem (4-1) has a very specific mathematical structure, since it involves the conditions to be satisfied pointwise. This is the consequence of the integrand in (P_1) being of linear growth. Since the integrand in (3-19) has also a linear growth, the problem dual to (3-19) will have again the mathematical form similar to (4-1); the modification will touch the shape of the ball B, called the locking locus. As mentioned in Section 1, the ball B is now defined by the norm dual to the norm $|||\cdot|||$ involved in (3-19), hence

$$B = \big\{ \boldsymbol{\varepsilon} \in \mathbb{E}^2_s \mid |||\boldsymbol{\varepsilon}|||^* \le 1 \big\}, \tag{4-2}$$

while the norm $|||\cdot|||^*$ is defined by (1-6). A passage from (3-19) to (4-1)–(4-2) can be done by using the arguments invoked in [Czarnecki and Lewiński 2014a], along the lines of the derivation shown in [Strang and Kohn 1983], where, however, other norms are involved.

Our aim now is now to find the explicit form of the norm $|||\cdot|||^*$ given by (1-6). The scalar product $\boldsymbol{\tau}\cdot\boldsymbol{\varepsilon}$ can be decomposed into the hydrostatic and deviatoric parts:

$$\boldsymbol{\tau}\cdot\boldsymbol{\varepsilon} = \tfrac{1}{3}(\operatorname{tr}\boldsymbol{\tau})(\operatorname{tr}\boldsymbol{\varepsilon}) + \operatorname{dev}\boldsymbol{\tau}\cdot\operatorname{dev}\boldsymbol{\varepsilon}.$$

Let $\eta = \operatorname{tr}\boldsymbol{\tau}$, $\boldsymbol{s} = \operatorname{dev}\boldsymbol{\tau}$. Let us rewrite (1-6) using definition (1-3) of the norm $|||\cdot|||$:

$$|||\boldsymbol{\varepsilon}|||^* = \frac{1}{\alpha}\max_{\substack{\eta\in\mathbb{R},\,\boldsymbol{s}\in\mathbb{E}^2_s\\ \operatorname{tr}\boldsymbol{s}=0,\,\boldsymbol{s}\neq\boldsymbol{0}}} \frac{\frac{1}{3}\eta(\operatorname{tr}\boldsymbol{\varepsilon}) + \boldsymbol{s}\cdot\operatorname{dev}\boldsymbol{\varepsilon}}{|\eta| + \left(\frac{\beta}{\alpha}\right)\|\boldsymbol{s}\|}. \tag{4-3}$$

Now we shall make use of the following elementary result, valid for positive a and b:

$$\max_{x\in\mathbb{R}}\frac{cx+a}{|x|+b} = \max\left(|c|, \frac{a}{b}\right). \tag{4-4}$$

This result will be used by interpreting

$$x = \eta, \quad c = \tfrac{1}{3}\operatorname{tr}\boldsymbol{\varepsilon}, \quad a = \boldsymbol{s}\cdot\operatorname{dev}\boldsymbol{\varepsilon}, \quad b = \frac{\beta}{\alpha}\|\boldsymbol{s}\|. \tag{4-5}$$

Tensor $\boldsymbol{s}$ can always be chosen such that $a > 0$. Thus the norm (4-3) assumes the form

$$|||\boldsymbol{\varepsilon}|||^* = \frac{1}{\alpha}\max\left\{\tfrac{1}{3}|\operatorname{tr}\boldsymbol{\varepsilon}|,\ \frac{\alpha}{\beta}\max_{\substack{\boldsymbol{s}\in\mathbb{E}^2_s\\ \operatorname{tr}\boldsymbol{s}=0,\,\boldsymbol{s}\neq\boldsymbol{0}}}\frac{\boldsymbol{s}\cdot\operatorname{dev}\boldsymbol{\varepsilon}}{\|\boldsymbol{s}\|}\right\}, \tag{4-6}$$

hence

$$|||\boldsymbol{\varepsilon}|||^* = \max\left\{\frac{1}{3\alpha}|\operatorname{tr}\boldsymbol{\varepsilon}|,\ \frac{1}{\beta}\|\operatorname{dev}\boldsymbol{\varepsilon}\|\right\} \tag{4-7}$$

since

$$\max_{\substack{\boldsymbol{s}\in\mathbb{E}^2_s\\ \operatorname{tr}\boldsymbol{s}=0,\,\boldsymbol{s}\neq\boldsymbol{0}}}\frac{\boldsymbol{s}\cdot\operatorname{dev}\boldsymbol{\varepsilon}}{\|\boldsymbol{s}\|} = \max_{\substack{\boldsymbol{s}\in\mathbb{E}^2_s\\ \boldsymbol{s}\neq\boldsymbol{0}}}\frac{\boldsymbol{s}\cdot\operatorname{dev}\boldsymbol{\varepsilon}}{\|\boldsymbol{s}\|} = \|\operatorname{dev}\boldsymbol{\varepsilon}\|.$$

We omit the proof that $|||\cdot|||^*$ given by (4-7) is a norm in $\mathbb{E}^2_s$.

If the cost of the design is expressed by the trace of $\boldsymbol{C}$ then one should put $\alpha = \frac{\sqrt{3}}{3}$ and $\beta = \sqrt{2}$ into (4-7) to find the locking locus in the form

$$\max\left\{\tfrac{\sqrt{3}}{3}|\operatorname{tr}\boldsymbol{\varepsilon}|,\ \tfrac{\sqrt{2}}{2}\|\operatorname{dev}\boldsymbol{\varepsilon}\|\right\} \le 1. \tag{4-8}$$

The above set can be expressed in terms of principal strains upon using the formulae

$$|\operatorname{tr}\boldsymbol{\varepsilon}| = |\varepsilon_{\mathrm{I}} + \varepsilon_{\mathrm{II}} + \varepsilon_{\mathrm{III}}|, \qquad \|\operatorname{dev}\boldsymbol{\varepsilon}\| = \tfrac{\sqrt{3}}{3}\sqrt{(\varepsilon_{\mathrm{I}}-\varepsilon_{\mathrm{II}})^2 + (\varepsilon_{\mathrm{II}}-\varepsilon_{\mathrm{III}})^2 + (\varepsilon_{\mathrm{I}}-\varepsilon_{\mathrm{III}})^2}. \tag{4-9}$$

In the space of principal strains the locking locus assumes the shape of a cylindrical domain of the axis along the vector of $\boldsymbol{e} = (1, 1, 1)$; see Figure 1. The length of the cylinder equals 2, while its radius equals $\frac{2\sqrt{3}}{3}$.

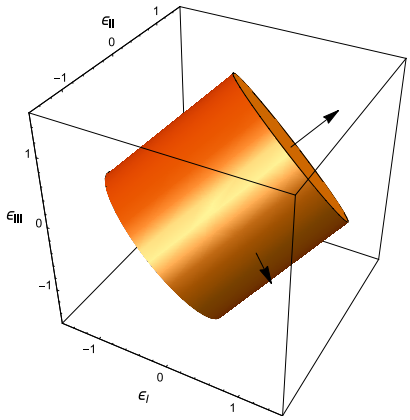

Figure 1. The locking locus for the isoperimetric condition expressed by $\operatorname{tr} \boldsymbol{C}$.

5. The question of correctness of the equilibrium problem of the optimal structure

The equilibrium of the optimal structure is governed by the following variational problem: find $\boldsymbol{u} \in V(\Omega)$ such that

$$\mathsf{a}^*(\boldsymbol{u}, \boldsymbol{v}) = f(\boldsymbol{v}) \quad \text{for all } \boldsymbol{v} \in V(\Omega), \tag{5-1}$$

the bilinear form being associated with the optimal Hooke tensor $\boldsymbol{C}^*$

$$\mathsf{a}^*(\boldsymbol{u}, \boldsymbol{v}) = \int_\Omega \boldsymbol{\varepsilon}(\boldsymbol{v}) \cdot (\boldsymbol{C}^* \boldsymbol{\varepsilon}(\boldsymbol{u}))\, \mathrm{d}x \tag{5-2}$$

given by the formula (3-27) in case $\alpha_2 < \alpha_3$ and by the formula (3-35) if $\alpha_2 > \alpha_3$. Consider the case of $\alpha_2 > \alpha_3$ encompassing the case of the isoperimetric condition expressed by $\operatorname{tr} \boldsymbol{C}$. The bilinear form $\mathsf{a}^*(\,\cdot\,,\cdot\,)$ is nonnegative, since

$$\begin{aligned} \boldsymbol{\varepsilon} \cdot (\boldsymbol{C}^* \boldsymbol{\varepsilon}) &= a^*(\boldsymbol{\varepsilon} \cdot (\boldsymbol{J}\boldsymbol{\varepsilon})) + c^*\big[\boldsymbol{\varepsilon} \cdot (\boldsymbol{S}\boldsymbol{\varepsilon}) - \boldsymbol{\varepsilon} \cdot (\boldsymbol{J}\boldsymbol{\varepsilon})\big] \\ &= \tfrac{1}{3} a^* (\operatorname{tr} \boldsymbol{\varepsilon})^2 + c^*\big(\boldsymbol{\varepsilon} \cdot (\boldsymbol{S}\boldsymbol{\varepsilon}) - \tfrac{1}{3}(\operatorname{tr} \boldsymbol{\varepsilon})^2\big) \geq 0. \end{aligned} \tag{5-3}$$

Let $\mathscr{R}$ be the kernel of the bilinear form $\mathsf{a}^*(\,\cdot\,,\cdot\,)$:

$$\mathscr{R} = \big\{\boldsymbol{v} \in H^1(\Omega, \mathbb{R}^3) \mid \mathsf{a}^*(\boldsymbol{v}, \boldsymbol{v}) = 0\big\}. \tag{5-4}$$

Any field v of the class $\mathscr{R}$ is such that there exists a field $\boldsymbol{w} \in H^1(\Omega, \mathbb{R}^3)$ such that

$$\boldsymbol{\varepsilon}(\boldsymbol{v}) = \boldsymbol{L}\boldsymbol{\varepsilon}(\boldsymbol{w}), \tag{5-5}$$

where $\boldsymbol{L} = \overset{4}{\boldsymbol{I}} - \boldsymbol{S}$; cf. (1-9).

Let us compute the integrand of $\mathsf{a}^*(\boldsymbol{v}, \boldsymbol{v})$:

$$\boldsymbol{\varepsilon}(\boldsymbol{v}) \cdot (\boldsymbol{C}^* \boldsymbol{\varepsilon}(\boldsymbol{v})) = (\boldsymbol{L}\boldsymbol{\varepsilon}(\boldsymbol{w})) \cdot (\boldsymbol{C}^* \boldsymbol{L}\boldsymbol{\varepsilon}(\boldsymbol{w})).$$

According to (3-35) and using (1-12) we find

$$\boldsymbol{C}^* \boldsymbol{L} = (a^* \boldsymbol{J} + c^* \boldsymbol{M})\boldsymbol{L} = a^*(\boldsymbol{J}\boldsymbol{L}) + c^*(\boldsymbol{M}\boldsymbol{L}) = \boldsymbol{0},$$

which proves that $\boldsymbol{v} \in \mathcal{R}$.

Let us proceed now to prove

$$f(\boldsymbol{v}) = 0 \quad \text{for all } \boldsymbol{v} \in \mathcal{R} \cap V(\Omega), \tag{5-6}$$

which is the main necessary condition of well-posedness of problem (5-1). Let us note that the minimizer $\boldsymbol{\tau} = \boldsymbol{\sigma}$ of (3-19) satisfies (2-1). Thus the linear form $f(\cdot)$ may be represented by

$$f(\boldsymbol{v}) = \int_\Omega \boldsymbol{\sigma} \cdot \boldsymbol{\varepsilon}(\boldsymbol{v})\, \mathrm{d}x \quad \text{for all } \boldsymbol{v} \in V(\Omega). \tag{5-7}$$

For showing (5-6) it is sufficient to prove that

$$\boldsymbol{\sigma} \cdot \boldsymbol{\varepsilon}(\boldsymbol{v}) = 0 \tag{5-8}$$

holds if the field $\boldsymbol{v}$ is chosen such that $\boldsymbol{\varepsilon}(\boldsymbol{v}) = \boldsymbol{L}\boldsymbol{\varepsilon}(\boldsymbol{w})$ and $\boldsymbol{w} \in H^1(\Omega, \mathbb{R}^3)$. We compute

$$\boldsymbol{\sigma} \cdot \boldsymbol{\varepsilon}(\boldsymbol{v}) = \boldsymbol{\sigma} \cdot (\boldsymbol{L}\boldsymbol{\varepsilon}(\boldsymbol{w})) = \boldsymbol{\sigma} \cdot ((\overset{4}{\boldsymbol{I}} - \boldsymbol{S})\boldsymbol{\varepsilon}(\boldsymbol{w})) = \boldsymbol{\sigma} \cdot \boldsymbol{\varepsilon}(\boldsymbol{w}) - \boldsymbol{\sigma} \cdot (\boldsymbol{S}\boldsymbol{\varepsilon}(\boldsymbol{w})). \tag{5-9}$$

Let $\overset{m}{\sigma}, \overset{m}{\boldsymbol{n}}$ be the eigenvalues and eigenvectors of the tensor $\boldsymbol{\sigma}$, $m = 1, 2, 3$. In the case when $\alpha_2 > \alpha_3$, the following representations hold:

$$\begin{aligned} S_{ijkl} &= \overset{1}{n}_i \overset{1}{n}_j \overset{1}{n}_k \overset{1}{n}_l + \overset{2}{n}_i \overset{2}{n}_j \overset{2}{n}_k \overset{2}{n}_l + \overset{3}{n}_i \overset{3}{n}_j \overset{3}{n}_k \overset{3}{n}_l, \\ \sigma_{ij} &= \overset{1}{\sigma} \overset{1}{n}_i \overset{1}{n}_j + \overset{2}{\sigma} \overset{2}{n}_i \overset{2}{n}_j + \overset{3}{\sigma} \overset{3}{n}_i \overset{3}{n}_j, \end{aligned} \tag{5-10}$$

since the triplet $(\boldsymbol{m}^*, \boldsymbol{n}^*, \boldsymbol{p}^*)$ coincides with the eigenvectors of $\boldsymbol{\sigma}$. Let us write $\eta_{ij} = \varepsilon_{ij}(\boldsymbol{w})$ for brevity and compute

$$\boldsymbol{\sigma} \cdot \boldsymbol{\varepsilon}(\boldsymbol{w}) = \sum_{m=1}^{3} \overset{m}{\sigma} (\overset{m}{n}_i \eta_{ij} \overset{m}{n}_j) \tag{5-11}$$

as well as

$$\boldsymbol{\sigma} \cdot (\boldsymbol{S}\boldsymbol{\varepsilon}(\boldsymbol{w})) = \boldsymbol{\sigma} \cdot (\boldsymbol{S}\boldsymbol{\eta}) = \sigma_{ij} S_{ijkl} \eta_{kl} = \sum_{m=1}^{3} \sigma_{ij} \overset{m}{n}_i \overset{m}{n}_j \overset{m}{n}_k \overset{m}{n}_l \eta_{kl}. \tag{5-12}$$

Taking into account that

$$\sigma_{ij} \overset{m}{n}_i \overset{m}{n}_j = \overset{m}{\sigma}, \tag{5-13}$$

we find

$$\boldsymbol{\sigma} \cdot (\boldsymbol{S}\boldsymbol{\varepsilon}(\boldsymbol{w})) = \sum_{m=1}^{3} \overset{m}{\sigma} (\overset{m}{n}_k \eta_{kl} \overset{m}{n}_l), \tag{5-14}$$

which proves that $\boldsymbol{\sigma} \cdot \boldsymbol{\varepsilon}(\boldsymbol{v}) = 0$ if $\boldsymbol{v}$ satisfies the condition (5-5). Consequently, the condition (5-6) is fulfilled.

Assume that the problem (5-1) possesses two solutions $\overset{1}{\boldsymbol{u}}, \overset{2}{\boldsymbol{u}}$. Then

$$\mathsf{a}^*(\overset{1}{\boldsymbol{u}} - \overset{2}{\boldsymbol{u}}, \boldsymbol{v}) = 0 \quad \text{for all } \boldsymbol{v} \in V(\Omega). \tag{5-15}$$

Let us choose $\boldsymbol{v} = \overset{1}{\boldsymbol{u}} - \overset{2}{\boldsymbol{u}}$ to conclude that $\overset{1}{\boldsymbol{u}} - \overset{2}{\boldsymbol{u}} \in \mathcal{R}$. By (5-5) a field $\boldsymbol{w}$ exists such that

$$\boldsymbol{\varepsilon}(\overset{1}{\boldsymbol{u}} - \overset{2}{\boldsymbol{u}}) = \boldsymbol{L}\boldsymbol{\varepsilon}(\boldsymbol{w}). \tag{5-16}$$

Then

$$\boldsymbol{C}^*\boldsymbol{\varepsilon}(\overset{1}{\boldsymbol{u}}) - \boldsymbol{C}^*\boldsymbol{\varepsilon}(\overset{2}{\boldsymbol{u}}) = 0 \tag{5-17}$$

since

$$\boldsymbol{C}^*\boldsymbol{L} = \boldsymbol{0}.$$

Hence to both the fields $\overset{1}{\boldsymbol{u}}$ and $\overset{2}{\boldsymbol{u}}$ the same stress tensor is assigned:

$$\tilde{\boldsymbol{\sigma}} = \boldsymbol{C}^*\boldsymbol{\varepsilon}(\overset{1}{\boldsymbol{u}}) = \boldsymbol{C}^*\boldsymbol{\varepsilon}(\overset{2}{\boldsymbol{u}}). \tag{5-18}$$

We conclude that the stress field in the optimal structure is uniquely determined, provided it exists. We have previously noted that this stress field is simultaneously the minimizer of the problem (3-19), except for some specific cases when the eigenvectors of the stress field are not uniquely determined.

Let us stress that the displacement field and strain field are not uniquely determined, but this property does not contradict uniqueness of the stress field. Moreover, the compliance $f(\boldsymbol{u})$ is uniquely determined since $\boldsymbol{u}$, a solution to (5-1), is determined modulo fields from $\mathcal{R}$ on which the linear form $f(\cdot)$ vanishes.

6. Final remarks

The minimum compliance problem (2-4) has been reduced to the auxiliary, stress-based problem (3-19) with the integrand of linear growth. A numerical method for this problem is now available; it has been successfully developed by Czarnecki [2015] to construct optimum isotropic bodies. Case studies concerning cubic symmetry will be published in separate papers.

The optimal designs depend drastically on the sign of $(\alpha_2 - \alpha_3)$, α_i being the weight coefficients in the isoperimetric condition (1-17). In case of $\alpha_2 < \alpha_3$ the eigenvalues of the optimal Hooke tensor $\boldsymbol{C}^*$ are $(a, b, b, b, 0, 0)$. In case of $\alpha_2 > \alpha_3$ these eigenvalues are $(a, 0, 0, 0, c, c)$. Moreover, in the latter case the stress field in the optimal body coincides (except for very specific cases) with the stress field being the minimizer of the auxiliary problem (3-19). In particular, the trajectories of both the stress fields are the same.

References

[Aste and Weaire 2008] T. Aste and D. Weaire, *The pursuit of perfect packing*, 2nd ed., Taylor & Francis, New York, 2008.

[Bendsøe et al. 1994] M. P. Bendsøe, J. M. Guedes, R. B. Haber, P. Pedersen, and J. E. Taylor, "An analytical model to predict optimal material properties in the context of optimal structural design", *J. Appl. Mech.* (*ASME*) **61**:4 (1994), 930–937.

[Bouchitté et al. 2005] G. Bouchitté, T. Champion, and C. Jimenez, "Completion of the space of measures in the Kantorovich norm", *Riv. Mat. Univ. Parma* (7) **4** (2005), 127–139.

[Bouchitté et al. 2010] G. Bouchitté, G. Buttazzo, and L. de Pascale, "The Monge–Kantorovich problem for distributions and applications", *J. Convex Anal.* **17**:3-4 (2010), 925–943.

[Christensen 1999] R. M. Christensen, "Mechanics of cellular and other low-density materials", *Int. J. Solids Struct.* **37**:1-2 (1999), 93–104.

[Czarnecki 2015] S. Czarnecki, "Isotropic material design", *Comput. Methods. Sci. Technol.* **21**:2 (2015), 49–64.

[Czarnecki and Lewiński 2012] S. Czarnecki and T. Lewiński, "A stress-based formulation of the free material design problem with the trace constraint and single loading condition", *Bull. Acad. Pol. Sci. Tech.* **60**:2 (2012), 191–204.

[Czarnecki and Lewiński 2014a] S. Czarnecki and T. Lewiński, "The *free material design* in linear elasticity", pp. 213–257 in *Topology optimization in structural and continuum mechanics*, edited by G. I. N. Rozvany and T. Lewiński, CISM Courses and Lectures **549**, Springer, Vienna, 2014.

[Czarnecki and Lewiński 2014b] S. Czarnecki and T. Lewiński, "A stress-based formulation of the free material design problem with the trace constraint and multiple load conditions", *Struct. Multidiscip. Optim.* **49**:5 (2014), 707–731.

[Czarnecki and Wawruch 2015] S. Czarnecki and P. Wawruch, "The emergence of auxetic material as a result of optimal isotropic design", *Phys. Status Solidi B* **252**:7 (2015), 1620–1630.

[Demengel and Suquet 1986] F. Demengel and P. Suquet, "On locking materials", *Acta Appl. Math.* **6**:2 (1986), 185–211.

[Friis et al. 1988] E. A. Friis, R. S. Lakes, and J. B. Park, "Negative Poisson's ratio polymeric and metallic foams", *J. Mater. Sci.* **23**:12 (1988), 4406–4414.

[Grigoliuk and Filshtinskii 1970] E. I. Grigoliuk and L. A. Filshtinskii, *Perforated plates and shells*, Nauka, Moscow, 1970. In Russian.

[Haslinger et al. 2010] J. Haslinger, M. Kočvara, G. Leugering, and M. Stingl, "Multidisciplinary free material optimization", *SIAM J. Appl. Math.* **70**:7 (2010), 2709–2728.

[Łukasiak 2013] T. Łukasiak, "Recovery of two-phase microstructures of planar isotropic elastic composites", in *10th World Congress on Structural and Multidisciplinary Optimization* (WCSMO-10) (Orlando, FL, 2013), 2013.

[Łukasiak 2014] T. Łukasiak, "Two-phase isotropic composites with prescribed bulk and shear moduli", pp. 213–222 in *Recent advances in computational mechanics*, edited by T. Łodygowski et al., Taylor & Francis, London, 2014.

[Norris 2006] A. N. Norris, "Optimal orientation of anisotropic solids", *Quart. J. Mech. Appl. Math.* **59**:1 (2006), 29–53.

[Strang and Kohn 1983] G. Strang and R. V. Kohn, "Hencky–Prandtl nets and constrained Michell trusses", *Comput. Methods Appl. Mech. Eng.* **36**:2 (1983), 207–222.

[Telega and Jemioło 1998] J. J. Telega and S. Jemioło, "Macroscopic behaviour of locing materials with microstructure, I: Primal and dual elastic-locking potential: Relaxation", *Bull. Acad. Pol. Sci. Tech.* **46**:3 (1998), 265–576.

[Ting 2003] T. C. T. Ting, "Generalized Cowin–Mehrabadi theorems and a direct proof that the number of linear elastic symmetries is eight", *Int. J. Solids Struct.* **40**:25 (2003), 7129–7142.

[Walpole 1984] L. J. Walpole, "Fourth-rank tensors of the thirty-two crystal classes: Multiplication tables", *Proc. R. Soc. Lond. A* **391**:1800 (1984), 149–179.

[Weaire 1996] D. Weaire (editor), *The Kelvin problem: Foam structures of minimal surface area*, Taylor & Francis, London, 1996.

[Xiao 1997] H. Xiao, "On constitutive equations of Cauchy elastic solids: All kinds of crystals and quasicrystals", *J. Elasticity* **48**:3 (1997), 241–283.

[Xie et al. 2004] Z. Xie, T. Ikeda, Y. Okuda, and H. Nakajima, "Sound absorption characteristics of lotus - type porous copper fabricated by unidirectional solidification", *Mater. Sci. Eng. A* **386**:1-2 (2004), 390–395.

[Zohdi 2001] T. I. Zohdi, "Computational optimization of vortex manufacturing of advanced materials", *Comput. Methods Appl. Mech. Eng.* **190**:46-47 (2001), 6231–6256.

[Zohdi 2003a] T. I. Zohdi, "Constrained inverse formulations in random material design", *Comput. Methods Appl. Mech. Eng.* **192**:28-30 (2003), 3179–3194.

[Zohdi 2003b] T. I. Zohdi, "Genetic design of solids possessing a random-particulate microstructure", *Phil. Trans. R. Soc. A* **361**:1806 (2003), 1021–1043.

Received 17 Apr 2015. Revised 26 Jun 2015. Accepted 4 Jul 2015.

RADOSŁAW CZUBACKI: r.czubacki@il.pw.edu.pl
Department of Structural Mechanics and Computer Aided Engineering, Faculty of Civil Engineering, Warsaw University of Technology, ul. Armii Ludowej 16, 00-637 Warsaw, Poland

TOMASZ LEWIŃSKI: t.lewinski@il.pw.edu.pl
Department of Structural Mechanics and Computer Aided Engineering, Faculty of Civil Engineering, Warsaw University of Technology, ul. Armii Ludowej 16, 00-637 Warsaw, Poland

SUBMISSION GUIDELINES

ORIGINALITY

Authors may submit manuscripts in PDF format online at the Submissions page. Submission of a manuscript acknowledges that the manuscript is original and has neither previously, nor simultaneously, in whole or in part, been submitted elsewhere. Information regarding the preparation of manuscripts is provided below. Correspondence by email is requested for convenience and speed. For further information, write to contact@msp.org.

LANGUAGE

Manuscripts must be in English. A brief abstract of about 150 words or less must be included. The abstract should be self-contained and not make any reference to the bibliography. Also required are keywords and subject classification for the article, and, for each author, postal address, affiliation (if appropriate), and email address if available. A home-page URL is optional.

FORMAT

Authors can use their preferred manuscript-preparation software, including for example Microsoft Word or any variant of TEX. The journal itself is produced in LATEX, so accepted articles prepared using other software will be converted to LATEX at production time. Authors wishing to prepare their document in LATEX can follow the example file at www.jomms.net (but the use of other class files is acceptable). At submission time only a PDF file is required. After acceptance, authors must submit all source material (see especially Figures below).

REFERENCES

Bibliographical references should be complete, including article titles and page ranges. All references in the bibliography should be cited in the text. The use of BibTEX is preferred but not required. Tags will be converted to the house format (see a current issue for examples); however, for submission you may use the format of your choice. Links will be provided to all literature with known web locations; authors can supply their own links in addition to those provided by the editorial process.

FIGURES

Figures must be of publication quality. After acceptance, you will need to submit the original source files in vector format for all diagrams and graphs in your manuscript: vector EPS or vector PDF files are the most useful. (EPS stands for Encapsulated PostScript.)

Most drawing and graphing packages—Mathematica, Adobe Illustrator, Corel Draw, MATLAB, etc.—allow the user to save files in one of these formats. Make sure that what you're saving is vector graphics and not a bitmap. If you need help, please write to graphics@msp.org with as many details as you can about how your graphics were generated.

Please also include the original data for any plots. This is particularly important if you are unable to save Excel-generated plots in vector format. Saving them as bitmaps is not useful; please send the Excel (.xls) spreadsheets instead. Bundle your figure files into a single archive (using zip, tar, rar or other format of your choice) and upload on the link you been given at acceptance time.

Each figure should be captioned and numbered so that it can float. Small figures occupying no more than three lines of vertical space can be kept in the text ("the curve looks like this:"). It is acceptable to submit a manuscript with all figures at the end, if their placement is specified in the text by means of comments such as "Place Figure 1 here". The same considerations apply to tables.

WHITE SPACE

Forced line breaks or page breaks should not be inserted in the document. There is no point in your trying to optimize line and page breaks in the original manuscript. The manuscript will be reformatted to use the journal's preferred fonts and layout.

PROOFS

Page proofs will be made available to authors (or to the designated corresponding author) at a Web site in PDF format. Failure to acknowledge the receipt of proofs or to return corrections within the requested deadline may cause publication to be postponed.

Journal of Mechanics of Materials and Structures

Volume 10, No. 4 July 2015